12

Platinum Group Element Traces of CAMP Volcanism Associated With Low-Latitude Environmental and Biological Disruptions

Jessica H. Whiteside[1], Paul E. Olsen[2], Sean T. Kinney[2], and Mohammed Et-Touhami[3]

ABSTRACT

Multiple lines of evidence suggest that volcanic and thermogenic gas emanations from the voluminous eruptions of the Central Atlantic Magmatic Province (CAMP) triggered the end-Triassic mass extinction. However, a comparison of the timing and duration of the biotic and environmental crises with the timing and duration of the magmatic activity is difficult with existing data, especially when comparing the sedimentary archives below radioisotopically dated CAMP lavas. Here, we report multiple iridium anomalies interpreted to be the remnants of weathered basaltic ashes or aerosols of CAMP eruptions from three basins across a 15° swath of paleolatitude. Milankovitch-controlled climate cycles pace the lacustrine strata of these basins, and in conjunction with paleomagnetic reversal stratigraphy and abundant palynological data, allow us to constrain the timing of magmatic events to be coincident with the extinctions. Thus, platinum group element concentrations provide geochemical traces of CAMP eruptions and can serve as potential proxies for CAMP eruptive pulses in both marine and nonmarine Triassic-Jurassic boundary successions, permitting evaluation of correlations worldwide.

12.1. INTRODUCTION

The end-Triassic extinction (ETE) closely coincided with eruptions of the Central Atlantic Magmatic Province (CAMP) (Marzoli et al., 1999), a massive large igneous province (LIP) considered responsible for a greenhouse warming episode (McElwain et al., 1999; Schaller et al., 2011) and one of the five largest biodiversity crises of the Phanerozoic (Raup & Sepkoski, 1982). Relating the biotic and environmental changes to specific magmatic events of the CAMP has proved challenging due to an inability to establish reliable high-resolution correlations between biotic events recorded in sedimentary archives and the lava sequences that might have caused them. Here we present new data on platinum group element (PGE) anomalies in six continental rift basins in eastern North America and Morocco, where CAMP lava flows are intercalated with lacustrine sedimentary sequences with direct evidence of the ETE.

Motivated by the discovery of a modest Ir anomaly at a "fern spike" at the palynological Triassic-Jurassic transition in the Jacksonwald Syncline of the Newark Basin (Fig. 12.1) (Cornet, 1977; Fowell, 1993; Fowell et al., 1994; Olsen et al., 2002) (Appendix Note 1) resembling the K-Pg boundary in the Raton Basin (Fig. 12.1; e.g., Tschudy et al., 1984), we sampled 13 more sections across 15° paleolatitude and found multiple anomalies at two additional areas. Below we describe these findings in paleotropical eastern North America and Morocco and Europe, and place these new data in the context of new stable carbon isotopic, biotic, and geochronologic information and previously published reports of Triassic-Jurassic Ir anomalies (e.g., Tanner & Kyte, 2005, 2016; Tanner et al., 2008, 2016; Whiteside et al., 2010; Dal Corso et al., 2014; Percival et al., 2017;

[1] *National Oceanography Centre, Southampton, University of Southampton, Southampton, United Kingdom*

[2] *Lamont-Doherty Earth Observatory of Columbia University, Palisades, New York, USA*

[3] *2GPMH, Département des Sciences de la Terre, Université Mohammed Premier, Oujda, Morocco*

Large Igneous Provinces: A Driver of Global Environmental and Biotic Changes, Geophysical Monograph 255, First Edition.
Edited by Richard E. Ernst, Alexander J. Dickson, and Andrey Bekker.
© 2021 The Authors. Co-published 2021 by the American Geophysical Union and John Wiley and Sons, Inc.
DOI: 10.1002/9781119507444.ch12
This is an open access publication under the terms of the Creative Commons Attribution License, which permits use, distribution and reproduction in any medium, provided the original work is properly cited.

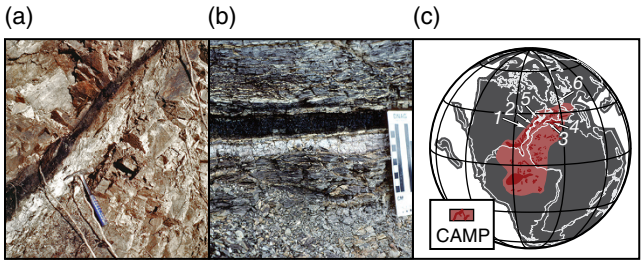

Figure 12.1 Comparison between the ETE in Newark Basin and the K-Pg boundary in the Raton Basin and location of sites described in text. (a) Exeter section of the base of the continental ETE in the Newark Basin, Exeter Township, Pennsylvania; an Ir anomaly (Olsen et al., 2002) is in the white layer (for scale, hammer is 30 cm). (b) K-Pg boundary in the Raton Basin, Colorado; Ir anomaly is in the white layer (photo courtesy of Mark Anders and Walter Alvarez). (c) Paleogeographic reconstruction of the end-Triassic world, adapted from Whiteside et al. (2010) with the study sites; the inferred extent of the CAMP is in red and the present preserved extent of the CAMP in darker red: 1, Newark Basin; 2, Hartford-Deerfield basins; 3, Argana Basin; 4, Central High Atlas Basin 5, Fundy Basin; and 6, St. Audrie's Bay section in the Bristol Channel Basin.

Cornet, 1977; Fowell et al., 1994; Olsen et al., 2002; Whiteside et al., 2007; Guex et al., 2012; Blackburn et al., 2013; Wotzlaw et al., 2014; Davies et al., 2017).

12.2. GEOLOGICAL CONTEXT

Rift basins of the Central Atlantic Margin (CAM) (Olsen, 1997) formed at low latitudes during the incipient fragmentation of Pangea in the Late Permian extending into at least the Early Jurassic (Sinemurian), terminating at the initial stages of Atlantic seafloor spreading. This broad CAM rifting zone extended roughly NE-SW across 23° of latitude on at least three plates (North American, African, and Iberian) and composed the central part of a much larger rift province extending from northern Europe and Greenland to at least the Gulf of Mexico and plausibly to the Pacific (Fig. 12.1).

Strata in these rift basins (except eastern Morocco) are continental in origin with sedimentary sections generally dominated by red clastic rocks, but also contain much lesser amounts of grey and black mudstones and more minor carbonates. The intervals described here are predominantly lacustrine. Lacustrine and fluvio-lacustrine facies are arranged in a hierarchy of cycles which constitute a cyclostratigraphy paced by variations in the orientation of the Earth's spin axis and orbit (Van Houten, 1964; Olsen, 1986; Olsen & Kent, 1996, 1999; Kent & Olsen, 2000; Kent & Olsen, 2008; Blackburn et al., 2013; Kent et al., 2017; Olsen et al., 2019a).

12.2.1. Resolving the ETE and Asserted Hiatus in the CAM Basins

The end-Triassic extinction (ETE) is recognized as one of the largest mass extinctions of the Phanerozoic (Colbert, 1958; Newell, 1967; Hallam, 1981; Raup & Sepkoski, 1982; but see Weems, 1992; Benton, 1994; Lucas & Tanner 2007, 2018). Here we focus on PGE evidence from individual sections and how those sections correlate, and include an encompassing overview of how the PGE anomalies relate to the biotic events. Below we present PGE evidence for individual sections, identify correlations among these sections, and present a synthesis of the relationships between the PGE anomalies and biotic events. We begin with a demonstration that the archive is not distorted by a reported regional hiatus; the size of the global record for the ETE relative to other extinctions is not considered.

Of the CAM rifts, strata of the Newark Basin are the best characterized from over 160 years of mapping, extensive drilling and coring, and sedimentological and stratigraphic study (e.g., reviewed in Olsen et al., 1996; Kent et al., 1995; Smoot, 2010; Withjack et al., 2013). The cyclostratigraphy and magnetic polarity stratigraphy are known in great detail and are demonstrably of astronomical origin (Olsen & Kent, 1996, 1999; Li et al., 2018; Kent et al., 2018; Olsen et al., 2019a). The Newark Basin section is also the only CAM basin that has both tetrapod and palynological data at multiple levels below and above the CAMP basalts fully integrated with the cyclostratigraphy, magnetostratigraphy, and high resolution U-Pb zircon geochronology (Kent et al., 1995; Kent & Olsen, 1999; Olsen et al., 2002; Whiteside et al., 2007; Blackburn et al., 2013).

The ETE is recognized in the Newark Basin on the basis of sporomorphs, tetrapod footprints, and to a lesser extent, skeletal remains (Olsen et al., 2002). Best seen in the Exeter section of the Jacksonwald Syncline (Pennsylvania), the Newark Basin sporomorph transition has been examined by Cornet (1977), Cornet et al. (1973), Cornet and Traverse (1975), Fowell et al. (1994), Fowell and Olsen (1993); and Olsen et al. (2002a, b). A diverse assemblage of pollen and spores in the uppermost Passaic Formation with abundant vesicate pollen (*Patinasporites*) is replaced by a low diversity assemblage strongly dominated by *Corollina meyeriana* (>90%) with no *Patinasporites*. At the transition is the aforementioned fern spore-dominated interval (Fig. 12.2a).

Several footprint taxa abundant through the Norian and Rhaetian age portions of the Newark Basin section have their last appearances in the upper few tens of meters of the Passaic Formation, just beneath the sporomorph transition that occurs immediately below the

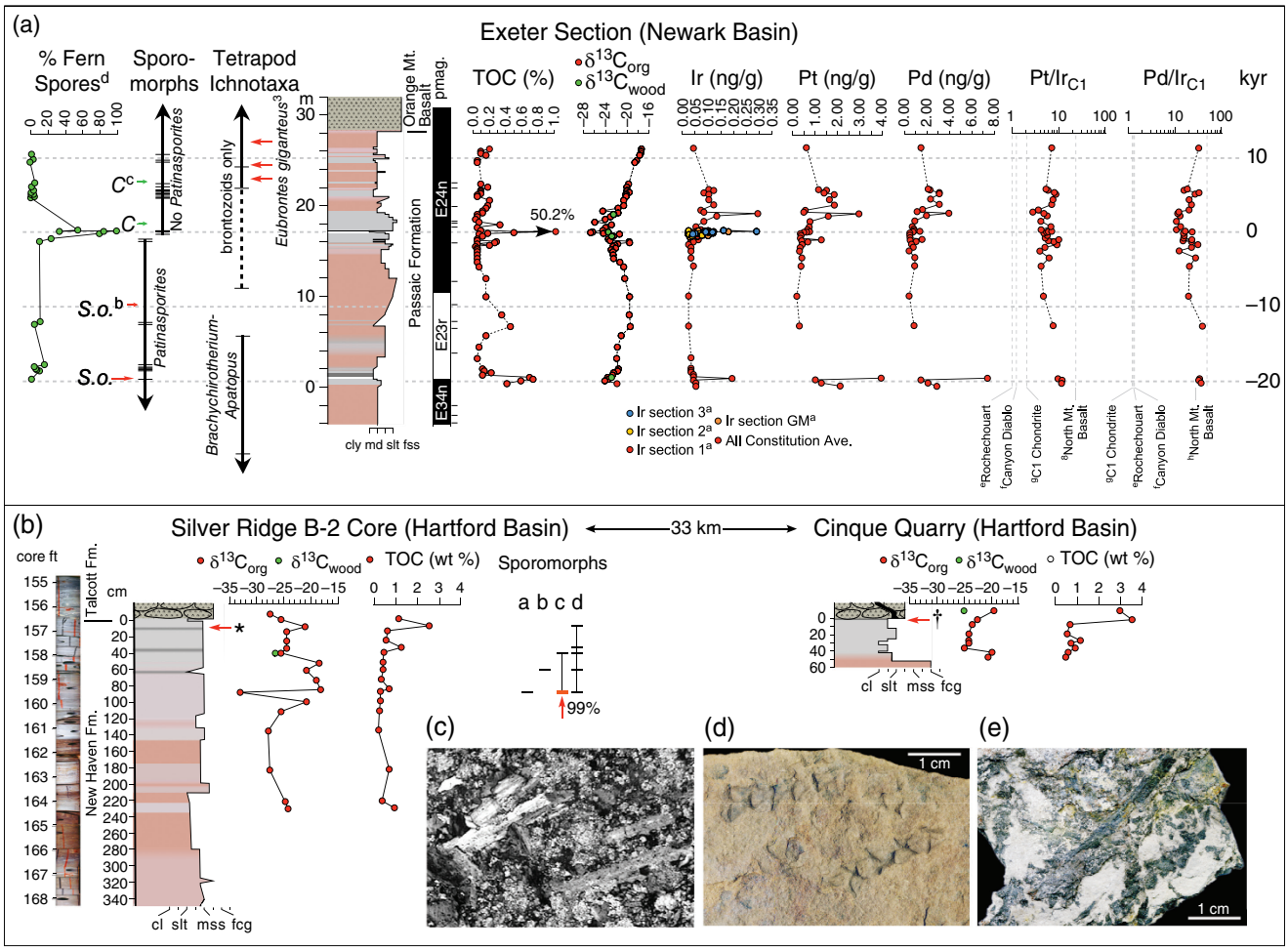

Figure 12.2 (a) Exeter section composite from the Newark Basin including new data (red, Constitution Avenue) and previously published outcrop data from the Exeter area as well data from the Martinsville no. 1 core (Appendix Note 7), and outcrops at Woodland Park, N.J. (Appendix Note 8), projected in with scaling shown in Olsen et al. (2016b, Fig. 34). C = *Clathropteris* leaf fragments; S. o. = spinocaudatan *Shipingia olseni*. Notes: [a]from Olsen et al., 2002; [b]occurrence of *Shipingia olseni* in Martinsville no. 1 core anchored by being in the upper part of E23r of Kent et al. (1995) in that core; [c]occurrences of track taxon *Eubrontes giganteus* from exposures at Woodland Park; [d]fern spore percentages from Olsen et al. (2002) and Olsen et al. (2016b); [e]Rochechouart data from Tagle et al. (2009), normalized to C1 chondrite; [f]Canyon Diablo data from Tagle et al. (2009), normalized to C1 chondrite; [g]C1 chondrite data from Lodders and Fegley (1998); [h]North Mountain Basalt data from Greenough and Fryer (1995). In sporomorphs and tetrapod ichnotaxa, the horizontal ticks mark the position of occurrences. (b) Hartford Basin sections in upper New Haven Formation below the Talcott (basalt) Formation. Note: *position of *Brachyphyllum* mat and possible felsic ash; †position of *Brachyphyllum* mat; sporomorph taxa = a, *Deltaspora* sp.; b, *Alisporites* sp.; c, *Pilasporites* sp.; d, *Classopollis meyeriana*); (c) thin section of possible felsic ash clast in Silver Ridge B-2 core; (d) *Brachyphyllum* cf. *B scotti*, exposure of *Brachyphyllum* mat on east side of CT 15 at Silver Ridge; (e) *Brachyphyllum* cf. *B scotti* mat from Cinque Quarry.

oldest lava flows (Orange Mountain Basalt) in the basin. Reviewed by Olsen et al. (2002), these include forms attributed to phytosaurs (*Apatopus*), large pseudosuchians (*Brachychirotherium*), and small tanystropheiids; none of these are known above the ETE globally. Above these last occurrences and the palynological ETE, but still below the Orange Mountain Basalt, are assemblages with abundant tracks attributed to the oldest occurrence of large theropod dinosaurs (*Eubrontes giganteus*) in eastern North America. These tracks display an abrupt 20% increase in size compared with older theropod tracks (brontozoids), consistent with the global skeletal record (Olsen et al., 2002; Griffin & Nesbitt, 2019) (Appendix Notes 2 and 3) (Fig. 12.2a). Above this level, tracks

attributed to ornithischian dinosaurs appear. The less sampled skeletal record is consistent with the footprints (Olsen et al., 2002). Palynological and tetrapod data of the other CAM basins are consistent though less studied (Cornet, 1977; Olsen et al., 2002; Cirilli et al., 2009; Sues & Olsen, 2015). Both in sporomorphs and footprints, little discernable change exists at the supraspecies level above the zone of concentrated biotic change of the ETE, except for the addition of ornithischian and prosauropod skeletal remains and footprints in the Hartford and Fundy basins (Sues & Olsen, 2015).

Below the ETE in the Newark Basin, there are two less-dramatic turnover intervals. One of these is based solely on sporomorph assemblages in the lower Passaic Formation and appears middle Norian in age. The other involves the last appearance of a footprint taxon attributed to nondinosaurian dinosauromorphs close to the projected Rhaetian-Norian boundary (Appendix Note 4). Both are minor compared with the Newark ETE, and are consistent with data from other CAM basins (Olsen et al., 2002).

Critical to the assessment of the relationship between the PGE (and other geochemical) anomalies and the ETE are repeated and persistent assertions that there is a major hiatus or dramatic accumulation rate drop in pre-CAMP strata of CAM basins (e.g., Van Veen, 1995; Kozur & Weems, 2007, 2010; Tanner & Lucas, 2015). Based on biostratigrapic data of sporomorphs and clam shrimp (the spinocaudatan *Shipingia*), and lacking empirical evidence of an erosional surface or surface of nondeposition, this hiatus has been asserted to span nearly the entire Rhaetain, a duration of nearly five million years. Were this the case, the meaning of the evidence for mass extinction and the significance of the PGE and other geochemical data we describe here would be entirely different.

Although the biostratigraphic interpretation for such a hiatus can be questioned on its own merits (Appendix Note 5), CA-ID-TIMS zircon U-Pb dates and paleomagnetic polarity stratigraphy from the Chinle Formation of the western United States, combined with that of the Newark and Fundy basins (Kent et al., 2018; Olsen et al., 2019a), falsify the hypothesized presence of this hiatus. Such a gap is also difficult to understand in light of the consistent position of the oldest CAMP basalts relative to the underlying magnetic polarity reversal sequence (Olsen et al., 2016b).

Four conclusions can be drawn from the faunal, floral, and related stratigraphic and geochronological data from these CAM basins: (1) the biotic transition, the base of the continental ETE, is in a consistent position relative to the high-resolution paleomagnetic polarity record across eastern North America and Morocco; (2) there is no discernable hiatus at this biotic event; (3) it is the largest magnitude shift in the fauna and flora in the basins; and (4) although the base of the interval of last appearances is dramatic, some evidence suggests that the transition was spatially complex and diachronous for 50 to100 ky through the older basalt flows to the top of the "upper basalt formation," as extrapolated from dates in Blackburn et al. (2013) and the astrochronology in Olsen et al. (2019a) (Appendix Note 6).

12.3. METHODS

Channel samples (continuous and contiguous samples spanning intervals) were collected from outcrop successions for PGE, stable carbon isotope, and sporomorph analysis. Data are depicted by the sample midpoint to facilitate comparison with published data. Geographic coordinates are given in decimal latitude and longitude with the WGS84 datum.

Samples were cleaned with deionized water, broken into mm-scale fragments in a jaw crusher with porcelain plates, and subsampled. For chemical analysis, the samples were ground to rock flour in an agate mortar and pestle.

For the Newark and Central High Atlas basin samples, PGE and Au concentrations (Ir, Ru, Rh, Pt, Pd, Au) were determined by ICP-MS after NiS preconcentration (NiS fire assay method) at the Geoscience Laboratories of the Ontario Geological Survey (Sudbury, Canada) (Richardson & Burnham, 2002) in 2008 and 2014 (Appendix 12.2) with results reported in ng/g. Detection limits are: Ir = 0.01 ng/g; Au = 0.71 ng/g; Pd = 0.12 ng/g; Pt = 0.17 ng/g; Rh = 0.02 ng/g; and Ru = 0.08 ng/g. Precision is 0.02 ng/g (Tanner & Kyte, 2005). Results on the same samples using neutron activation and NiS fire assay and ICP-MS are similar (Tanner & Kyte, 2005). For comparison with extraterrestrial materials, PGE concentrations were normalized to CI Chondrite of Lodders and Fegley (1998).

The bulk organic matter of sediment was analyzed to determine the ratio of $^{13}C/^{12}C$ by mass spectrometry with results expressed using the delta notation as ‰ $\delta^{13}C_{org}$. Precautions used to prevent sample cross contamination included rinsing equipment with high-purity acetone, methanol, and dichloromethane between samples. Powdered samples were placed in a 15 ml centrifuge tube. 10 ml of 10% HCl was added and agitated with a vortex mixer and placed in a 60°C water bath for 24 hours to ensure complete dissolution of carbonates. The acidic slurry was diluted with distilled, deionized (DDI) water, centrifuged, and decanted until a neutral solute *p*H was achieved (verified by litmus paper test). Once dried, residues were weighed into clean tin capsules (20–60 mg) on a Sartorius ME5 microbalance based on their TOC content and analyzed in the IRMS facility at University of

Southampton on an Isoprime VisION continuous flow isotope ratio mass spectrometer (IRMS) with an Elementar PYRO Cube Elemental Analyzer running in CNS mode and equipped with a TCD (thermal conductivity detector). Acetanilide and sulfanilamide were the elemental standards for C, and USGS40 and USGS41 were used as international reference materials for the normalization of the isotope ratios. Precision of the analytical system is 0.12‰ (1σ) for C at the typical sample sizes (4 μm C) used here.

12.4. STUDIED SECTIONS AND PREVIOUS PGE WORK

12.4.1. Eastern North America

Newark Basin

The Newark Basin section provided the first sedimentary measurements of PGEs (IR) (Olsen et al., 2002). The cyclical lacustrine and marginal lacustrine part of the section spans the upper Stockton, Lockatong, and Passaic formations of Norian to Rhaetian age and overlying CAMP lava-bearing sequence of latest Rhaetian through Hettangian age. As previously described, the Newark Basin section is the most extensively studied of the CAM basins with a well-developed astronomically tuned cyclostratigraphy, magnetostratigraphic polarity stratigraphy, and zircon U-Pb geochronology.

Exeter (Constitution Avenue) Section (40.313247°, -75.843174°) Deposited at about 20° N in the latest Triassic (Kent & Tauxe, 2005), the cyclical lacustrine section in the Jacksonwald Syncline in the southwestern part of the basin was intensely studied during housing construction in the 1970s though 1990s. Olsen et al. (2002a) analyzed four stratigraphically equivalent but thin (<1 m) sections spanning 1.3 km along strike (Appendix Note 7) to test the possibility that the Ir anomaly was lithologically controlled. Neutron activation was used for Ir and thus other PGEs were not measured. Because of the rich paleontological material, we added stratigraphic scope in this area by analyzing over 30 m of section for PGEs using NiS-ICP-MS as well as carbon isotopes and placed it in context with core and other outcrops that produce relevant fossils (Appendix Notes 7, 8, 9) (Fig. 12.2a).

Hartford Basin

Lacustrine strata of the Hartford Basin span the uppermost New Haven Formation of Late Triassic age, which is otherwise fluvial, through the middle Portland Formation of Sinemurian age (Fig. 12.1) deposited at ~21° N during CAMP (Kent & Tauxe, 2005). These strata are well characterized from outcrop study (e.g., Hubert et al., 1976) and extensive coring for geotechnical purposes (Whiteside et al., 2011; Steinen et al., 2015). The stratigraphy down to the fine-scale, sub-orbital level is remarkably similar to contemporaneous sequences in the Newark Basin. The ETE transition is poorly understood in this basin because of a dearth of Triassic aspect forms. The oldest relevant fossil floral assemblages are just below the Talcott Formation (i.e., the oldest CAMP flows in the basin). Although of pos-tinitial ETE aspect, these floral assemblages are consistent in pattern with the Newark Basin.

Holyoke Clathropteris *Locality (42.217205°, -72.662327°)* A small, stratigraphically isolated set of exposures along Southampton Road in Holyoke, Massachusetts, have produced the best-preserved examples of *Clathropteris meniscoides* in the Newark Supergroup (Cornet, 1977; Cornet & Traverse, 1975), an Ir anomaly of similar magnitude (Tanner & Kyte, 2016) to that at the fern spike in the Jacksonwald Syncline (Exeter) section, and in a succession with a similar sedimentology (Olsen et al., 2003c) (Appendix Note 10).

Although there are strong biotic, lithologic, and stratigraphic similarities between the *Clathropteris* locality and the Exeter section, there is no independent verification that this section represents the same fern spike, apart from the PGE anomaly. Due to stratigraphic isolation, there is furthermore no direct evidence from palynology, tetrapod footprints, or magnetostratigraphy bearing on the relationship to the biotic turnover seen in the Newark Basin. No $\delta^{13}C_{org}$ analyses were conducted on this outcrop because of the generally coarse-grained and weathered nature of the exposures. There are no other similar sequences known from the entire Hartford Basin. No taxa limited to the Triassic (e.g., *Patinasporites*) have been identified.

Silver Ridge Cores and Exposures, Berlin, Conn. The Silver Ridge B-2 (41.584217°, -72.760783°) and B-3 (41.583500°, -72.760917°) cores were drilled in 2002 (Olsen et al., 2003c, 2005) (Fig. 12.2). The cores sample the lower Talcott Formation, homotaxial with and chemically similar to the Orange Mountain Basalt of the Newark Basin, and the upper New Haven Formation, homotaxial to the uppermost Passaic Formation of the Newark Basin. The cores have sedimentary sections that plausibly overlap the Exeter section (Fig. 12.2). Core B-2 is the more extensive, sampling 44.5 m (146 ft) of Talcott Formation and 58.8 m (193 ft) of New Haven Formation. In contrast, Core B-3 has 1 m (3.3 ft) of Talcott Formation and 3.6 m (11.7 ft) of New Haven Formation. A thin layer of volcaniclastics is present ~10 cm below the contact with the Talcott Formation in the B-2 core at 156.8 ft (47.8 m). This ~1 cm interval has abundant small lithic

fragments (~1 mm), consisting of euhedral plagioclase laths in a groundmass of smaller feldspar crystals and chalcedony (Fig. 12.2c), with carbonate occurring around many of the euhedral feldspar crystals. The petrology suggests a trachyte or rhyolite rather than a basalt (Philpotts in Olsen et al., 2016a). We examined 3.4 m of lacustrine strata from the uppermost New Haven Formation in Silver Ridge B-2 to test the generality of the palynological and carbon isotopic pattern seen in the Newark Basin (Fig. 12.2b) (Appendix Note 11).

Cinque Quarry (approx. 41.299167°, -72.863611°) A section exposed in the Cinque Quarry in East Haven, Connecticut, reveals the uppermost New Haven Formation and overlying pillowed base of the Talcott basalt (Heilman, 1987). Here, the uppermost 40 cm of the New Haven Formation is grey (Fig. 12.2b) mudstone with abundant *Brachyphyllum* shoots and cones and a palynoflorule by *Classopollis* (Heilman, 1987) in the topmost few centimeters.

Fundy Basin

Sections in the Fundy Basin (see Figs. 12.1,12.4,12.6) have well-studied sporomorph assemblages below the CAMP (North Mountain) basalt (Fowell & Traverse, 1995; Cirilli et al., 2009), paleomagnetic polarity chron E23r (Deenen et al., 2011), and a well-characterized vertebrate assemblage directly above the basalt described by Olsen et al. (1987), Sues and Olsen (2015), and Fedak et al. (2015).

The key sections for PGE anomalies are Partridge Island and Central Clarence, Nova Scotia (see Figs. 12.4, 12.6) in the Partridge Island Member (Sues & Olsen, 2015), the uppermost division of the Blomidon Formation. Deposited at about 26° N (Kent & Tauxe, 2005), these sections consist of a thin (<10 m) sequence of variegated strata remarkably similar to the strata below the oldest CAMP basalts in Morocco. Facies bearing pollen and spores indistinguishable from the type section extend >460 km^2 (Olsen & Et-Touhami, 2008). It is not a local unit as asserted by Kozur and Weems (2010) (see the seven sections shown in Sues & Olsen, 2015). However, at some localities, such as due east of "The Old Wife" basalt pinnacle in Five Islands Provincial Park (45.389365°, -64.061596°), the overlying North Mountain Basalt metamorphosed strata of this unit (Sues & Olsen, 2015). As is the case for the Moroccan facies, there is abundant evidence for the role of salt dissolution in the Partridge Island Member (see below).

Partridge Island (45.369246°, -64.336145°) The second of the CAM basin sections that yielded PGE anomalies (0.20–0.23 ng/g (NiS ICP-MS) and 0.240–0.310 ng/g (NA) from Tanner & Kyte, 2005; and 0.273–0.449 (NA) from Tanner et al., 2008) was at Partridge Island (see Fig. 12.4b). Sporomorph assemblages recovered from three sampling efforts (Fowell & Traverse, 1995; Whiteside et al., 2007; Cirilli et al., 2009) produced identical results. Preservation was good (except in red strata), although the grains were dark, *Circumpolles* group species dominated (e.g., *Classopollis* spp.), and the stratigraphically highest samples consistently lack vesicate forms (e.g., *Patinasporites densus*). The latter pattern mirrors that seen in the Newark Basin section below the Orange Mountain Basalt.

Central Clarence, Nova Scotia (44.909208°, -65.217383°) Orth et al. (1990; republished by Mossman et al., 1998) report a sample with 0.150 ng/g Ir (Instrumental Neutron Activation Analysis) that "scarcely constitutes an anomaly" ~30 cm beneath the North Mountain Basalt (see Fig. 12.6b) in the Partridge Island Member. This member is unusually thick at this location (about 4 m) and coarse, consisting of white sandstone and pink and pale-grey to cream-colored mudstone. The only macroflora-producing locality in the Blomidon Formation, the fossils are almost entirely of the filicalean fern *Cladophlebis* (Baird, 1972; Olsen & Et-Touhami, 2008). Bracketing this fern-bearing unit are thinly bedded strata that contain abundant halite hoppers. Apparent metamorphism or intense weathering has removed most of the organic matter from these beds, although some pollen that is too fragile to be recovered, can still be found in residues following treatment with hydrofluoric acid (Sues & Olsen, 2015). Here, a biotite-bearing, apparent ash bed produced a K-Ar age of 195 ± 4 Ma (Armstrong & Besancon, 1970).

Red Head, Nova Sciotia (near 45.389365°, -64.061596°) Orth et al. (1990; republished by Mossman et al., 1998) also reported a 0.200 ng/g anomaly in the metamorphosed Partridge Island Member 2 m below the North Mountain Basalt at Red Head, Five Islands Provincial Park (approximately 45.389320°, -64.058948°). However, this value is only twice the detection limit for the combined NiS fire assay and ICP-MS method that was used.

12.4.2. Morocco

The lithology and stratigraphy of the Moroccan and Fundy basins (at 24°–25° N subtropical latitudes during CAMP emplacement; Kent & Tauxe, 2005; Olsen & Et-Touhami, 2008) are similar to each other (Fig. 12.1) but quite distinct from the more paleotropical Hartford and Newark basins. While the strata intercalated with CAMP flows are predominately lacustrine or marginal lacustrine, contemporaneous strata in the higher latitudes have

much lower accumulation rates, abundant evaporitic facies, particularly sand patch massive mudstones (Smoot & Olsen, 1988) that formed from trapped grains in evaporitic efflorescent crusts (Appendix Note 12) .

A distinct facies associated with the strata directly below the oldest flows in Morocco is closely comparable to the Partridge Island Member of the Fundy Basin and consists of decimeter-scale, predominantly clastic interbeds of red, grey, black, and white mudstones, some of which can be carbonate rich, with common evaporite pseudomorphs. Alternation of thin beds of such dramatically contrasting color is unusual in the CAM basins. These beds are variable in thickness over short distances, forming meter-scale salt dissolution and growth structures with indistinct boundaries. They contrast with the underlying, exclusively red clastic rocks bounded by the basalt, and differ from the strata between flows, which often have distinct carbonate sequences. In the Khémisset Basin, these variegated strata below the basalt pass down-dip into a thick sequence of similarly variegated halite and potash (Olsen et al., 2003a) (see below).

Argana Basin

We examined sections at the West Argana and Igounan (see Figs. 12.1, 12.4) areas within the Argana Basin. Although samples have not been processed for PGEs, the sections have produced substantial paleontological, magnetostratigraphic, and chemostratigraphic data relating to correlative strata with PGE data in the Central High Atlas and the Fundy Basin. The sections illustrate lateral changes in both thickness and facies, related to various degrees of halite dissolution. They are characterized by thin (<4 m) sequences of variegated mudstones (red, grey, and black) that are often palyniferous.

West Argana, Morocco (30.773482°, -9.151919°) Whiteside et al. (2007) and Deenen et al. (2010) studied two geographically close sections with similar stratigraphies (Appendix Note 13) in the uppermost Bigoudine Formation overlain by the Tasguint Formation of the Argana basalts (El Hachimi et al., 2011). Deenen et al. (2010) identified a very thin (<2 m) zone of reverse polarity within the uppermost few meters of Bigoudine Formation, correlative to E23r in the Newark Basin (see Fig. 12.4a). The sporomorph biostratigraphy also appears similar between the two sections, with the last appearance of *Patinasporites* occurring in the same nonfossiliferous grey bed and limited to the Triassic above this level. However, Marzoli et al. (2004) reported the last appearance of *Patinasporites* higher at two localities, Alemzi (<5 cm below the basalt) and Aguerouine (20 cm below the basalt) (Appendix Note 14). The dark color and poor preservation of the sporomorphs limits the usefulness of the lateral correlations (Deenen et al., 2010), and the thermal effects of the overlying basalt may have preferentially destroyed the more fragile *Patinasporites* in the uppermost layers at the Whiteside/Deenen sites, while better preservation and lighter grains characterize the Marzoli sites, suggesting less thermal effects. In a more northern locality (30.818159°, -9.150383°), the thermal effects are visible in that there is no palynomorph recovery and the section is discolored several meters below the basalt (see section 12, Discussion).

Igounane (30.803220°, -9.152590°) A series of outcrops north of the village of Igouane, about 3.4 km north of the West Argana localities of Whiteside et al. (2007) and Deenen et al. (2010), reveals the rapid lateral change in beds along strike that we interpret as related to salt dissolution in the beds in the uppermost Bigoudine Formation just below the Tasguint Formation basalt flows. Percival et al. (2017) describe the northernmost (Site I1) of three sections (see Fig. 12.4a) and provide mercury (Hg) concentrations as a tracer of volcanic Hg gas. Concentrations are low (<0.015 ng/g) except for three modest anomalies between 0.030 and 0.035 ng/g in the uppermost 1 m of sedimentary strata, each associated with a thin black mudstone or carbonate. However, the other dark mudstones do not contain enriched Hg concentrations. Although this section is similar in thickness and pattern to those at West Argana, two locations < 200 m south (I2, I4) have profound differences (see Fig. 12.4). Site I2 has a well-developed salt dissolution "bowl" identical to ones in the Blomidon Formation (Olsen & Touhami, Fig. 67, 2008). Superficially resembling channels, they are easily differentiated from them because the infill does not cut into older layers; rather the older layers are warped downward below the bowl and growth features often indicate greater accommodation space. More subtle salt dissolution features might cause the lateral discrepancy between sections. Thick halite sequences underlay the basal basalts in the subsurface Agadir-Essaouira Basin (Mader et al., 2017; Echarfaoui et al., 2002) to which the Argana Basin is attached and composes its up-dip, exposed portion.

Despite the differences between outcrop sections in the Argana Basin, there is a general pattern of an upper cluster of irregular, thin (2–30 cm) red, grey, black, white, and variegated beds and a lower cluster of three grey to black mudstone beds interbedded with red strata (see Fig. 12.4). This general stratigraphy is consistent for >3.5 km and allows the data from Whiteside et al. (2007), Deenen et al. (2011), and Percival et al. (2017) to be viewed in a common stratigraphic context. Within this reference frame, the Hg relative peaks all fall above chron E23r.

Khémisset Basin

The Khémisset Basin is located ~400 km to the northeast of the Argana Basin (see Figs. 12.1, 12.5). Unlike other Moroccan sections described here, there is subsurface information relating the outcrops to stratigraphy at depth, particularly the facies just below the oldest basalts in the Moroccan and Fundy basins, which is important because it places the stratigraphy of these sections into a larger facies context of salt basins and rampant penecontemporaneous dissolution that would otherwise not be apparent. Salt tectonics explains both the abrupt lateral changes in facies and thicknesses of units resulting in apparent discrepancies between different sections measured by various workers, or even the same worker, even when sections are only meters away from each other.

The Khémisset Basin section (see Fig. 12.5a) consists of correlatives of only the youngest strata seen in the Argana and Central High Atlas basins. The basal formation is the "lower clay formation," which looks virtually identical to the upper Bigoudine Formation of the Argana Basin, overlain by basalt flows of "lower basalt" and "intermediate basalt" chemistries (Panfili et al., 2019). In outcrop (see Fig. 12.4c,d), the uppermost "lower clay formation" is a 2 m thick palyniferous interval of red, grey, and black mudstone very similar to the Partridge Island Member of the Fundy Basin. In the subsurface, however, the 2 m variegated unit member passes laterally into >100 m of bedded salt (halite and potash salt; see Fig. 12.5a,b), which is similarly variegated (Et-Touhami, 2000), including the black layers. Likewise, the lower "upper clay formation" passes laterally into >500 m of salt, cyclically interbedded with thin red mudstones, followed upward by red gypsiferous mudstone. The same relationship is present between outcrops of the Berrechid Basin (~100 km west of the Khémisset Basin) (Appendix Note 15). The simplest hypothesis is that the halite was dissolved syndepositionally in small increments in shallower parts of the basin, leaving the residuum of variegated mudstone beds in outcrop.

Nif El Gour (33.647444°, -6.405790°) This section reveals the lower clay formation and the overlying basalt units as well as a thin interbedded dark grey carbonate and mudstone sequence (Appendix Note 16). We examined the upper 3 m of the lower clay formation for sporomorphs to test the pattern of last occurrences below the basalt sequence.

Central High Atlas

The High Atlas Basin is a loosely defined complex of deformed Late Permian to Early Jurassic strata that crop out in the High Atlas Mountains (see Fig. 12.4) (Appendix Note 17). The boundaries of the depositional basin or basins have not been fully delimited because of alpine and halokinetic deformation of younger sedimentary cover and erosion, although multiple, often fault-bound, depocenters have been defined (e.g., Mattis, 1977; Beauchamp et al., 1996). The eastern part of the Central High Atlas region is characterized by well-developed halokinetic structures developed by Late Triassic salt that are sometimes invaded by Middle Jurassic igneous intrusions, influencing sedimentation (Bensalah et al., 2013; Saura et al., 2014; Mártin-Mártin et al., 2017).

Sidi Rahal (31.595557°, -7.427255°) Outcrops along the north side of the anticline, south of Sidi Rahal in the northern depositional basin (as defined by Mattis, 1977) in the western part of Central High Atlas, display the stratigraphy of the upper parts of the pre-CAMP sedimentary section (T6 formation of Mattis, 1977; Appendix Note 17) and overlying basalts, interbedded and overlying sedimentary strata (Whiteside et al., 2007, 2008). This site was first sampled in September 2003 and has substantially deteriorated since then by slumping (see Fig. 12.5). The uppermost red mudstone unit below the basalts (T6) is similar in aspect to strata immediately below the basalts in Morocco (and the Fundy Basin), except at this section the strata are fine grained, consisting of 1.2 m of variegated white, grey, black, and red unconsolidated claystone and siltstone (see Fig. 12.6a).

As with the Argana and Khémisset sections, we argue that the thin variegated beds within a few meters of the basalt are a residuum of clastic material in an evaporitic environment with substantial penecontemporaneous salt dissolution that account for significant lateral thickness and facies changes and make detailed comparisons among sections at different localities difficult. The rest of the visible portion of the T6 formation shows little distinct bedding and mined zones of brecciated red mudstone in red halite matrix outcrop in the valley <1 km to the south in T6 (at 31.587250°, -7.424067°) (see Fig. 12.5e,f) and halite diapirism is prominent in contiguous strata in the High Atlas Basin to the northeast (Saura et al., 2014; Mártin-Mártin et al., 2017). It is possible that these salt features reflect fully exhumed salt structures.

Other Central High Atlas Localities Dal Corso et al. (2014) described two sections with $\delta^{13}C_{org}$ and mineralogical data that have the same style of variegated beds as our Sidi Rahal section (Appendix Note 18): the Oued Lahr section, at 31.612500°, -7.381389°; and the Tiourjdal section, at 31.129000°, -7.378333. Lithology, especially color, is not reported in sufficient detail to make comparisons with the other sections discussed here.

The Oued Lahr section is only ~4.9 km north, northeast of our Sidi Rahal section, but it appears truncated by a basalt breccia of unknown origin. The apparently more expanded Tiourjdal section is 52 km south, on the other side of the Atlas Mountains, and has a similar facies and $\delta^{13}C$ stratigraphy (see Fig. 12.7).

12.5. RESULTS

We provide new PGE data relevant to the paleontological, palynological, and carbon isotopic data from sections in the Newark, Hartford, and Fundy basins of eastern North America and the Argana, Khémisset, and Central High Atlas basins of Morocco. These new results are described in context with previously published data relevant to interpreting the PGE and carbon isotopic anomalies.

12.5.1. Newark Basin

For Jacksonwald Syncline, we analyzed 55 samples for PGEs and Au and 60 samples for $\delta^{13}C_{org}$ from the uppermost 30 m of the Passaic Formation at the Exeter section in the Jacksonwald area (Appendix Table 12.A1). This is approximately the same exposure as section II of Olsen et al (2002) and sections 5 and 6 of Fowell et al. (1994)'s study on sporomorphs (Fig. 12.2a).

Our data reveal that the ~30 m section below the Orange Mountain Basalt have at least three PGE anomalies (at 0.95, ~17.17, and 19.12 m), only one of which is associated with a distinct biotic change (~17.17 m) (Fig. 12.2). Although four geographically disparate sites produced a distinct Ir anomaly in the same stratigraphic position in the neutron activation data (Olsen et al., 2002), an anomaly was not detected in the same position (at ~17.17 m) in our new NiS Fire Assay data (Fig. 12.2), while two other anomalies were detected (Fig. 12.2). The failure to find the 2002 anomaly could be because a small undetected bedding plane fault cut it out or because of detection interference with the very high organic content of the bed (~50%) (cf. method reports by Richardson & Burnham, 2002).

All three peaks in Ir concentrations are at or adjacent to the most negative $\delta^{13}C_{org}$ values in the section and two of these are associated with high TOC values (Fig. 12.2), although there is no significant linear correlation among any of these variables, even excluding the ~50% TOC sample (Figs. 12.2 and 12.3a,g,h).

The fern spore spike occurs at the level of the 2002 Ir anomaly within a coaly unit and white claystone (Figs. 12.1 and 12.2) directly above the last occurrence of *Patinasporites densus*. The other two Ir anomalies occur in association with unremarkable sporomorph fluctuations. The dominant spore taxon present in the spore spike is *Granulatisporites infirmis*, produced by the dipteridaceous fern *Clathropteris menicoides* (Cornet & Traverse, 1975, see below). Distinctive fragments of *Clathropteris menicoides* occur in the sandstone unit overlying the fern spike and a rhizome mat of this fern composes the coaly layer at this locality. Strata above this horizon have produced no *Patinasporites* or vesicate taxa at this section (Fig. 12.2a) or in any other Newark Basin stratigraphic equivalent.

The lowest Ir anomaly at 0.95 m occurs at the base of E23r in a dark grey clayey siltstone dominated by *Patinasporites densus* (Fowell et al., 1994), conifer shoots, and *Shipingia olseni* (Fig. 12.2), which can be correlated in detail with other sections in the basin (Appendix Notes 7, 8).

12.5.2. Hartford Basin

Silver Ridge Core B-2 and Exposures, Berlin, Conn.

Sporomorphs were recovered in grey mudstones and siltstones between 157.7 and 159.5 ft in the Silver Ridge core B-2 (Fig. 12.2b). The lowermost productive sample at 159.5 ft produced predominantly *Pilasporites* sp. (horsetail) spores, with one *Deltoidspora* sp. and one *Classopollis meyerania*. Samples at 158.6, 157.9, and 157.7 ft were strongly dominated by *Classopollis meyerania*, with less common *Alisporites* sp. (158.6 ft) and *Pilasporites* (157.9 ft). Pollen appears thermally mature (dark), but preservation is good. Typical Triassic taxa (e.g., *Patinasporites*) are absent. All of the samples have woody debris and leaf cuticle.

Twenty-one rock samples from this grey interval, two wood samples, and one basalt sample were processed for TOC (Fig. 12.2b). Among the sedimentary rock samples, a broad range of $\delta^{13}C_{org}$ values between -28 and −18‰ plausibly reflects different carbon sources (see section 12.7 Discussion and Appendix 12.2). The sample at 159.9 ft, however, has a strikingly ^{13}C-depleted value (33.1‰) that could be due to hydrocarbons (see section 12.7 Discussion). The basalt sample from the base of the Talcott Formation has a $\delta^{13}C_{org}$ value of −27.6‰, again suggesting the presence of hydrocarbons.

No PGE data exist for the B-2 cores, however a ~1 m exposure of uppermost New Haven Formation ~169 m northwest of the B-2 core on the east side of CT Route 15 did not contain an Ir enrichment (Tanner & Kyte, 2016). Plant macrofossil fragments are present throughout the grey beds in core B-2 and shoots of *Brachyphyllum* sp. similar to those at Woodland Park in the Newark Basin (see Fig. 12.7) and at the Cinque Quarry (see below) have been recovered in weathered siltstones from this exposure equivalent to the uppermost few tens of centimeters of core B-2 (Fig. 12.2).

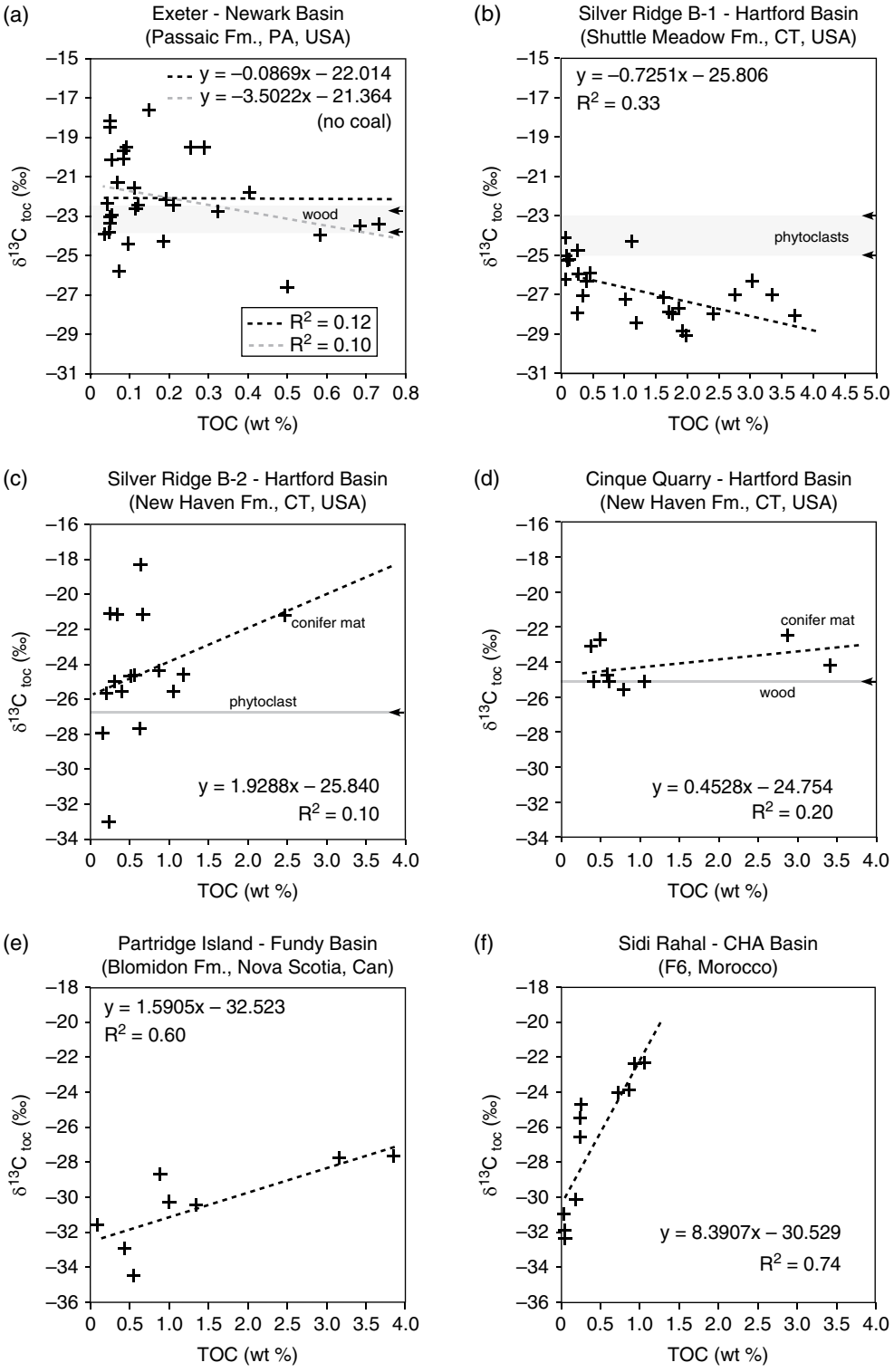

Figure 12.3 (a–f) Correlations between $\delta^{13}C_{org}$ and total organic carbon (TOC) for the sites described here for gray and black strata only). In (a) and (b) (Exeter and Silver Ridge core B-1), grey bars (with arrows indicating each datum) indicate range of $\delta^{13}C_{org}$ values from wood or other phytoclasts (reported in Spiker et al., 1988, for (d)). In (a), nc = the coaly layer with a 50.2% TOC that is omitted from this correlation and graph. Data in (b) from Whiteside et al. (2011). Note weakly negative relationship between $\delta^{13}C_{org}$ in (a) and (b), which are cyclical lacustrine sequences (upper Passaic and lower Shuttle Meadow formations) in contrast to the positive relationship seen in (e) and (f) (Partridge Island, Fundy Basin and Sidi Rahal, Central High Atlas Basin) in which the organic-poor samples are interpreted to be dominated by migrated hydrocarbons as opposed to indigenous organic remains (e.g., woody material and kerogen), both within 2 m of overlying basalts. (c) and (d) (Silver Ridge B-2 core and the Cinque Quarry) show similar but much weaker positive relationships, both in the Hartford Basin below the Talcott Formation lava flows. (g–j) Lack of correlation between TOC or $\delta^{13}C_{org}$ and Ir (black) alone or Ir + Pd + Pt (red) at the Exeter and Sidi Rahal sections. In (g) no coal = the coaly layer with a 50.2% TOC that is omitted from this correlation and graph.

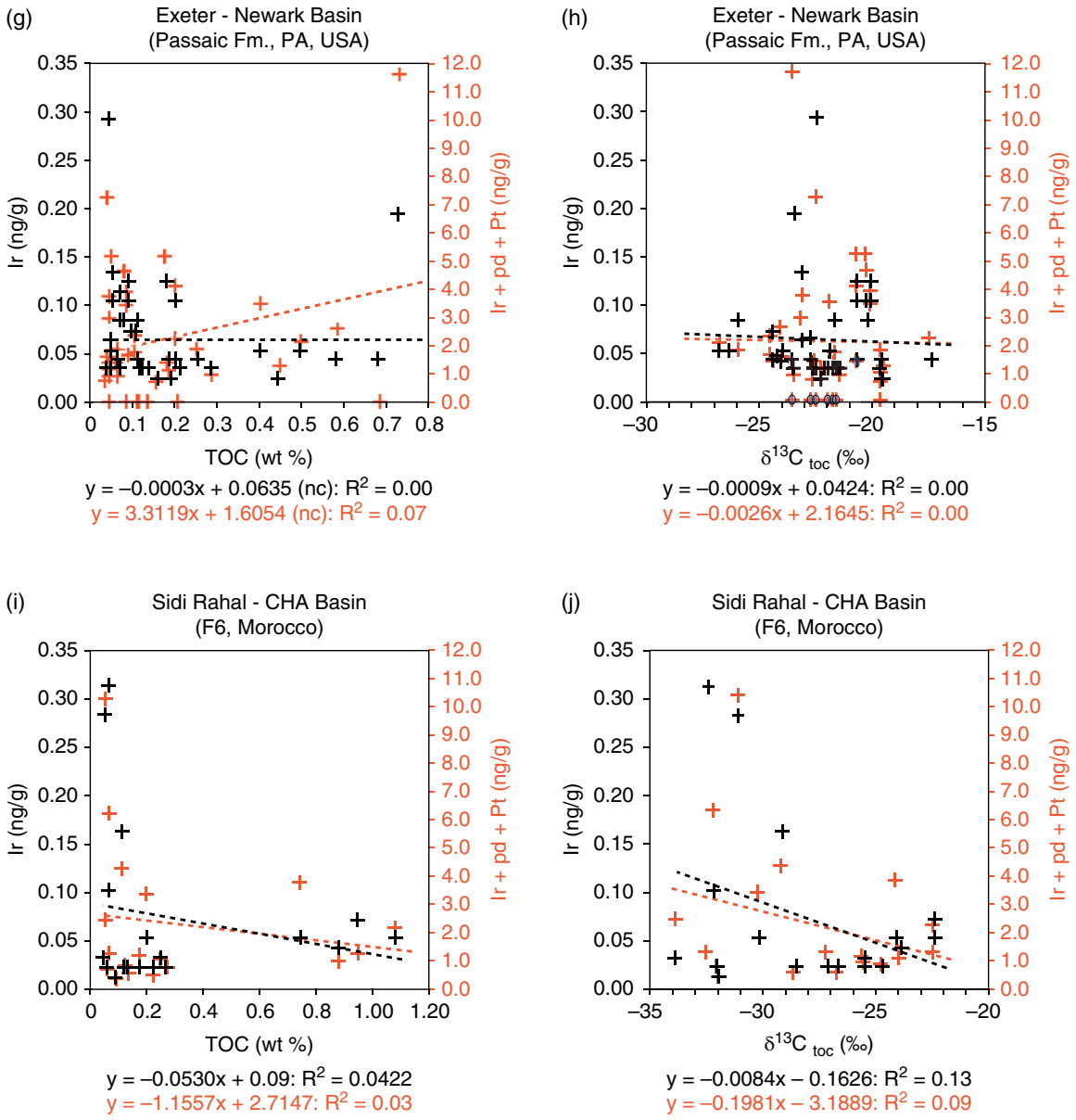

Figure 12.3 (Continued)

Cinque Quarry (approx. 41.299167°, -72.863611°)

For $\delta^{13}C_{org}$, we processed nine samples of rock, including one with a mat of *Brachyphyllum* and another with an upright stem in the basalt pillows, close to the base of the Talcott Formation basalt. The highest TOC measurements for sediment were in the mat layer and overlying interpillow sediment. The woody stem had a TOC of 42% (not shown in Fig. 12.2b). In our analysis, only the highest sample (08/15/00) directly beneath the Talcott basalt produced palynomorphs. The layer contains abundant shoots of *Brachyphyllum* cf. *B. scottii*. The palynoflora is strongly dominated by *Corollina meyeriana*, and abundant cuticle is present. Preservation is surprisingly good for a sample so close to pillow basalts. This section has not been analyzed for PGEs, but demonstrates the widespread (though not ubiquitous) occurrence of a lacustrine to marginal lacustrine environment in the Hartford Basin prior to deposition of the Talcott basalt in which floras of postinitial ETE aspect occur (see section 12.7 Discussion).

12.5.3. Fundy Basin

Partridge Island (45.369246°, -64.336145°)

For a $\delta^{13}C_{org}$ profile, 45 contiguous channel samples were processed with 13 in duplicate (Fig. 12.4b). This profile allows the relationship of TOC and $\delta^{13}C_{org}$ to be analyzed (Fig. 12.3e) and permits registry of the paleomagnetic polarity stratigraphy of Deenen et al. (2011), including chron E23r (Fig. 12.4), to the mercury data of Percival (2014), which were derived from the same samples as the carbon isotope data, as well as the PGE data of Tanner and Kyte (2005) and Tanner et al. (2008). As in the case with the Sidi Rahal and Tiourjdal $\delta^{13}C_{org}$ profiles, the samples closest to the basalt are the most ^{13}C-depleted and TOC and $\delta^{13}C_{org}$ correlate, with lower TOC values having the most ^{12}C-enriched values (Figs. 12.3e and 12.4b). As in the Newark Basin, the last appearance of *Patinasporites densus*, and sporomorph transition in general, occurs within E24n. *Patinasporites densus* is not known above this level in the Fundy Basin, although another sporomorph form genus, *Lunatisporites* spp., thought to have its last appearance at or close to the ETE, is known ~1 m above the North Mountain Basalt from the basal McCoy Brook Formation at Scots Bay (Cirilli et al., 2009). We correlated our results to the sporomorph data of Fowell and Traverse (1995) (Appendix Note 19). Whiteside et al. (2007) and Cirilli et al. (2009) using a common depth scale (Fig. 12.4b), showing that the pollen data are reproducible, notably the last occurrence of *Patinasporites densus*.

12.5.4. Morocco

Nif El Gour (33.647444°, -6.405790°)

Well-preserved *Patinasporites densus* and *Ovalipollis ovalis* occur in the youngest palyniferous sample that is also in contact with the overlying basalt (Fig. 12.5c,d), as well as in lower samples, consistent with Marzoli et al. (2004) who indicated that, where pollen and spores are well preserved, Triassic-aspect taxa occur in the youngest sedimentary strata below the basalts. This is a distinctly different pattern than that seen in the Newark, Hartford, and Fundy basins where strata lacking *Patinasporites* are consistently present just below the oldest basalts.

Sidi Rahal (31.595557°, -7.427255°)

Eighteen samples were processed for pollen, $\delta^{13}C_{org}$, and PGEs. The uppermost four samples had varying contributions of basaltic debris with the uppermost sample consisting of basaltic rubble. Given the unconsolidated yet unweathered nature of the underlying units, it is unclear if this material represents Triassic volcaniclastics, tectonized basalt at the contact, or broken up basalt along a modern slip surface.

Two modest PGE anomalies are evident: the lowest and largest have marked chondritic ratios (Fig. 12.6). There is no apparent correlation between TOC or $\delta^{13}C_{org}$ and PGE concentrations ($R^2 < 0.13$) (Fig. 12.3j) or similarity in concentration patterns (Fig. 12.6a). There is

Figure 12.4 Sections from the Argana (Morocco) and Fundy (Eastern Canada) basins. (a) Argana Basin sections. Locations: a2, Argana West from Deenen et al. (2011) (30.771707°, -9.152153°); a1, Argana West from Whiteside et al. (2007) (30.773482°, -9.151919°); I4, Igounane (30.801646°, -9.153156°); I2, Igounane (30.802093°, -9.152680°); I1, Igounane from Percival et al. (2017) (30.803220°, -9.152590°). Levels for *Patinasporites densus* (includes *Enzonalisporites*) are from d, Deenen et al. (2011); m, projected onto this section from Marzoli et al. (2004); w, Whiteside et al. (2007). (b) Partridge Island section in Fundy Basin; all sections are within 20 m of each other on the same outcrop. Sporomorph taxa are as follows: Fowell and Traverse (1994) (abundance data not provided): a, *Corollina meyeriana*; b, *Corollina torosa,* c, *Corollina murphyae,* d, *Corollina simplex,* e, *Dictyophyllidites harrisii*; f, *Spheripollenites* sp.; g, *Microreticulatisporites fuscus*; h, *Converrucosisporites cameronii*; i, *Carnisporites spiniger*; j, *Patinasporites densus*; k, *Alisporites parvus*; l, *Alisporites tenuicorpus*; m, *Klausipollenites gouldii*; n, *Parvisaccites triassicus*; o, *Densoisporites velatus*; p, *Cycadopites follicularis*; q, *Cycadopites tattoo*; r, *Cycadopites ginker*; s, *Cycadopites schlischii*; t, *Vitreisporites pallidus*; u, *Ovalipollis septimus*; v, *Cycadopites andrewsii*; w, *Granulatisporites infirmus*; x, *Calamospora mesozoica*; y, *Obtusisporis* sp.; z, *Indusiisporites parvisaccatus*. Whiteside et al. (2007): a, *Cycadopites follicularis*; b, *Klausipollenites gouldii*; c, *Vitreisporites palidus*; d, *Alisporites parvus*; e, *Patinasporites densus*; f, *Carnisporites* cf. *spiniger*; g, cf. *Dictyophyllidites*; h, *Cycadopites* cf. *ginker*; i, *Corollina* cf. *murphae*; j, *Corollina simplex*; k, *Corollina torosa*; l, *Corollina meyeriana*. Cirilli et al., 2009: a, *Desoisporites* sp.; b, *Ovalipollis septimus*; c, *Patinasporites densus*; d, *Converrucosisporites cameroni*; e, *Dictyophyllidites harrisii*; f, *Dictyophyllidites* sp.; g, *Spheripollinites* sp.; h, *Alisporites parvus*; i, *Alisporites tenuicorpis*; j, *Calamospora mesozoica*; k, *Combacullatisporites mesozoicus*; l, *Todisporites rotundiformis*; m, *Cycadopites* sp.; n, *Porcellispora longdonensis*; o, *Kraeuselisporites* sp.; p, *Carnisporites spiniger*; q, *Classopollis* sp.; r, *Corollina murphyae*; s, *Gliscopollis meyeriana*; t, *Classopollis torosus*.

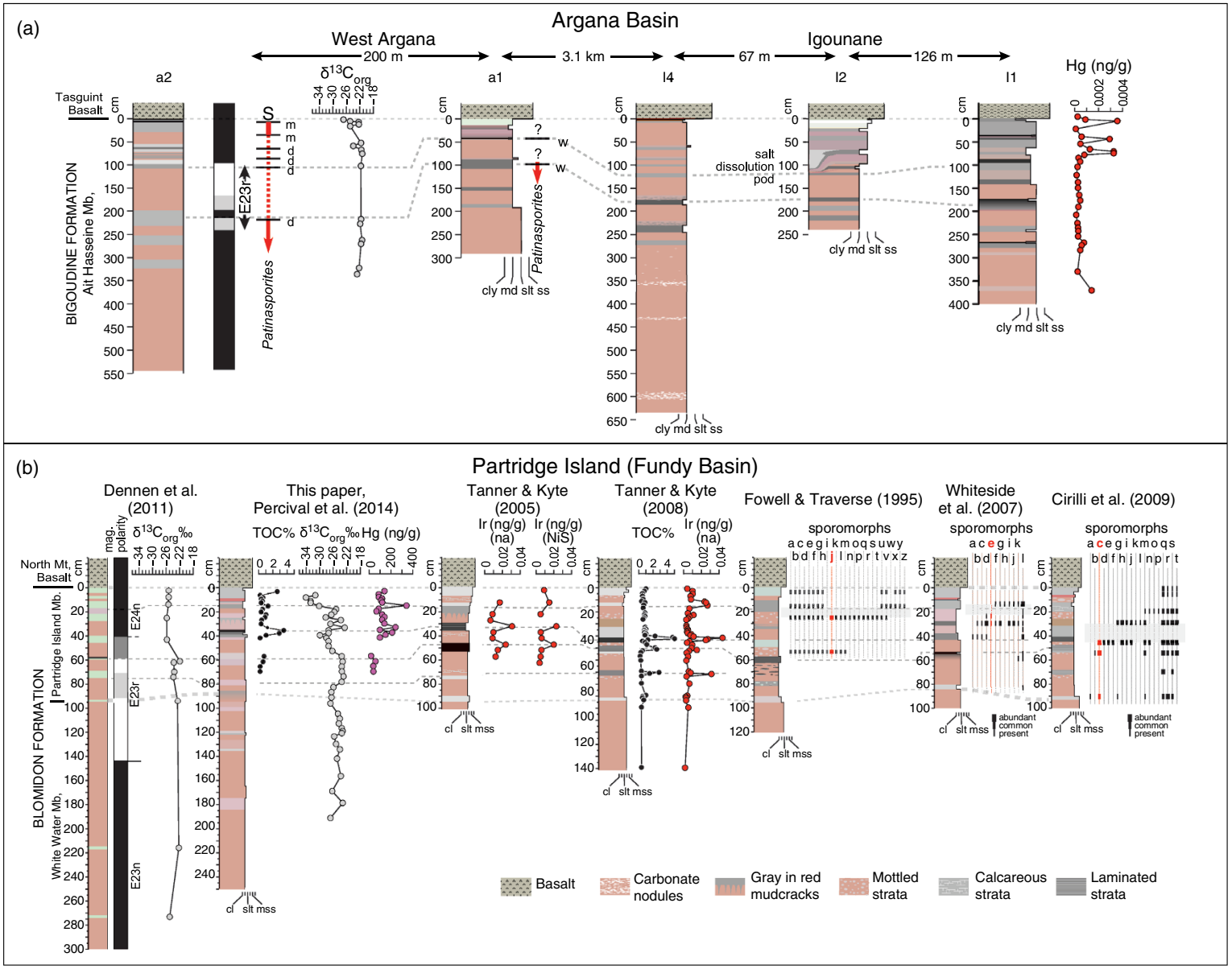
(a)
Argana Basin
West Argana
200 m
3.1 km
67 m
Igounane
126 m
a2
a1
l4
l2
l1
Hg (ng/g)
Tasguint Basalt
BIGOUDINE FORMATION
Ait Hasseine Mb,
E23r
Patinasporites
salt dissolution pod
cly md slt ss
(b)
Partridge Island (Fundy Basin)
Dennen et al. (2011)
This paper, Percival et al. (2014)
Tanner & Kyte (2005)
Tanner & Kyte (2008)
Fowell & Traverse (1995)
Whiteside et al. (2007)
Cirilli et al. (2009)
North Mt, Basalt
BLOMIDON FORMATION
Partridge Island Mb.
White Water Mb,
E24n
E23r
E23n
sporomorphs
abundant
common
present
cl slt mss
Basalt
Carbonate nodules
Gray in red mudcracks
Mottled strata
Calcareous strata
Laminated strata

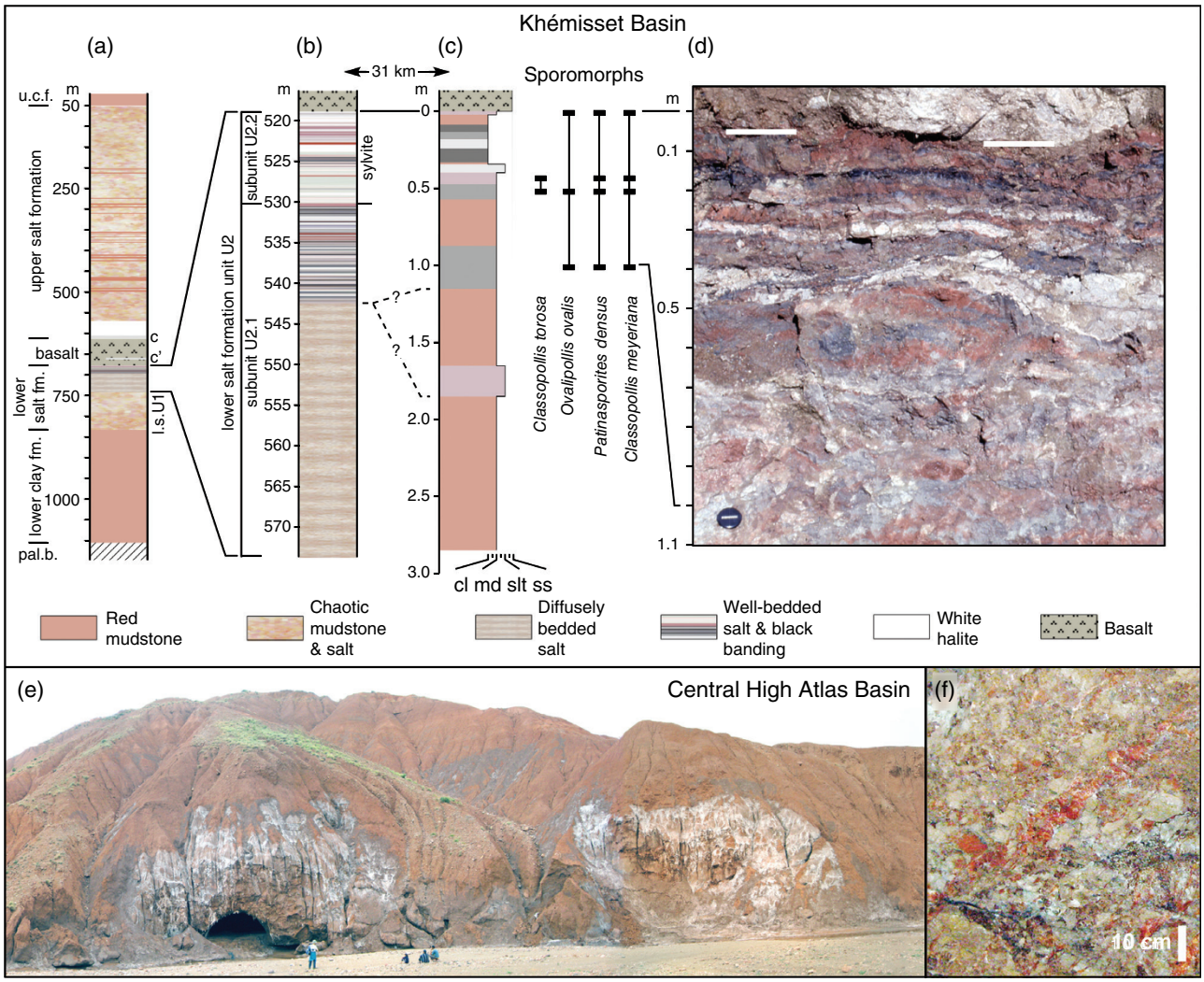

Figure 12.5 Moroccan salt basins and CAMP and ETE. (a–d) Khémisset basin: (a) Section of Triassic-earliest Jurassic Khémisset Basin based largely on cores Pz1 and PKB3 as compiled by Et-Touhami (1996); (b) upper part of the "lower salt formation" in core Pz1, the upper part of which is in contact with the CAMP lavas and bears the potash salt, sylvite; note the thick sequence of banded salt in which many layers are black; (c) outcrop section at Nif El Gour, Morocco, about 31 km west of core Pz1 showing major sporomorph taxa including abundant *Patinasporites* in contact with basalt flow; (d) outcrop of "lower clay formation" in contact with "lower basalt formation" (above white lines); note low angle faults and lateral changes in thickness of units. Abbreviations: c = carbonate bed at base of "upper salt formation"; c′ = discontinuous carbonate interbed between "lower basalt formation" and "intermediate basalt formation"; l. basalt fm.= "lower basalt formation"; pal.b.= Paleozoic basement; u.cf. = "upper clay formation". (e–f) Central High Atlas Basin salt diapric or dissolution structures in the middle of unit F6: (e) diapir-like structures in unit F6 mudstones consisting largely of red halite-mudstone breccia (appearing white where reprecipitated as salt encrustations), which is the local source for an artisanal salt industry; (f) wall of mine in (e) showing halite mudstone breccia (some halite is bright red and some is white).

no correlation between TOC and Ir, although the sample with the highest Ir value is adjacent to the sample with the highest TOC value. More ^{13}C-depleted values track upward in general with the most depleted value in the uppermost basaltic unit (Figs. 12.6a and 12.7a). TOC and $\delta^{13}C_{org}$ correlate ($R^2 = 0.74$), with more ^{13}C-depleted values associated with the lowest TOC values (Fig. 12.3f).

Five samples were selected for palynological processing based on their darker color. All five were productive, with moderate palynomorph preservation and diverse assemblages. There is no apparent trend of preservation with

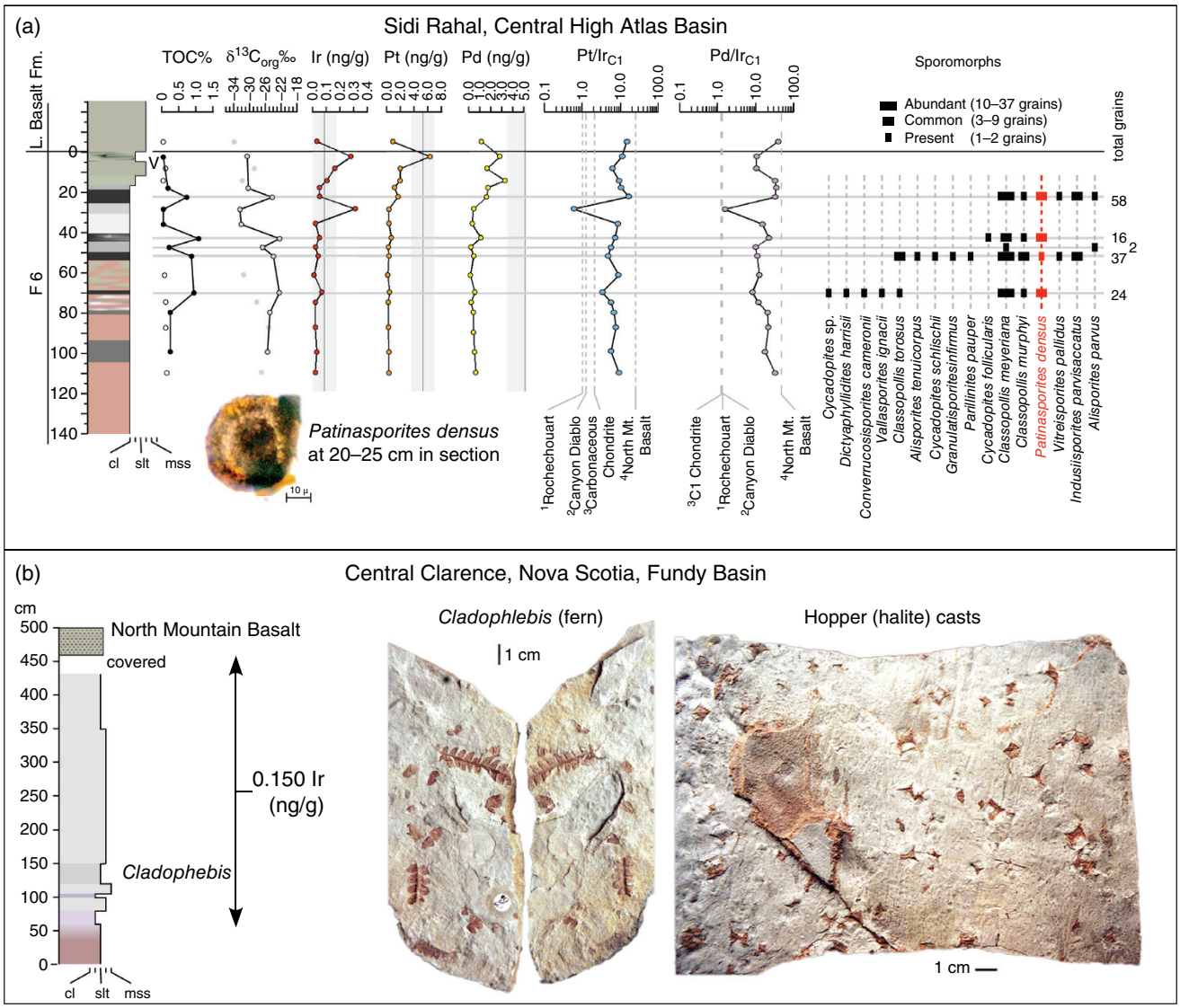

Figure 12.6 (a) Sidi Rahal, Morocco (Central High Atlas Basin), section with sporomorph ranges; figured *Patinasporites* grain from sample 27-09-03 18 (see Appendix, data files). (b) Central Clarence, Nova Scotia (Fundy Basin), exact position of sample analyzed by Orth et al. (1990) is unknown. *Cladophlebis* part and counterpart are in the collection of the Nova Scotia Museum of Natural History (987 GF 61.1) and the hoppers are in the same repository, uncatalogued.

distance from the basalt. As at Nif El Gour in the Khémisset Basin, the highest sample yielded *Patinasporites densus* (Fig. 12.6) where it makes up nearly 9% of the assemblage (Appendix Table 12.A2).

Other Central High Atlas Localities

The Tiourjdal $\delta^{13}C_{org}$ stratigraphy has its most ^{13}C-depleted values in contact with the basalt, with dramatic shifts of 5 to 7‰ in the last two meters. There are no published TOC data to test the extent of the inverse relationship seen at Sidi Rahal. The Oued Lahr section does not resemble Tiourjdal or Sidi Rahal and has its most ^{13}C enriched values in contact with the basalt breccia, suggesting the section is truncated at the top by erosion, a bedding fault, or recent glide plane.

12.6. DISCUSSION

12.6.1. PGE Anomalies and Possible Ashes or Aerosols

Our analyses of sections from the Newark Supergroup and Central High Atlas show the presence of multiple

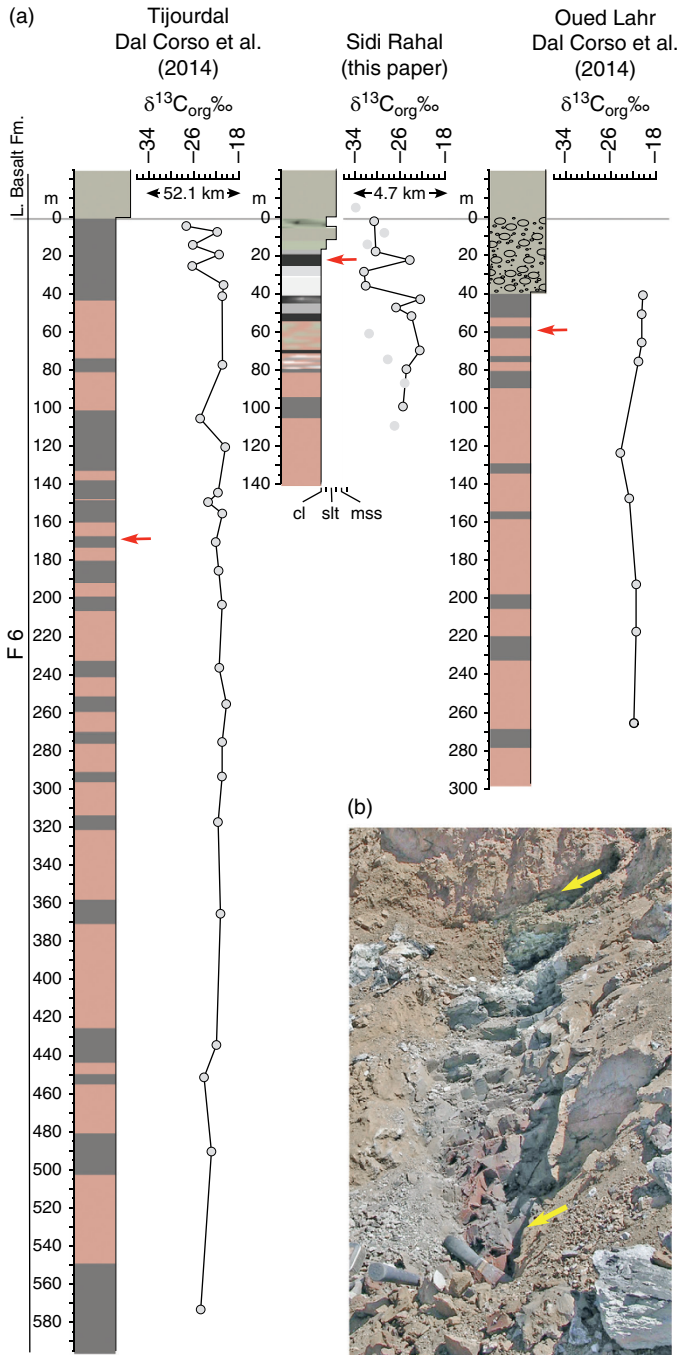

Figure 12.7 (a) Correlation between the Sidi Rahal section and the two sections described by Dal Corso et al. (2014) in the Central High Atlas Basin plotted on a common depth scale with the base of the "lower basalt formation" as the correlative datum. Grey vertical bars are values and error estimates for the North Mountain Basalt from Greenough and Fryer (1995). Arrows represent highest level with sporomorphs, including *Patinasporites densus*. (b) Sampled part of the Sidi Rahal section showing contact with basalt (arrow) and unconsolidated nature (sampled with a putty knife).

modest PGE anomalies that generally track organic carbon concentrations but are not quantitatively correlated (Fig. 12.3g–j). This finding suggests that the PGE distributions were caused by diagenetic migration and enhancement at redox boundaries, as has been observed for Ir anomalies of the same magnitude in onshore and offshore marine strata at the K-Pg boundary (Colodner et al., 1992; Miller et al., 2010). Tanner and Kyte (2005)

and Tanner et al. (2008) consider the overlying CAMP flows or CAMP volcanic aerosols as possible sources for the PGEs without excluding an impact as a source, but they do not identify how these options might be distinguished. Schmitz and Asaro (1996) demonstrated that many basaltic ashes from the Paleogene North Atlantic Igneous Province have modest Ir anomalies similar in magnitude to those observed here; however, these were deposited in laminated marine strata and are well preserved. We argue below that thin CAMP basaltic ashes and/or aerosols are a likely source of PGEs in the older CAMP lacustrine deposits, but would leave little to no obvious visible trace once weathered and bioturbated (see section 12.7.3, Correlations and Synthesis).

A clue that CAMP volcanic aerosols or ash events could be the source of the PGE anomalies is provided by the PGE elemental ratios (Norris et al., 2000; Robinson et al., 2009) that allow discrimination of the Ir sources. NiS Fire Assay data for this are available from the sections at Exeter (Fig. 12.2), Partridge Island (Fig. 12.4), and Sidi Rahal (Fig. 12.6). Normalized to the C1 chondrite, most of the Pt/Ir and Pd/Ir ratios exceed those for ordinary chondrites by nearly an order of magnitude (e.g., Tanner & Kyte, 2005; Tanner et al., 2008), but are not as elevated as basalts. Unfortunately, coverage of Pt, Pd, and Au data for the other sections is fragmentary because neutron methods do not routinely produce data for other PGEs.

An exception to the basaltic ratios of the PGE anomalies reported here are the chondritic or super-chondritic C1-normalized PGE ratios (Figs. 12.6, 12.8) of the lowest anomaly sampled at Sidi Rahal. The importance of this result is that it is difficult to imagine a scenario in which PGEs diffusing down from the basalt, or diffusing upward from fluids from below the basalt, would produce discrete anomalies at redox boundaries with *different* PGE ratios. A simpler hypothesis is that the PGE spikes represent PGE inputs from discrete CAMP events (ashes or volcanic aerosols) that then migrated some centimeters to nearby redox boundaries (i.e., the PGE enrichments are the consequence of specific eruptive events). There is furthermore no correlation between TOC or $\delta^{13}C_{org}$. For example, the PGE anomaly at the fern spike at Exeter may be a distal record of the "lower basalt formation," and the upper anomaly could be a trace of the lower "intermediate basalt formation" and North Mountain Basalt eruptions. The middle anomaly at the Partridge Island section could be linked to a precursor to the lower basalt formation, but this possibility would require support from a high-resolution correlation between sections (e.g., some independent correlation tool such as magnetic polarity stratigraphy).

The chondritic ratios could possibly result from an extraterrestrial source, such as the Rochechouart impact. It was initially reported with an age of 201 ± 2 Ma (Schmieder et al., 2010), but recent redating efforts show that the impact is actually >5 Myr too old (Cohen et al., 2017). Alternatively, some basalts and peridotites are known to exhibit chondritic ratios (e.g., McDonough & Sun, 1995; Rehkämper et al., 1999). For instance, ash from the 1991 Hekla eruption on Iceland is enriched in Ir (30 fg/g compared to background of ~1 fg/g in snow) and at least for Pt/Ir has a slightly suprachondritic ratio of 0.9 (C1 normalized) (Gabrielli et al., 2008). Thus, a CAMP origin cannot be ruled out, but this assertion awaits studies demonstrating the presence of CAMP material with near chondritic ratios of PGEs. Chemistry of the lower basalt formation suggests correlation to the basalt flows in the Argana Basin, but correlation of PGE anomalies at Sidi Rahal to other sections is problematic because there are no independent correlation tools for lower in the section.

We do not have PGE ratios sampled at the same level of resolution as Ir for Partridge Island and Tanner and Kyte's (2005) data did not extend that low in the section (Figs. 12.4, 12.8). Likewise, the Exeter section is not sampled with sufficient density below the fern spike to reveal whether the PGE pattern resembles that seen at Partridge Island or Sidi Rahal. Given the large variation in the PGE ratios, fuller coverage for Pt and Pd in these various sections are required to test possible correlations.

Apart from the one slight anomaly near the bottom of the Exeter section, all of the PGE anomalies reported here are either known, or are inferred by correlation, to be above chron E23r. If these do represent the products of individual major CAMP eruptions, U-Pb zircon ages would be expected to be within error of each other because E23r is estimated to be 23 kyr older than the Orange Mountain Basalt (Blackburn et al., 2013). Given that the lavas would all be expected to be of normal polarity as well (except possibly the lowest at Partridge Island/Sidi Rahal), lavas or intrusions would be difficult to tie to specific PGE anomalies without the benefit of superposition. The PGE excursion at the base of the ETE at Exeter and Partridge Island seems to line up with the lower and intermediate basalt formations. The oldest anomaly reported here at Exeter is ~20 ky older than the fern spike and again would not be recognizably different from the other early CAMP eruptions without superposition. It is possible that this anomaly is within the base of E23r and therefore of reverse polarity, which would in itself be distinctive because reverse polarity CAMP flows have yet to be identified (Olsen et al., 2003b; Font et al., 2011). Any of these anomalies could be due to eruptions tied to the recently dated CAMP intrusives that are nominally older than the ETE (Davies et al., 2017), namely the Messejana Dike of Spain

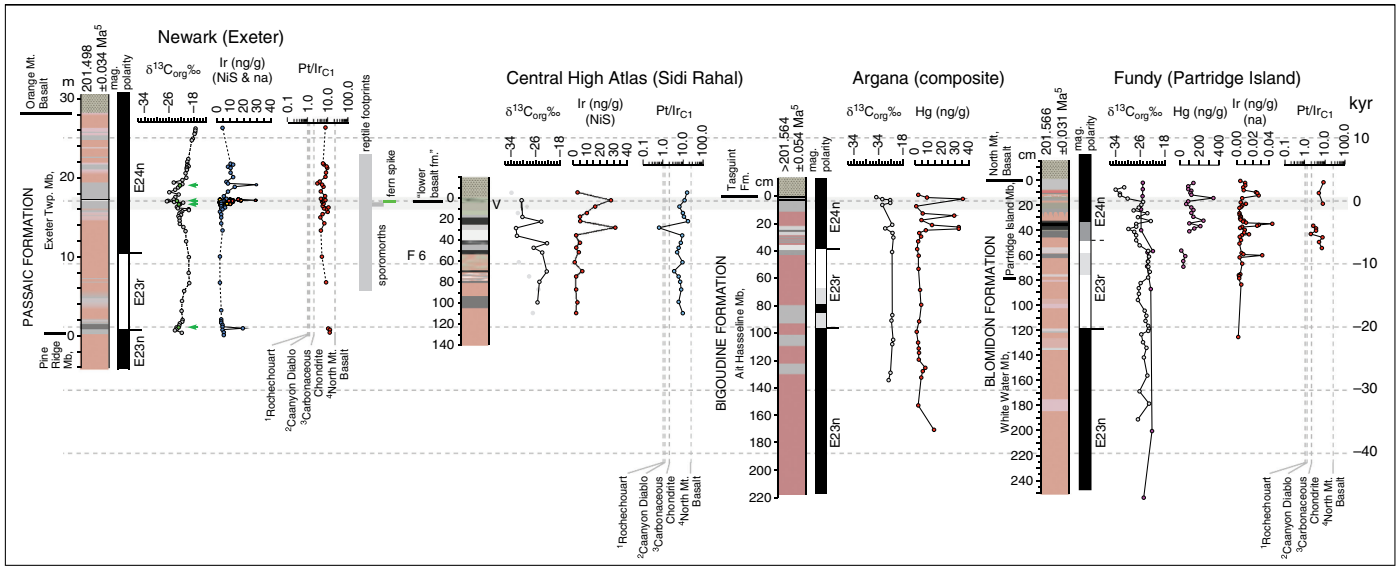

Figure 12.8 Correlations among CAM basins with PGE or Hg profiles. Newark, Argana, and Fundy (Partridge Island) are composites based on new and published data. Note: [1]Rochechouart data from Tagle et al. (2009), normalized to C1 chondrite; [2]Canyon Diablo data from Tagle et al. (2009), normalized to C1 chondrite; [3]C1 chondrite data from Lodders and Fegley (1998); [4]North Mountain Basalt data from Greenough and Fryer (1995); [5]dates from Blackburn et al. (2013). Kyr from ETE (fern spike) based on astrochronology from Blackburn et al. (2013).

(201.585 ± 0.034 Ma), the Tarabuco Sill of Bolivia (201.612 ± 0.046 Ma), and the Kakoulima Pluton of Guinea (201.635 ± 0.029 Ma), all within error of the projected age of all the PGE anomalies.

Although use of the PGE anomalies for correlation is promising, some caveats remain: (1) we do not have consistent independent correlation constraints for all sections; (2) we do not have enough stratigraphic scope to know if PGE anomalies are a common part of the record outside the CAMP window in these continental basins; (3) as of yet, we cannot reliably correlate any specific PGE anomaly to any specific CAMP eruption; and (4) there has been no thorough search for other distinctive tracers of volcanic activities in the sediments below the CAMP flows except for the mineralogical work of Dal Corso et al. (2014).

12.6.2. Carbon Isotope Excursions

A goal of much recent work is to use $\delta^{13}C$ excursions to correlate among various sections spanning diverse locations and environments, from pelagic marine (Kuroda et al., 2010) and continental shelves (Yager et al., 2017), to nonmarine settings (Whiteside et al., 2010). The underlying assumption is that the isotopic excursions are caused by changes in the global exchangeable carbon reservoirs (cf. the approach for the PETM and the Toarcian Ocean Anoxic event). For the end-Triassic extinction, the most familiar example is the mixed marine-continental section at St. Audrie's Bay. This section has a marked, 5‰ shift toward ^{13}C-depleted values in bulk organic matter at or close to the last appearances of several typically Triassic marine taxa, and dramatic shifts in marine and terrestrial palynomorphs, including the local last appearances of several characteristic Rhaetian sporomorph species. In its original interpretation, this initial carbon isotopic excursion (ICIE) was attributed to the addition of ^{13}C-depleted carbon from marine methane clathrates, released to the atmosphere by CO_2-triggered warming from CAMP (Hesselbo et al., 2002). This ICIE has proved an attractive correlation target for isotopic curves showing excursions of various magnitudes, with multiple alternative, nonunique correlations being offered (e.g., Ruhl et al., 2009; Tanner, 2010; Zaffani et al., 2018; Lindström et al., 2017).

Ideally, a distinctive isotopic excursion would be found in sections containing CAMP materials that could be directly correlated with the ICIE in the marine records, thus tightly linking the marine biotic changes with the terrestrial changes and the CAMP itself. This chemostratigraphic marker could then be related to far-field effects of CAMP eruptions of other sorts, such as PGEs, Hg, or mineralogical anomalies and associated biological changes (e.g., Percival et al., 2017; Dal Corso et al., 2014). The reality, however, is complex and nuanced.

The first nonmarine section associated with CAMP flows and exhibiting a negative $\delta^{13}C$ excursion that could be plausibly correlated to the CAMP was in the Exeter section in the Newark Basin (Whiteside et al., 2010). There, a marked negative excursion is associated with the fern spike and Ir anomaly (Fig. 12.2). As this level is at the sporomorph transition and within sampling uncertainty of the tetrapod footprint turnover, a case was made that this $\delta^{13}C$ anomaly correlated directly with the ICIE at St. Audrie's Bay. However, lower in the Exeter section is another $\delta^{13}C$ excursion that is associated with a laminated dark grey mudstone with lacustrine fossils (spinocaudatans and ostracodes; Fig. 12.2) making the proposed chemostratigraphic correlation nonunique.

A more extensive and continuous section in the younger Shuttle Meadow Formation B-1 core (Whiteside et al., 2011) presents additional issues. This section has a 3–5‰ negative shift $\delta^{13}C_{org}$ similar in magnitude to an "excursion" at every deeper-water grey and black mudstone in this cyclical lacustrine sequence. The simplest explanation for these isotopic shifts is cyclically changing sources of carbon controlled by ecosystem responses to lake-level change paced by Milankovitch climate change as described by Whiteside et al. (2011) and supported by the U-Pb dates of Blackburn et al. (2013). The more ^{13}C-depleted intervals are interpreted to have larger contributions of lipid-rich microbial material from deeper lake levels, whereas more recalcitrant vascular plant material dominates the organic matter of the shallower-water intervals. The same argument could apply to the Exeter section, where it is supported by $\delta^{13}C$ values from wood and *n*-alkanes from the same section that do not show similar fluctuations (Fig. 12.2). Given what seems to be a general relationship among deeper-water units, $\delta^{13}C_{org}$, and lacustrine cyclicity in these nonmarine sections, it seems possible that these more local source factors are more significant than any isotopic shifts in the global exchangeable carbon reservoirs. This alternative hypothesis for the origin of the excursion(s) can be tested by examining the correlation between the negative excursion at the floral and faunal break at the Exeter section and the ICIE at St. Audrie's Bay and elsewhere using independent high-resolution correlation tools (e.g., magnetostratigraphy and radioisotopic dating).

Cross-plots of TOC and $\delta^{13}C_{org}$ from the Exeter and Silver Ridge B-1 core (Fig. 12.3) show that negative values tend to be associated with higher TOCs (negative slope), although the correlations are weak (R^2 <0.4),

perhaps more easily seen in the data curves from these sites (Fig. 12.2) (Whiteside et al., 2011). Consistent with the well-known positive correlation between $\delta^{13}C_{org}$ and thermal maturity (Stahl, 1977) (a correlation that extends to graphite in Phanerozoic, Proterozoic, and Archean rocks; Tashiro et al., 2017), mudrock data from Exeter are also shifted to higher $\delta^{13}C$ values relative to the Silver Ridge B-1 core, with Exeter being significantly more thermally mature (R_0 = 1.0%) (Malinconaco, 2002, 2010) compared with the Shuttle Meadow Formation near the B-1 core (R_0 = 0.5 to 0.65%; Cornet et al., 1973; Braghetta, 1985; Spiker et al., 1988). The average $\delta^{13}C$ values of phytoclasts and wood at Exeter and the Shuttle Meadow Formation near the Silver Ridge B-1 core are offset by a similar amount (−4.10‰) compared with average $\delta^{13}C_{org}$ (−4.41‰, all grey and black), whereas the offset between the phytoclasts and wood at the Silver Ridge B-2 core and the Shuttle Meadow Formation near the Silver Ridge B-1 core (−0.22‰), or the offset for $\delta^{13}C_{org}$ at the same sites (−2.03‰), is significantly less.

In contrast to the Exeter and the Silver Ridge B-1 core, organic matter in the Silver Ridge B-2 core and Cinque Quarry show an opposite relationship between TOC and $\delta^{13}C_{org}$ (Fig. 12.3), with higher TOC samples tending to be more ^{13}C enriched (positive slope), although the relationship is also weak ($R^2 \leq 0.2$).

The lowest sporomorph-bearing sample (159.4), the Silver Ridge B-2 core is dominated by the horsetail spore *Pilasporites* (99%), and could be characterized as a spore spike. This sample also yields the most ^{13}C enriched value (18.4‰) in the core. This is difficult to reconcile with the abundance of horsetail spores, as the tissue of sphenopsids tends to be much more depleted in ^{13}C (−23 to −35‰; Tütken, 2011). However, the directly underlying sample (159.5) is the most ^{13}C depleted. We speculate this might represent migrated *n*-alkanes.

A similar but much stronger positive relationship ($R^2 \geq 0.6$) between TOC and $\delta^{13}C_{org}$ is observed at the Partridge Island (Fundy Basin) and Sidi Rahal (Central High Atlas Basin) sections (Fig. 12.3). Along with the West Argana (Argana Basin) and Tiourjdal (Central High Atlas Basin) sections, they are characterized by having their most negative values adjacent to (or in) the basalt. Dal Corso et al. (2014) and Percival et al. (2017) suggested that these ^{13}C-depleted excursions immediately below the oldest basalt correlate to the ICIE at St. Audrie's Bay. Because these sections have organic-rich strata <1 m from the basalt, an alternative origin of these excursions is related to the thermal alteration by the basalt flow, as suggested by the relationship between the ^{13}C depletion, the TOC values, and organic matter in the basalt itself.

The carbon isotopic excursions below the basalts range from −5‰ to −12‰, a variance that is hard to explain by a change in atmospheric $\delta^{13}C$. The simplest explanation is that this range represents different carbon sources that might not show up as visible differences in kerogen type. This could happen even if the excursion were part of a global signal augmented by local effects. We hypothesize that the end-members on the ^{13}C-enriched side are vascular plant-dominated carbon indigenous to the mudrock, while those on the ^{13}C-depleted side (~ −30‰ to −34‰) are migrated hydrocarbons (e.g., Stahl, 1977), originating from the more organic-rich beds, with either the basalt or burial depth (and/or hydrothermal heat) acting as heat source first, and the basalt acting as a relative seal second. The presence of very negative $\delta^{13}C_{org}$ values in the basalt, which should have essentially no organic matter (although graphite could be present in undetected xenoliths), argues for migrated hydrocarbons. Support for this hypothesis is the striking correlation between TOC and $\delta^{13}C_{org}$ (Fig. 12.3) with more ^{13}C-depleted values associated with the lowest TOC values. This correlation is opposite of what is observed in the cyclical lacustrine strata above the CAMP basalt (and thus unaffected by contact metamorphism) in the Silver Ridge B-1 core or in the Exeter section in which organic rich strata are ≥10 m from the overlying basalt and thus minimally affected. As at the other sections discussed here, the more ^{13}C enriched values associated with the high TOC are close to what might be expected for C3 vegetation, similar to the values from phytoclasts and wood described here (mean −25.33‰), or all of the phytoclasts reported by Spiker et al. (1988; mean −25.54‰); therefore, the ^{13}C-depleted values are more consistent with hydrocarbons. For example, the average value of lipids extracted from Triassic-Jurassic mudstones by Spiker et al. (1988) is −30.0 ± 1.4‰, and migrated oils in the lacustrine Triassic Yanchang Formation of the Ordos Basin China average −32.3 ± 0.5‰ (Li et al., 2016). Thus, the apparent $\delta^{13}C_{org}$ excursion at the base of the oldest CAMP basalts in the Argana, Central High Atlas, and Fundy basins may be the result of migrated hydrocarbons, a viable alternative to the hypothesis that the excursion is a correlative of a global ICIE. A similar negative relationship between TOC and $\delta^{13}C_{org}$ is also seen in far more thermally altered graphitic metasediments (e.g., Tashiro et al., 2017). This could be tested in the Triassic rift basins with more detailed geochemical analysis (e.g., by kerogen extraction and compound specific isotope analysis). A very similar pattern is evident in the Central High Atlas in Morocco, again suggestive of hydrocarbon migration toward the basalt (Figs. 12.3f, 12.6a, 12.7a).

Relevant to the issue of hydrocarbon generation and migration are the assertions that there is little or no contact metamorphism associated with the CAMP flows (Bernet, 2008; Dal Corso et al., 2014) and that any apparent alteration or additions of zeolites to the basalts are due instead to basin-scale hydrothermal brine activity or even prehnite-pumpellyite facies metamorphism (in excess of 150°C to 289°C) (Armstrong & Besancon, 1970; Greenberger et al., 2015; Puffer et al., 2018). Although older (and much more deeply buried) strata are significantly thermally altered well into the gas window of thermal maturity (R_o = 3) (e.g., Malinconaco, 2002, 2010), and conduits of heated brine may have reached the latest Triassic and Early Jurassic sedimentary sequence, there is no direct evidence of regional metamorphism associated with strata close to or in contact with the CAMP. In fact, extensive regional metamorphism in the prehnite-pumpellyite facies temperature range is excluded by the widespread presence of well-preserved biomarkers, incompatibly low vitrinite reflectance values (~0.3–1.2% R_o), low TAI (Thermal Alteration Index) indexes of pollen and spores, and other indications of thermal maturity in the oil window in many strata interbedded with and immediately below CAMP flows in the Newark, Hartford, and Fundy basins (e.g., Spiker et al., 1988; Pratt et al., 1988; Wade et al., 1996; Malinconaco, 2002, 2010; Whiteside et al., 2011). Permeating high temperature hydrothermal activity in these youngest strata is also unreasonable in light of the lack of a paleomagnetic overprint in these same strata with low thermal maturity indicators (Kent & Olsen, 2008).

Conversely, clear visual indications of contact metamorphism are present below a number of CAMP flows. For example, grey to purple zones in contact with the basalt extend downward for a meter or so, gradually turning the typical greyish-maroon color of the many meters of underlying strata in the Hampden and parts of the Holyoke basalts of the Hartford Basin (April, 1980, 1981), the Orange Mountain Basalt in the Martinsville no. 1 core, and the Hook Mountain Basalt in the Newark Basin (Fox et al., 2019). These alteration zones look identical to those described by April (1980) in which clay mineralogical changes are found associated with the local metamorphism, but such data are not yet available for the Newark basin strata. A simple explanation for the color change is that it is due to a thermochemical increase in grain size or clustering of hematite grains (e.g., Steinwehr, 1969; Walker et al., 1981; Torrent & Schwetman, 1987). This distinctive alteration occurs where the basalt is massive in the Newark and Hartford basins and is absent where pillow lavas are present, even for the same overlying basalt formation at different localities suggesting that water limited thermal alteration in the latter. Well-preserved pollen can occur even at the contact with the pillow lava, which is to be expected as the pillows are already relatively cool when they contact the sediment under water. Therefore, because of the plausible contact-heating origin for the negative $\delta^{13}C_{org}$ excursions in the Fundy, Argana, and Central High Atlas sections, we do not regard them as reliable correlation tools.

The origin of the St. Audrie's Bay ICIE and its global nature is problematic (Fox et al., 2019). This excursion, the "type" for the ETE, occurs in a continental interlude in an otherwise marine sequence spanning the Triassic-Jurassic transition. Continental fossils such as the bryophyte *Naiadita*, spinocaudatans, and darwinulid ostracodes occur in and near the interval with the ICIE in the Cotham Member (Warrington & Ivimey-Cook, 1992), which may strongly bias the apparent position of the extinction level (see discussion in Radley et al., 2008). Extensive work on biomarkers and their $\delta^{13}C$ composition (Whiteside et al., 2010) suggests dramatic changes in carbon sources through this interval, providing evidence that the entire excursion is a result of basin-wide ecosystem change due to salinity and water-depth reductions as opposed to changes in the global exchangeable reservoirs (Fox et al., 2019). Another excursion of smaller magnitude (~4‰, once the Cotham excursion is discounted), at the base of the Blue Lias reported at St. Audrie's Bay and seen at least regionally, is another plausible candidate for an excursion related to global carbon reservoirs associated with an alternative location for the ETE, at the last appearances of conodonts, several marine invertebrate taxa (regional extirpations), and phytosaurs (Mander et al. 2008; Maisch & Kapitzke, 2010; Fox et al., 2019). This again highlights the difficulty in finding unique correlations for these isotopic fluctuations in the absence of independent correlation tools, particularly magnetostratigraphy, astrochronology, or datable ashes or additional potential chemostratigraphic markers such as PGE or Hg anomalies (Percival et al., 2017).

Magnetic polarity stratigraphy offers a powerful tool for correlation among these sections (e.g., Fig. 12.8). Chron E23r, despite its brevity, is clearly a distinctive and repeatable marker within the continental sequences of eastern North America and Morocco. Candidate reverse-polarity zones have been identified at the St. Audrie's Bay section (Hounslow et al., 2004) but none of these have been reproduced at any other marine sections. Particularly interesting are chrons SA5n.3r in the basal Cotham Member and SA5r in the lower preplanorbis zone in the Blue Lias. If the former were found to be reproducible, it would suggest that the St. Audrie's Bay ICIE does correlate with the base of the continental ETE, PGE anomaly,

and its apparent $\delta^{13}C_{org}$ excursion. As a consequence SA5r would have no counterpart in the repeatedly sampled eastern North America section, although it is possible the poorly understood intervals reported as of reverse polarity in the Moroccan Central High Atlas CAMP lavas by Marzoli et al. (2004) and Knight et al. (2004) are somehow correlative, although these have been reinterpreted as remagnetizations by Font et al. (2011). If SA5r were found to be reproducible, then the continental ETE would plausibly correlate to the pre-*planorbis* zone in the Blue Lias and the marine extinctions would apparently slightly precede the continental events, which is possible given the range of CAMP eruption ages. The recovery of a reproducible magnetostratigraphy in these marine sections is a high priority and could clarify the relative timing of events around the ETE.

12.6.3. Correlations and Synthesis

Strata immediately below the oldest basalts in the Newark and Fundy basins definitively record the largest and most concentrated floral and faunal turnover in the entire record of the CAM basins, which is most parsimoniously correlated to the ETE in the marine environment as supported by geochronological data. The turnover in these rift basins is associated with several new PGE anomalies described here and one or more carbon isotopic events that possibly reflect regional to global events. There is no evidence of a hiatus and strong geochronological evidence against one (e.g., Kent et al., 2018; Olsen et al., 2019a). In Morocco, sporomorph evidence, particularly the range of the vesicate conifer pollen forms *Patinasporites densus* and *Enzonalasporites vigens* show no consistent evidence of an extinction up to the base of the basalts where examined. This suggests that the flows with the lower basalt formation chemistry are older than the oldest basalts in eastern North America and are synchronous with or predate the ETE (Blackburn et al., 2013). However, *Patinasporites densus* also occurs above the upper basalt formation in the Central High Atlas Basin, suggesting either that the extinction of that plant group was spatially complex at time scales of tens of thousands of years or that the entire sequence of Moroccan basalts from the lower through upper basalt formations are older that the ETE. However, the latter scenario requires that available geochronological, geochemical, and cyclostratigraphic correlations of the basalts are incorrect, which is a less parsimonious argument than an irregular extirpation leading to extinction at the ~10 k level.

Circumstantial evidence suggests these PGE anomalies are diagenetically modified traces of CAMP ashes or vapor pulses, and internal evidence from the lower PGE anomaly at Sidi Rahal has apparent chondritic elemental ratios suggesting that diagenetic remobilization of basalt or nonvolcanogenic sediment PGEs cannot be solely responsible for the levels of PGE concentration. At least some definitive ash or detrital volcanic material occurs in the zone with these anomalies, but these seem to have been locally sourced from the basal basalts themselves. Dal Corso et al. (2014) interprets clay mineralogical data from the Central High Atlas to be of volcanogenic origin, however similar clay mineralogical data have also been interpreted to be of hydrothermal origin at other localities (Daoudi & Pot de Vin, 2002).

Given these generalities, two fundamental issues confront our ability to synthesize the diverse data from these sections. First, sampling strategies have been inconsistent at the different sections and by different researchers. In the absence of *a priori* expectation of the accumulation rate and the frequency of the phenomena that are being sought, "point samples" are inappropriate because of the danger of aliasing. Contiguous channel samples avoid this problem because anomalies can be captured but possibly diluted if the anomaly is stratigraphically thin and the sampling interval thick. Second, real lateral variability in the stratigraphy (e.g., salt dissolution) or unrecognized creep or small-scale faulting of sections over small distances, even for the same authors at the same locality, makes comparison between records difficult (e.g., Tanner & Kyte, 2005; Tanner et al., 2008: Fig. 12.4).

Nonetheless, with these caveats in mind, we have endeavored to produce synthetic sections combining data from ourselves and other authors in the same areas using lithologic markers such as distinctive mudstones and the base of basalt flows (Fig. 12.7). We recognize that even at this scale, these correlations may be nonunique. However, at present this is the only way to register polarity stratigraphy to sporomorph, carbon isotope, and PGE stratigraphy.

Correlation among these locally composite sections (Fig. 12.8) is broadly constrained among the Newark, Argana, and Fundy basins by reverse paleomagnetic chron E23r, the initiation of the ETE in the Newark and Fundy basins, the chemistry of the basalt flows (e.g., Deenen et al., 2010), and high resolution CA-ID-TIMS zircon U-Pb dates (Blackburn et al., 2013), with linear scaling between these available fiducials. The resulting correlation is consistent with that of Blackburn et al. (2013) and is independent of the PGE and $\delta^{13}C_{org}$ chemostratigraphy.

Given this correlation, we report two distinct PGE anomalies: an anomaly originally described by Olsen et al. (2002) at the Exeter section, and a second that is the lowest at Sidi Rahal (Fig. 12.8). The Exeter anomaly is directly associated with the spore spike and palynofloral transition and, based on its position relative to E23r, it

may correlate to the uppermost PGE anomaly in the Central High Atlas basins and the Fundy Basin, given the uncertainties. The uppermost Hg peaks in the Argana and Fundy basins (Percival et al., 2017) are also possible correlates. The upper PGE peak in the Central High Atlas section and the upper Hg peak in the Argana section lie directly in contact with the lower basalt formation and correlative Tasguint Formation, respectively, and might be related to their eruption or an immediate precursor that seems to be tied to the initiation of the ETE in the Newark and Fundy basins. This set of possibly correlative PGE anomalies have high PT/Ir ratios.

The lower PGE anomaly in the Central High Atlas section has chondritic or superchondritic ratios and may correlate with the largest PGE anomaly in the Fundy Basin, which has nearly chondritic ratios, slightly lower than carbonaceous chondrites (Fig. 12.8). Unfortunately, the peak Ir level of Tanner et al. (2008) does not seem to have been sampled by Tanner and Kyte (2005). Within the Fundy Basin section, this interval of near chondritic PGE ratios is associated with the lower Hg anomalies of Percival et al. (2017), although this is uncertain given the stratigraphic variability at that site and the fact that different samples were analyzed by different groups. The correlative part of the Newark Basin sections appears too undersampled to assess whether a similar chondritic PGE anomaly is present. The uppermost PGE anomaly in the Newark Basin section seems to correlate into the North Mountain Basalt and also seems to have near chondritic PGE ratios. The lowest anomaly in the Newark Basin section has no counterpart in other basins, which are also undersampled in the plausibly correlative interval.

Despite problems with correlations, the possibility that PGEs have migrated toward redox boundaries, and the overall low concentrations of PGEs, a meaningful pattern is emerging. The ETE is correlative to the eruption of the oldest flows in Morocco, those with lower basalt formation chemistries, with the distal products of the eruptions being a PGE anomaly in correlative sedimentary sections where those flows never reached (Fig. 12.8). Atmospheric CO_2, based on the soil carbonate proxy, indicates a sharp rise from 3,000 to 4,000 ppm in the interval associated with the PGE anomalies and the level of the ETE (Schaller et al., 2016; Jones et al., 2017). Thus, the CO_2 rise generally ascribed to the CAMP began approximately at the level of the associated Ir anomalies and the projected position of the Tasguint and lower basalt formation in Morocco. Additional increases occurred above the Orange Mountain Basalt and correlative formations (Schaller et al., 2011, 2012, 2015, 2016), with several sporomorph last appearances occurring just above the North Mountain Basalt in Nova Scotia and the upper basalt formation in the Central High Atlas Basin (Cirilli et al., 2009; Panfili et al., 2019). Above that there is little or no sporomorph evidence and no tetrapod evidence of extinctions in the CAM basins.

It is unclear how the PGE anomalies at the Hartford Basin *Clathropteris* locality (Tanner & Kyte, 2016) and the Fundy Basin Central Clarence *Cladophlebis* locality (Fig. 12.6) correlate to the others described here because there is inadequate outcrop to assess the stratigraphic context. They provide critical macrofossil context very close in time to the ETE, so their stratigraphic uncertainty is unfortunate. PGE analyses have yet to be conducted on the Silver Ridge B-2 and B-3 cores, the Cinque Quarry section in the Hartford Basin, or the Nif El Gour section in the Khémisset Basin.

CAMP intrusions older than the apparent age of the ETE, 201.564 ± 0.015 Ma (Blackburn et al., 2013), such as the Kakoulima intrusion in Guinea (201.635 ± 0.029 Ma) or the Tarabuco Sill of Bolivia (201.612 ± 0.046 Ma) (Davies et al., 2017) may have fed surface eruptions and contributed to environmental change prior to the apparent initiation of the continental ETE. Although no flows are present in West Africa near the Kakoulima intrusion (plausibly because the level of erosion is so deep) there are flows in Bolivia associated with the Tarabuco Sill (Bertrand et al., 2014). However, there are no studies of strata in the CAM basins that are appropriately far enough below the basalts to detect PGE anomalies that could relate to these eruptions, although there is at least one reported Hg anomaly that could be a record of such eruptions in the right stratigraphic level in the upper Passaic Formation (Jones et al., 2017). No known biotic events correlate with these intrusions.

There are a few published records of PGE anomalies in lacustrine strata interbedded with CAMP basalts. This includes Ir (neutron activation) anomalies in the upper Fall River Beds of the Sugarloaf Formation and the lower Turners Falls Formation in the Deerfield Basin (Tanner & Kyte, 2015), as well as in the Pompton Ash in the middle Towaco Formation of the Newark Basin and middle East Berlin Formation of the Hartford Basin (Olsen et al., 2016a). The Turners Falls Formation occurrence is noteworthy because it occurs entirely in red beds, and Beaty (2017) reported a Hg anomaly from what is close to or might be the same as the Ir level. These strata were deposited close to or during the eruption of the chemically distinct (Tollo & Gottfried, 1992) upper flows of the Preakness Basalt that have no counterparts in the Hartford or Deerfield basins (Olsen et al., 2019a, 2019b). The Ir and Hg anomalies could represent traces of these eruptions.

The Pompton Ash is particularly interesting as it is a 5-mm-thick bona fide volcanic airfall, made of euhedral,

nonrounded, plagioclase laths in clay or chalcedony matrix that was originally glass, fine-grained feathery feldspars, carbonate, and distinct sub-mm spherule-like volcanic grains at the base (Olsen et al., 2016b, 2019c). There are no zircons, in line with a basaltic to andesitic composition. Interbedded with microlaminated fish-bearing dark calcareous mudstone, the airfall has a PGE anomaly of similar magnitude to the anomalies below the basalt, an elevated Hg concentration, and ε_{Nd} values intermediate between the surrounding basalts and the sediments (Olsen et al., 2016b, 2019c). A thinner (1 mm) ash is present above it (Olsen et al., 2019c). These are the only airfalls (other than proximal lapillae) known from the entire CAMP. We interpret them to be cryptotephras (Lowe & Hunt, 2001; Alloway et al., 2005), with the glass completely altered to clay. If weathered and bioturbated in a paleosol or a bioturbated lacustrine deposit, the latter being typical of the associated Triassic-Jurassic sequences, they would leave little or no visible trace but could be detectible chemically. We argue that the absence of other airfall ashes in this gigantic region is a result of such alteration and bioturbation, rather than that no other explosive eruptions occurred. Although this leads credence to our argument that the PGE anomalies below the basalt could have originated as CAMP ashes, we caution that a diagenetic origin of this metal enrichment cannot be ruled out and that such focusing occurred, regardless of the ultimate source of the PGEs.

These observations are consistent with the hypothesis that the PGE anomalies are distal traces of CAMP eruptions related to the initiation of the ETE biotic events. However, despite the correlation of PGE, Hg, and $\delta^{13}C_{org}$ anomalies, our observations could reflect pervasive confirmation bias (e.g., Nickerson, 1998) because we are unaware of the distribution or absence of PGE anomalies in strata where there is no expectation of CAMP or other eruptive products, and there is evidence of diagenetic migration. Our windows of observation have been circumscribed close to the basalts and the hypothesis that similar anomalies are widespread and entirely of diagenetic origin has yet to be falsified. An analogous challenge faced the original discovery of the K-Pg Ir anomaly (Alvarez et al., 1980), which was tested by examination of a longer stratigraphic record (Kyte & Wasson, 1982, 1986), even before the detection of shocked quartz (Bohor et al., 1984) that demonstrated its extraterrestrial impact origin. Additional sampling using multiple geochemical techniques on aliquots of the same samples coupled with high-resolution paleomagnetic polarity stratigraphy, biostratigraphy, and compound specific isotopic analysis should resolve the uncertainties of correlation and test the origin of these PGE anomalies and their relationship to the ETE.

12.7. CONCLUSIONS

Whereas the extraterrestrial impact paradigm of Alvarez et al. (1980) was immensely successful in explaining the K-Pg extinction, and has been of great heuristic value to study of the ETE, the initial enthusiasm for its applicability to the ETE has diminished because many features fail to fit the impact hypothesis. The impact hypothesis has been succeeded by the hypothesis that Ir and other sedimentary metal anomalies associated with the ETE are the result of distal products of CAMP eruptions, the environmental effects of which resulted in the extinctions and subsequent rise to ecological domination of the dinosaurs.

Our results show multiple PGE anomalies at 13 localities in strata directly below the oldest CAMP lavas in three Central Atlantic Margin rift basin sequences on two continents: the Newark and Fundy basins of eastern North America (the latter by Tanner & Kyte, 2005; Tanner et al., 2008); and the Central High Atlas Basin of Morocco. This includes the first section in which an Ir anomaly was identified at the level of the ETE in the Newark Basin (Olsen et al., 2002).

We also confirm the presence of a negative $\delta^{13}C_{org}$ excursion in sedimentary strata at the base of the oldest basalts in the Fundy and Moroccan basins, but we caution that despite its position being appropriate for the excursion seen at the canonical St. Audrie's Bay section, it is more parsimoniously attributed to migrated hydrocarbons.

Our data show that the range of the key Triassic-aspect sporomorph taxon *Patinasporites densus* (related forms) extends to the base of the oldest basalts in Morocco (as suggested by Marzoli et al., 2004), but not to the oldest basalts in eastern North America. We note the discovery of that taxon above the upper basalt formation in the Central High Atlas Basin (Panfil et al., 2019) shows that the extinction of the conifer group that produced that sporomorph must have been characterized by a geographically patchy extirpation, which nonetheless removes any palynostratigraphic evidence for a major hiatus encompassing most of the Rhaetian in these basins, as well as falsifying the hypothesized restriction of *Patinasporites* and kin to early Rhaetian and older strata (e.g., Gradstein et al., 1994; Van Veen, 1995; Lucas & Tanner, 2007; Tanner & Lucas, 2015).

Our conclusions are tempered by the knowledge that rigorous tests of a diagenetic origin have yet to be conducted, and that there are inconsistencies and deficits in the sampling methodologies used to date, but we emphasize that the PGE anomalies and associated data and correlations presented here corroborate the hypothesis that the metal anomalies were produced by CAMP eruptions and are markers of the causes of the end-Triassic mass extinction, specifically the initiation of the palynological and tetrapod turnover.

ACKNOWLEDGMENTS

We thank Sarah Fowell for palynological results produced during 2011 from samples from the Argana, Khémisset (Nif El Gour, sampled in 1999), and Fundy basins; Bruce Cornet for pollen and spore processing and taxa identification during 2005 for the upper Exeter (sampled in 2000), the Partridge Island (sampled in 2003), the Argana Basin (rerun from samples collected in 1994), and Sidi Rahal (collected in 2003) sections; developers and contractors in the Exeter area during the 1990s and 2000s for their enthusiastic cooperation and access to temporary exposures; ONAREP for logistical support in Morocco on multiple occasions; and the numerous researchers who, in published discussion and dispute, have helped refine our understanding of the ETE and associated phenomena. We are grateful for support from NSF EAR 1147402 and a University of Southampton Annual Adventures in Research grant to JHW, NSF EAR9418464 to S. Fowell and P. E. Olsen, and EAR0753496 to PEO and Dennis Kent as well as multiple grants from the Lamont Climate Center that supported many of our analyses. This is Lamont contribution 8437.

REFERENCES

Afenzar, A. & Essamoud, R. (2017). Early Mesozoic detrital and evaporitic syn-rift series of Mohammedia-Benslimane-El Gara-Berrechid Basin (Meseta, Morocco): Sedimentary and palaeoenvironmental evolution and comparison with neighboring basins. *International Journal of Advanced Earth Science and Engineering, 6*(1), 596–621.

Alloway, B. V., Pillans, B. J., Carter, L., Naish, T. R. & Westgate, J. A. (2005). Onshore-offshore correlation of Pleistocene rhyolitic eruptions from New Zealand: Implications for TVZ eruptive history and paleoenvironmental construction. *Quaternary Science Reviews*, *24*(14–15), 1601–1622.

Alvarez, L. W., Alvarez, W., Asaro, F., & Michel, H. V. (1980). Extraterrestrial cause for the Cretaceous-Tertiary extinction. *Science*, *208*(4448), 1095–1108.

Armstrong, R. L., & Besançon, J. (1970). A Triassic timescale dilemma: K-Ar dating of Upper Triassic mafic igneous rocks, eastern U.S.A. and Canada and post-Upper Triassic plutons, western Idaho, U.S.A. *Eclogae Geologicae Helvetiae*, *63,* 15–28.

Baird, D. (1972). Burntcoat, Upper Triassic. In R. L. Carroll et al. (Eds), *Field excursion A59: Vertebrate paleontology of eastern Canada, guidebook* (pp. 22–30).Twenty-Fourth International Geological Congress, Montreal, Quebec, Canada.

Baird, D. (1986), Some upper Triassic reptiles, footprints, and an amphibian from New Jersey. *The Mosasaur, 3,* 125–153.

Beaty, B. (2017). *Mercury enrichments in the Triassic-Jurassic rift basins of eastern North America: Facies dependence, volcanic associations, and relationship to the End-Triassic extinction*. B.Sc. Thesis, Amherst College.

Beauchamp, J., & Petit, J.-P. (1983). Sédimentation et taphrogenèse triasique au Maroc: L'exemple du haut atlas de Marrakech. *Bulletin Centres de Recherches Exploration-Production Elf- Aquitaine, 7*(1), 389–397.

Beauchamp, W., Barazangi, M., Demnati, A., & El Alji, M. (1996). Intracontinental rifting and inversion: Missour Basin and Atlas Mountains, Morocco. *AAPG Bulletin*, *80*(9), 459–1482.

Bensalah, M. K., Youbi, N., Mata, J., Madeira, J., Martins, L., El Hachimi, H., Bertrand, H., et al. (2013). The Jurassic-Cretaceous basaltic magmatism of the Oued El-Abid syncline (High Atlas, Morocco): Physical volcanology, geochemistry and geodynamic implications. *Journal of African Earth Sciences, 81,* 60–81.

Benton, M. J. (1994). Late Triassic to Middle Jurassic extinctions among continental tetrapods: testing the pattern. In N. C. Fraser & H. D. Sues (Eds.), *In the shadow of the dinosaurs* (pp. 366–397). Cambridge: Cambridge University Press.

Bernet, M. (2008). Hot rocks in the Hartford Basin, thermochronology in rift basin analysis. In J. I. Garver & M. J. Montario (Eds.), *Proceedings from the 11th International Conference on Thermochronometry* (pp. 27–30), *Anchorage Alaska,* Sept. 2008.

Bertrand, H., Fornari, M., Marzoli, A., García-Duarte, R., & Sempere, T. (2014). The Central Atlantic magmatic province extends into Bolivia. *Lithos*, *188,* 33–43.

Biron, P. E. (1982). *Le Permo-Trias de la région de l'Ourika (Haut-Atlas de Marrakech, Maroc)*. Thèse 3rd cycle, Université de Grenoble.

Blackburn, T. J., Olsen, P. E., Bowring, S. A., McLean, N. M., Kent, D. V., Puffer, J., McHone, G., et al. (2013). Zircon U-Pb geochronology links the end-Triassic extinction with the Central Atlantic Magmatic Province. *Science*, *340*(6135), 941–945.

Bohor, B. F., Foord, E. E., Modreski, P. J., & Triplehorn, D. M. (1984). Mineralogic evidence for an impact event at the Cretaceous-Tertiary boundary. *Science*, *224*(4651), 867–869.

Braghetta, A. (1985). *A study of hydrocarbon maturity of the Hartford and Newark Basins by vitrinite reflectance*. Senior Thesis, Princeton University, Princeton, New Jersey.

Carroll, R. L., Belt, E. S., Dineley, D. L., Baird, D., & McGregor, D. C. (1972). *Field excursion A59: Vertebrate Paleontology of Eastern Canada, Guidebook*. Twenty-Fourth International Geological Congress, Montreal, Quebec.

Cirilli, S., Marzoli, A., Tanner, L., Bertrand, H., Buratti, N., Jourdan, F., Bellieni, G., et al. (2009). Latest Triassic onset of the Central Atlantic magmatic province (CAMP) volcanism in the Fundy basin (Nova Scotia): New stratigraphic constraints. *Earth and Planetary Science Letters*, *286*(3–4), 514–525.

Cohen, B. E., Mark, D. F., Lee, M. R., & Simpson, S. L. (2017). A new high-precision $^{40}Ar/^{39}Ar$ age for the Rochechouart impact structure: At least 5 Ma older than the Triassic-Jurassic boundary. *Meteoritics & Planetary Science, 52*(8), 1600–1611.

Colbert, E. H. (1958). Tetrapod extinctions at the end of the Triassic Period. *PNAS, 4,* 973–977.

Colodner, D. C., Boyle, E. A., Edmond, J. M., & Thomson, J. (1992). Post-depositional mobility of platinum, iridium and rhenium in marine sediments. *Nature*, *358*(6385), 402–404.

Cornet, B. (1977). *The Palynostratigraphy and age of the Newark supergroup*. PhD Thesis, The Pennsylvania State University, University Park.

Cornet, B. & Traverse, A., (1975). Palynological contributions to the chronology and stratigraphy of the Hartford Basin in Connecticut and Massachusetts. *Geoscience and Man*, *11*(1), 1–33.

Cornet, B., Traverse, A. & McDonald, N. G. (1973). Fossil spores, pollen, and fishes from Connecticut indicate Early Jurassic age for part of the Newark Group. *Science*, *182*(4118), 1243–1247.

Dal Corso, J., Marzoli, A., Tateo, F., Jenkyns, H. C., Bertrand, H., Youbi, N., Mahmoudi, A., et al. (2014). The dawn of CAMP volcanism and its bearing on the end-Triassic carbon cycle disruption. *Journal of the Geological Society*, *171*(2), 153–164.

Daoudi, L. & Pot De Vin, J. L. (2002). Effets thermique et hydrothermal de la coulée de basalte triasico-liasique sur les argiles du bassin d'Argana. (Maroc). *Comptes Rendus Géoscience*, *334,* 463–468.

Davies, J. H. F. L., Marzoli, A., Bertrand, H., Youbi, N., Ernesto, M., & Schaltegger, U. (2017). End-Triassic mass extinction started by intrusive CAMP activity. *Nature Communications*, *8*. doi:10.1038/ncomms15596

Deenen, M. H. L., Krijgsman, W., & Ruhl, M. (2011). The quest for chron E23r at Partridge Island, Bay of Fundy, Canada: CAMP emplacement postdates the end-Triassic extinction event at the North American craton. *Canadian Journal of Earth Sciences*, *48*(8), 1282–1291.

Deenen, M. H. L., Ruhl, M., Bonis, N. R., Krijgsman, W., Kuerschner, W. M., Reitsma, M., & van Bergen, M. J. (2010). A new chronology for the end-Triassic mass extinction. *Earth and Planetary Science Letters, 291*, 113–125.

Echarfaoui, H., Hafid, M., Aït Salem, A. & Aït Fora, A. (2002). Analyse sismo-stratigraphique du bassin d'Abda (Maroc occidental), exemple de structures inverses pendant le rifting atlantique. *Comptes Rendus Geoscience, 334,* 371–377.

El Hachimi, H., Youbi, N., Madeira, J., Khalil Bensalah, M., Martins, L., Mata, J., Medina, F., et al. (2011). Morphology, internal architecture and emplacement mechanisms of lava flows from the Central Atlantic Magmatic Province (CAMP) of Argana Basin (Morocco). In D. J. J. Van Hinsbergen et al. (Eds.), *The formation and evolution of Africa: A synopsis of 3.8 Ga of earth history* (pp. 167–193), Geological Society, London, Special Publications, 357. doi: 10.1144/SP357.9 0305-8719/11/$15.00 # The Geological Society of London.

Et-Touhami, M. (1996). L'origine des accumulations salifères du Trias marocain: Apport de la géochimie du brome du sel du bassin de Khémisset (Maroc central). *Comptes rendus de l'Académie des sciences, Série 2*, *323*(7), 591–598

Et-Touhami, M. (2000). Lithostratigraphy and depositional environments of Lower Mesozoic evaporites and associated red beds, Khémisset Basin, northwestern Morocco. *Zentralblatt fur Geologie und Palaontologie, Teil I*, *1998,* 1193–1216.

Fabuel-Perez, I., Redfern, J., & Hodgetts, D. (2009). Sedimentology of an intra-montane rift-controlled fluvial dominated succession: The Upper Triassic Oukaimeden Sandstone Formation, Central High Atlas, Morocco. *Sedimentary Geology*, *218*, 103–140.

Farabee, M. J. (1991). Botanical affinities of some *Triprojectacites* fossil pollen. *American Journal of Botany*, *78,* 1172–1181.

Fedak, T., Sues, H-D., & Olsen, P. E. (2015). First record of the tritylodontid cynodont *Oligokyphus* and cynodont postcranial bones from the McCoy Brook Formation of Nova Scotia, Canada. *Canadian Journal of Earth Science, 52,* 244–249.

Fedosh, M. S. & Smoot, J. P. (1988). A cored stratigraphic section through the northern Newark basin, New Jersey. *U.S. Geological Survey Bulletin 1776*, 19–24.

Font, E., Youbi, N., Fernandes, S., El Hachimi, H., Kratinova, Z., & Hamim, Y. (2011). Revisiting the magnetostratigraphy of the Central Atlantic Magmatic Province (CAMP) in Morocco. *Earth and Planetary Science Letters, 309*(3–4), 302–317.

Fowell, S. J. (1993). *Palynology of Triassic/Jurassic boundary sections from the Newark supergroup of eastern North America: Implications for catastrophic extinction scenarios*. (Doctoral dissertation). New York: Columbia University.

Fowell, S. J., & Olsen, P. E. (1993). Time-calibration of Triassic/Jurassic microfloral turnover, eastern North America. *Tectonophysics, 222,* 361–369.

Fowell, S. J., & Traverse, A. (1995). Palynology and age of the upper Blomidon Formation, Fundy Basin, Nova Scotia. *Review of Palaeobotany and Palynology, 86*, 211–233.

Fowell, S. J., Cornet, B., & Olsen, P. E. (1994). Geologically rapid Late Triassic extinctions: Palynological evidence from the Newark supergroup. In G. D. Klein (Ed.), Pangaea: Paleoclimate, Tectonics and Sedimentation During Accretion, Zenith and Break-up of a Supercontinent (pp. 197–206). Geological Society of America Special Paper 288,

Fox, C. P., Whiteside, J. H., Olsen, P. E., Cui, X., Summons, R. E., & Grice, K. (2019). End-Triassic mass extinction not associated with massive input of light carbon. *PNAS*, submitted.

Furin, S., Preto, N., Rigo, M., Roghi, G., Gianolla, P., Crowley, J. L., & Bowring, S. A. (2006). High-precision U\Pb zircon age from the Triassic of Italy: implications for the Triassic time scale and the Carnian origin of calcareous nannoplankton and dinosaurs. *Geology*, *34,* 1009–1012.

Gabrielli, P., Barbante, C., Plane, J. M., Boutron, C. F., Jaffrezo, J. L., Mather, T. A., Stenni, B., Gaspari, V., Cozzi, G., Ferrari, C. and Cescon, P. (2008). Siderophile metal fallout to Greenland from the 1991 winter eruption of Hekla (Iceland) and during the global atmospheric perturbation of Pinatubo. *Chemical Geology*, *255*(1–2), 78–86.

Gallagher, W. & Hanczaryk, P. (2006). The West Patterson quarry: An Early Jurassic dinosaur track site in the Newark Basin of New Jersey. In J. D. Harris et al. (Eds.), *The Triassic-Jurassic terrestrial transition* (pp. 238–240). Albuquerque: New Mexico Museum of Natural History & Science Bulletin 37.

Gradstein, F. M., Agterberg, F. P., Ogg, J. G., Hardenbol, J., van Veen, P., Thierry, J., & Huang, Z. (1994). A Mesozoic timescale. *Journal of Geophysical Research, 99,* 24051–24074.

Greenberger, R. N., Mustard, J. F., Cloutis, E. A., Mann, P., Wilson, J. H., Flemming, R. L., Robertson, K. M., et al. (2015). Hydrothermal alteration and diagenesis of terrestrial lacustrine pillow basalts: Coordination of hyperspectral imaging with laboratory measurements. *Geochimica et Cosmochimica Acta*, *171,* 174–200.

Greenough, J. D., & Fryer, B. J. (1995). Behavior of the platinum-group elements during differentiation of the North

Mountain basalt, Nova Scotia. *The Canadian Mineralogist*, *33*(1), 153–163.

Griffin, C. T. & Nesbitt, S. J. (2019). Does the maximum body size of theropods increase across the Triassic-Jurassic boundary? Integrating ontogeny, phylogeny, and body size. *The Anatomical Record (2019),* 1–12. doi: 10.1002/ar.24130

Guex, J., Schoene, B., Bartolini, A., Spangenberg, J., Schaltegger, U., O'Dogherty, L., Taylor, D., et al. (2012). Geochronological constraints on post-extinction recovery of the ammonoids and carbon cycle perturbations during the Early Jurassic. *Palaeogeography, Palaeoclimatology, PalaeoecoIogy, 1–11,* 346–347.

Hallam, A. (1981). The end-Triassic bivalve extinction event. *Palaeogeography, Palaeoclimatology, PalaeoecoIogy, 35,* 1–44.

Heilman, J. J. (1987). That catastrophic day in the Early Jurassic. *Connecticut Journal of Science Education*, *25,* 8–25.

Hesselbo, S. P., Robinson, S. A., Surlyk, F. & Piasecki, S. (2002). Terrestrial and marine extinction at the Triassic-Jurassic boundary synchronized with major carbon-cycle perturbation: A link to initiation of massive volcanism?. *Geology, 30*(3), 251–254.

Hethke, M. (2014). *A multiproxy approach to studying lake ecosystems in the Mesozoic*. Unpublished PhD thesis. Universität at Erlangen-Nurnberg.

Hethke, M., Fürsich, F. T., Morton, J. D. & Jiang, B. (2018). Analysis of morphological variability in the clam shrimp *Eosestheria middendorfii* (Crustacea, Spinicaudata) from the Lower Cretaceous of China, and its implications for spinicaudatan taxonomy. *Papers in Palaeontology, 4*(1), 21–53.

Hillebrandt, A. V., Krystyn, L., Kürschner, W. M., Bonis, N. R., Ruhl, M., Richoz, S., Schobben, M. A. N., et al. (2013). The global stratotype sections and point (GSSP) for the base of the Jurassic system at Kuhjoch (Karwendel Mountains, Northern Calcareous Alps, Tyrol, Austria). *Episodes*, *36*(3), 162–198.

Holser, W. T., Clement, G. P., Jansa, L. F., & Wade, J. A. (1988). Evaporite deposits of the North Atlantic Rift. In W. Manspeizer (Ed.), *Triassic-Jurassic rifting: Continental breakup, and the formation of the Atlantic Ocean and Passive Margins, Pt. B, Developments in Geotectonics, 22* (pp. 525–556). Elsevier.

Hounslow, M. W., Posen, P. E. & Warrington, G. (2004). Magnetostratigraphy and biostratigraphy of the Upper Triassic and lowermost Jurassic succession, St. Audrie's Bay, UK. *Palaeogeography, Palaeoclimatology, Palaeoecology, 213*(3), 331–358.

Hubert, J. F., Reed, A. A., & Carey, P. J. (1976). Paleogeography of the East Berlin Formation, Newark Group, Connecticut Valley. *American Journal of Science*, *276*(10), 1183–1207.

Irmis, R. B., Martz, J. W., Parker, W. G., & Nesbitt, S. J. (2010). Re-evaluating the correlation between Late Triassic terrestrial vertebrate biostratigraphy and the GSSP-defined marine stages. *Albertiana*, *38,* 40–52.

Jones, D. S., Beaty, B. J., Schaller, M. F., Kent, D. V., & Olsen, P. E. (2017). Sedimentary Hg in Upper Triassic rift basins of eastern North America: CAMP volcanism, CO_2, and end-Triassic extinction. *Geological Society of America Abstracts with Programs*, *49*(6), doi: 10.1130/abs/2017AM–307100,

Kent, D. V., & Olsen, P. E. (1999). Astronomically tuned geomagnetic polarity timescale for the Late Triassic. *Journal of Geophysical Research, Solid Earth*, *104*(B6), 12831–12841.

Kent, D. V., & Olsen, P. E. (2000). Magnetic polarity stratigraphy and paleolatitude of the Triassic-Jurassic Blomidon Formation in the Fundy basin (Canada): Implications for early Mesozoic tropical climate gradients. *Earth and Planetary Science Letters*, *179*(2), 311–324.

Kent, D. V., & Olsen, P. E. (2008). Early Jurassic magnetostratigraphy and paleolatitudes from the Hartford continental rift basin (eastern North America): Testing for polarity bias and abrupt polar wander in association with the central Atlantic magmatic province. *Journal of Geophysical Research*, *113*, B06105. doi: 10.1029/2007JB005407

Kent, D. V. & Tauxe, L. (2005). Corrected paleolatitudes for Pangea in the Late Triassic. *Science, 307,* 240–244.

Kent, D. V., Olsen, P. E., & Muttoni, G. (2017). Astrochronostratigraphic polarity time scale (APTS) for the Late Triassic and Early Jurassic from continental sediments and correlation with standard marine stages. *Earth-Science Reviews*, *166,* 153–180.

Kent, D. V., Olsen, P. E., & Witte, W. K. (1995). Late Triassic-Early Jurassic geomagnetic polarity and paleolatitudes from drill cores in the Newark rift basin (Eastern North America). *Journal of Geophysical Research, 100*(B8), 14,965–14,998.

Kent, D. V., Olsen, P. E., Rasmussen, C., Lepre, C, Mundil, R., Irmis, R. B., Gehrels, G., et al. (2018). Empirical evidence for stability of the 405-kiloyear Jupiter-Venus eccentricity cycle over hundreds of millions of years. *PNAS, 115*(24), 6153–6158.

Knight, K. B., Nomade, S., Renne, P.R., Marzoli, A., Bertrand, H., & Youbi, H. (2004). The Central Atlantic Magmatic Province at the Triassic-Jurassic boundary: Paleomagnetic and $^{40}Ar/^{39}Ar$ evidence from Morocco for brief, episodic volcanism. *Earth and Planetary Science Letters, 228,* 143–160.

Kozur, H. W., & Weems, R. E. (2005). Conchostracan evidence for a late Rhaetian to early Hettangian age for the CAMP volcanic event in the Newark Supergroup, and a Sevatian (late Norian) age for the immediately underlying beds. *Hallesches Jahrbuch für Geowissenschaften B*, *27,* 21–51.

Kozur, H. W., & Weems, R. E. (2007). Upper Triassic conchostracan biostratigraphy of the continental rift basins of eastern North America: Its importance for correlating Newark supergroup events with the Germanic basin and the international geologic timescale. *New Mexico Museum of Natural History and Science Bulletin*, *41*, 137–188.

Kozur, H. W., & Weems, R. E. (2010). The biostratigraphic importance of conchostracans in the continental Triassic of the northern hemisphere. In S. G. Lucas (Ed.), *The Triassic timescale* (pp. 315–417). Geological Society, London, Special Publications 334.

Krynine, P. D. (1950). Petrology, stratigraphy and origin of the Triassic sedimentary rocks of Connecticut. *Connecticut Geological and Natural History Survey Bulletin No. 73*.

Kuerschner, W. M., Bonis, N. R., & Krystyn, L. (2007). Carbon-isotope stratigraphy and palynostratigraphy of the Triassic-Jurassic transition in the Tiefengraben section-Northern Calcareous Alps (Austria). *Palaeogeograraphy, Palaeoclimatology, Palaeoecology, 244*, 257–280.

Kuroda, J., Hori, R. S., Suzuki, K., Gröcke, D. R.. & Ohkouchi, N. (2010). Marine osmium isotope record across the Triassic-Jurassic boundary from a Pacific pelagic site. *Geology, 38*(12), 1095–1098.

Kyte, F. T., & Wasson, J. T. (1982). A search for iridium anomalies in sediments deposited during the past 70 Ma. *Lunar and Planetary Science Conference, 13,* 411–412.

Kyte, F. T., & Wasson, J. T. (1986). Accretion rate of extraterrestrial matter: Iridium deposited 33 to 67 million years ago. *Science, 232,* 1225–1229.

Le Marrec, A. (1985). Carte géologique du Marroc, feuille Demnate. *Notes et Memoires du Service Géologique du Maroc*, 338.

Li, D., Li, R., Wang, B., Liu, Z., Wu, X., Liu, F., Zhao, B., et al. (2016). Study on oil-source correlation by analyzing organic geochemistry characteristics: A case study of the Upper Triassic Yanchang formation in the south of Ordos Basin, China. *Acta Geochimica, 35*(4), 408–420.

Li, M., Kump, L. R., Hinnov, L. A., & Mann, M. E. (2018). Tracking variable sedimentation rates and astronomical forcing in Phanerozoic paleoclimate proxy series with evolutionary correlation coefficients and hypothesis testing. *Earth and Planetary Science Letters*, *501*, 165–179.

Lindström, S., van de Schootbrugge, B., Hansen, K. H., Pedersen, G. K., Alsen, P., Thibault, N., Dybkjær, K., et al. (2017). A new correlation of Triassic-Jurassic boundary successions in NW Europe, Nevada and Peru, and the Central Atlantic Magmatic Province: A time-line for the end-Triassic mass extinction. *Palaeogeography, Palaeoclimatology, Palaeoecology, 478,* 80–102.

Lodders, K., & Fegley, B., Jr. (1998). *The planetary scientist's companion*. New York: Oxford University Press.

Lowe, D. J., & Hunt, J. B. (2001). A summary of terminology used in tephra-related studies. *Les Dossiers de I'Archéo-Logis, 1,* 17–22.

Lucas S. G., & Tanner, L. H. (2007). The nonmarine Triassic-Jurassic boundary in the Newark Supergroup of eastern North America. *Earth-Science Reviews*, *84*, 1–20.

Lucas, S. G., & Tanner, L. H. (2008). Reexamination of the end-Triassic mass extinction. In A. M. T. Elewa (Ed.), *Mass extinction* (pp. 66–103). New York: Springer Verlag.

Lucas, S. G., & Tanner, L. H. (2018). The Missing Mass Extinction at the Triassic-Jurassic Boundary. In: Tanner L. (Ed.), The Late Triassic World (pp. 721–785), Topics in Geobiology 46, Springer, Cham.

Lucas, S. G., Klein, H., Lockley, M. G., Spielmann, J. A., Gierlinski, G. D., Hunt, A. P., & Tanner, L. H. (2006). Triassic-Jurassic stratigraphic distribution of the theropod footprint ichnogenus *Eubrontes*. *New Mexico Museum of Natural History and Science Bulletin, 37,* 86–93.

Lucas, S. G., Tanner, L. H., Kozur, H. W., Weems, R. E., & Heckert, A. B. (2012). The Late Triassic timescale: Age and correlation of the Camian-Norian boundary. *Earth-Science Reviews, 114,* 1–18.

Mader, N. K., Redfern, J., & El Ouataoui, M. (2017). Sedimentology of the Essaouira Basin (Meskala Field) in context of regional sediment distribution patterns during upper Triassic pluvial events. *Journal of African Earth Sciences, 130,* 293–318.

Maisch, M. W., & Kapitzke, M. (2010). A presumably marine phytosaur (Reptilia: Archosauria) from the preplanorbis beds (Hettangian) of England. *Neues Jahrbuch für Geologie und Paläontologie-Abhandlungen*, *257*(3), 373–379.

Malinconico, M. L. (2002). *Lacustrine organic sedimentation, organic metamorphism, and thermal history of selected Early Mesozoic Newark Supergroup basins, Eastern U.S.A*. Ph.D. dissertation. New York: Columbia University.

Malinconico, M. L. (2010). Chapter C: Synrift to early postrift basin-scale groundwater history of the Newark Basin based on surface and borehole vitrinite reflectance data. In G. C. Herman & M. E. Serfes (Eds.), *Contributions to the geology and hydrogeology of the Newark basin* (pp. C1–C38). Trenton, N.J.: Geological Survey Bulletin 77.

Mander, L., Twitchett, R. J., & Benton, M. J. (2008). Palaeoecology of the Late Triassic extinction event in the SW UK. *Journal of the Geological Society*, *165,* 319–332.

Maron, M., Rigo, M., Bertinelli, A., Katz, M.E., Godfrey, L., Zaffani, M., & Muttoni, G., (2015). Magnetostratigraphy, biostratigraphy, and chemostratigraphy of the Pignola- Abriola section: New constraints for the Norian-Rhaetian boundary. *Geological Society of America Bulletin, 127*(7–8), 962–974.

Mártin-Mártin, J. D., Vergés, J., Saura, E., Moragas, M., Messager, G., Baqués, V., Razin, P., et al. (2017). Diapiric growth within an Early Jurassic rift basin: The Tazoult salt wall (central High Atlas, Morocco). *Tectonics*, *36,* 2–32.

Marzoli, A., Bertrand, H., Knight, K. B., Cirilli, S., Buratti, N., Verati, C., Nomade, S., et al. (2004). Synchrony of the Central Atlantic magmatic province and the Triassic-Jurassic boundary climatic and biotic crisis. *Geology, 32,* 973–976.

Marzoli, A., Bertrand, H., Youbi, N., Callegaro, S., Merle, R., Reisberg, L., Chiaradia, M., et al. (2019). The Central Atlantic Magmatic Province (CAMP) in Morocco. *Journal of Petrology, 60*(5), 945–996.

Marzoli, A., Callegaro, S., Dal Corso, J., Davies, J. H., Chiaradia, M., Youbi, N., Bertrand, H., et al. (2018). The Central Atlantic Magmatic Province (CAMP): A review. In L. Tanner (Ed.), *The Late Triassic world* (pp. 91–125). Cham.: Springer.

Marzoli, A., Renne, P. R, Piccirillo, E. M., Ernesto, M., Bellieni, G., & DeMin, A. (1999). Extensive 200 million years old continental flood basalts from the Central Atlantic Magmatic Province. *Science, 248,* 616–618.

Mattis, A. F. (1977). Nonmarine Triassic sedimentation, Central High Atlas, Morocco. *Journal of Sedimentary Petrology, 47*(1), 107–119.

McDonough, W. F., & Sun, S. S. (1995). The composition of the Earth. *Chemical Geology*, *120*(3–4), 223–253.

McElwain, J. C., Beerling, D. J., & Woodward, F. I. (1999). Fossil plants and global warming at the Triassic-Jurassic boundary. *Science*, *285*(5432), 1386–1390.

Miller, K. G., Sherrell, R. M., Browning, J. V., Field, M. P., Gallagher, W., Olsson, R. K., Sugarman, P.J., et al. (2010). Relationship between mass extinction and iridium across the Cretaceous-Paleogene boundary in New Jersey. *Geology*, *38*(10), 867–870.

Morton, J. D., Whiteside, D. I., Hethke, M., & Benton, M. J. (2017). Biostratigraphy and geometric morphometrics of

conchostracans (Crustacea, Branchiopoda) from the Late Triassic fissure deposits of Cromhall Quarry, UK. *Palaeontology*, *60*(3), 349–374.

Mossman, D. J., Grantham, R. G. & Langenhorst, F. (1998). A search for shocked quartz at the Triassic-Jurassic boundary in the Fundy and Newark basins of the Newark Supergroup. *Canadian Journal of Earth Science*, *35,* 101–109.

Muttoni, G., Kent, D. V., Olsen, P. E., Stefano, P. D., Lowrie, W., Bernasconi, S. M., & Hernández, F. M. (2004). Tethyan magnetostratigraphy from Pizzo Mondello (Sicily) and correlation to the Late Triassic Newark astrochronological polarity time scale. *Geological Society of America, Bulletin, 16*(9–10), 1043–1058.

Newell, N. D. (1967). Revolutions in the history of life. In C. C. Albritton Jr., et al. (Eds.), *Uniformity and simplicity: A symposium on the principle of the uniformity of nature* (pp. 63–91). Geological Society of America Special Paper, 89.

Nickerson, R. S. (1998). Confirmation bias: A ubiquitous phenomenon in many guises. *Review of General Psychology, 2* (2), 175–220.

Norris, R. D., Firth, J., Blusztajn, J. S., & Ravizza, G. (2000). Mass failure of the North Atlantic margin triggered by the Cretaceous-Paleogene bolide impact. *Geology*, *28*(12), 1119–1122.

Olsen, P. E. (1986). A 40-million-year lake record of early Mesozoic orbital climatic forcing. *Science*, *234*(4778), 842–848.

Olsen, P. E., & Et-Touhami, M. (2008). *Field trip #1: Tropical to subtropical syntectonic sedimentation in the Permian to Jurassic Fundy rift basin, Atlantic Canada, in relation to the Moroccan conjugate margin*. Central Atlantic Conjugate Margins Conference Halifax, Nova Scotia, Canada, August 2008.

Olsen, P. E., & Kent, D. V. (1996). Milankovitch climate forcing in the tropics of Pangea during the Late Triassic. *Palaeogeography, Palaeoclimatology, Palaeoecology*, *122*(1–4), 1–26.

Olsen, P. E., & Kent, D. V. (1999). Long-period Milankovitch cycles from the Late Triassic and Early Jurassic of eastern North America and their implications for the calibration of the early Mesozoic time scale and the long-term behavior of the planets. *Philosophical Transactions of the Royal Society of London A*, *357,* 1761–1787.

Olsen, P. E., Kent, D. V., & Et-Touhami, M. (2003a). Chronology and stratigraphy of the Fundy and related Nova Scotia offshore basins and Morocco based on core and outcrop. In D. Brown (Ed.), *Conventional core workshop* (pp. 51–63.). Geological Society of America (NE Section) and Atlantic Geoscience Society, Halifax.

Olsen, P. E., Kent, D. V., & Whiteside, J. H. (2011). Implications of the Newark Supergroup-based astrochronology and geomagnetic polarity time scale (Newark-APTS) for the tempo and mode of the early diversification of the Dinosauria. *Earth and Environmental Science Transactions of the Royal Society of Edinburgh*, *101,* 201–229.

Olsen, P. E., Kent, D. V., Cornet, B., Witte, W. K., & Schlische, R. W. (1996a). High-resolution stratigraphy of the Newark rift basin (Early Mesozoic, Eastern North America). *Geological Society of America Bulletin*, *108,* 40–77.

Olsen, P. E., Kent, D. V., Et-Touhami, M., & Puffer, J. (2003b). Cyclo-, magneto-, and bio-stratigraphic constraints on the duration of the CAMP event and its relationship to the Triassic-Jurassic boundary. *Geophysical Monographs, 136,* 7–32.

Olsen, P. E., Kent, D. V., Sues, H.-D., Koeberl, C., Huber, H., Montanari, A., Rainforth, E. C., et al. (2002a). Ascent of dinosaurs linked to an iridium anomaly at the Triassic-Jurassic boundary. *Science*, *296*(5571), 1305–1307.

Olsen, P. E., Kinney, S. T., Stüeken, E., Jaret, S., Percival, L., Philpotts, A. R., & Whiteside, J. H. (2019c). Two CAMP explosive eruptions. *Goldschmidt Abstracts, 2019*. https://goldschmidt.info/2019/abstracts/abstractView?id=2019005267

Olsen, P. E., Kinney, S. T., Zakharova, N. V., Schlische, R. W, Withjack, M. O., Kent, D. V., Goldberg, D. S., et al. (2016b). New insights on rift basin development and the geological carbon cycle, mass extinction, and carbon sequestration from outcrops and new core, drill holes, and seismic lines from the northern Newark Basin (New York and New Jersey). In A. E. Gates (Ed.), *88th Annual New York State Geological Field Conference, guidebook, geologic diversity in the New York metropolitan area* (pp. 190–274). New York State Geological Association.

Olsen, P. E., Koeberl, C., Huber, H., Montanari, A., Fowell, S. J., Et-Touhami, M. & Kent, D. V. (2002b). Continental Triassic-Jurassic boundary in central Pangea: Recent progress and discussion of an Ir anomaly. In C. Koeberl & K. G. MacLeod (Eds.), *Continental Triassic-Jurassic boundary in central Pangea: Recent progress and discussion of an Ir anomaly* (pp. 505–522). Geological Society of America Special Paper 356, Boulder, Colorado, Geological Society of America.

Olsen, P. E., Laskar, J., Kent, D. V., Kinney, S. T., Reynolds, D. J., Sha, J., & Whiteside, J. H. (2019a). The geological orrery: Mapping chaos in the solar system. *PNAS,* in press.

Olsen. P. E., Philpotts, A. R., McDonald, N. G., Steinen, R. P., Kinney, S. T., Jaret, S. J., & Rasbury, E. T. (2016a). Wild and wonderful implications of the 5 mm Pompton Ash of the Hartford and Newark basins (Early Jurassic, Eastern North America). *Geological Society of America Abstracts with Programs, Northeastern Section*, *48*(2). doi: 10.1130/abs/2016NE–272509

Olsen P. E., Schlische, R. W., & Fedosh, M. S. (1996b). 580 ky duration of the Early Jurassic flood basalt event in eastern North America estimated using Milankovitch cyclostratigraphy. In M. Morales (Ed.), *The continental Jurassic* (pp. 11–22)*, vol. 60, Albuquerque: Museum of Northern Arizona Bulletin*. Albuquerque: New Mexico Museum of Natural History and Science.

Olsen, P. E., Shubin, N. H., & Anders, P. E. (1987). New Early Jurassic tetrapod assemblages constrain Triassic-Jurassic tetrapod extinction event. *Science*, *237,* 1025–1029.

Olsen, P. E., Whiteside, J. H., & Huber, P. (2003c). Causes and consequences of the Triassic-Jurassic mass extinction as seen from the Hartford basin. In J. B. Brady & J. T. Cheney (Eds.), *Guidebook for field trips in the five college region, 95th New England Intercollegiate Geological Conference*

(pp. B5-1–B5-41). Northampton, Mass.: Department of Geology, Smith College.

Olsen, P. E., Whiteside, J. H., LeTourneau, P. M., & Huber, P. (2005). Jurassic cyclostratigraphy and paleontology of the Hartford basin. In B. J. Skinner & A. R. Philpotts (Eds.), *97th New England intercollegiate geological conference* (pp. A4-1–A4-51). New Haven: Department of Geology and Geophysics, Yale University.

Olsen, P. E., Whiteside, J. H, Steinen, R. P., & Kinney, S. T. (2019b). New cores resolve an old geochronological conundrum for the Central Atlantic Magmatic Province (CAMP) extrusive zone in the Newark, Hartford, and Deerfield Basins. *Geological Society of America Abstracts with Programs*. doi: 10.1130/abs/2019NE-328007

Orth, C. J ., Attrep, M., & Quintana, L. R. (1990). Iridium abundance patterns across bio-event horizons in the fossil record. In V. L. Sharpton & P. D. Ward (Eds.), *Global catastrophes in earth history: An interdisciplinary conference on impacts, volcanism, and mass mortality* (pp. 45–59). GeoScience World.

Panfili, G., Cirilli, S., Dal Corso, J., Bertrand, H., Medina, F., Youbi, N., & Marzoli, A. (2019). New biostratigraphic constraints show rapid emplacement of the Central Atlantic Magmatic Province (CAMP) during the end-Triassic mass extinction interval. *Global and Planetary Change, 172,* 60–68.

Parker, R. A., Houghton, H. F., & McDowell, R. C. (1988). Stratigraphic framework and distribution of early Mesozoic rocks of the northern Newark Basin, New Jersey and New York. *U.S. Geological Survey Bulletin 1776*, 31–39.

Percival, L. M., Ruhl, M., Hesselbo, S. P., Jenkyns, H. C., Mather, T. A. & Whiteside, J. H., (2017). Mercury evidence for pulsed volcanism during the end-Triassic mass extinction. *Proceedings of the National Academy of Sciences, 114*(30), 7929–7934.

Pratt, L. M., Shaw C. A., & Burruss, R. C. (1988). Thermal histories of the Hartford and Newark basins inferred from maturation indices of organic matter. In A. J. Froelich & G. R. Robinson (Eds.), *Studies of the Early Mesozoic basins of the eastern United States* (pp. 58–63). U.S. Geological Survey Bulletin 1776.

Puffer, J. H., Block, K. A., Steiner, J. C., & Laskowich, C. (2018). Complex layering of the Orange Mountain Basalt: New Jersey, USA. *Bulletin of Volcanology*, *80*(6), 54.

Radley, J. D., Twitchett, R. J., Mander, L. & Cope, J. C. W. (2008). Discussion on palaeoecology of the Late Triassic extinction event in the SW UK. *Journal of the Geological Society*, *165*(5), 988–992.

Raup, D. M., & Sepkoski, J. J. (1982). Mass extinctions in the marine fossil record. *Science, 215,* 1501–1503.

Rehkämper, M., Halliday, A. N., Alt, J., Fitton, J. G., Zipfel, J. & Takazawa, E. (1999). Non-chondritic platinum-group element ratios in oceanic mantle lithosphere: petrogenetic signature of melt percolation? *Earth and Planetary Science Letters*, *172*(1–2), 65–81.

Richardson, T., & Burnham, O. M. (2002). *Precious metal analysis at the Geosciences Laboratories: results from the new low-level analytical facility*. (Open File Report 6100). Sudbury, Ontario, Canada: Ontario Geological Survey.

Robinson, N., Ravizza, G., Coccioni, R., Peucker-Ehrenbrink, B., & Norris, R. (2009). A high-resolution marine 187Os/188Os record for the late Maastrichtian: Distinguishing the chemical fingerprints of Deccan volcanism and the KP impact event. *Earth and Planetary Science Letters*, *281*(3–4),159–168.

Ruhl, M., Kürschner, W. M., & Krystyn, L. (2009). Triassic-Jurassic organic carbon isotope stratigraphy of key sections in the western Tethys realm (Austria). *Earth and Planetary Science Letters*, *281*(3–4), 169–187.

Saito, T., Yamanoi, T., & Kaiho, K. (1986). Devastation of the terrestrial flora at the end of the Cretaceous in the Boreal Far East. *Nature*, *323*, 253–256.

Saura, E., Vergés, J., Martín-Martín, J. D., Messager, G., Moragas, M., Razin, P., Grélaud, C., et al. (2014). Syn-to post-rift diapirism and minibasins of the Central High Atlas (Morocco): The changing face of a mountain belt. *Journal of the Geological Society*, *171*(1), 97–105.

Schaller, M., Olsen, P. E., Wright, J. D., & Kent, D. V. (2016). A gradual increase in pCO_2 across the abrupt across the abrupt end-Triassic extinction. *Geological Society of America, Abstracts with Programs, 47*(7), paper 267142.

Schaller, M. F., Wright, J. D., & Kent, D. V. (2011). Atmospheric pCO_2 perturbations associated with the Central Atlantic magmatic province. *Science*, *331*(6023), 1404–1409.

Schaller, M. F., Wright, J. D., & Kent, D. V. (2015). A 30 Myr record of Late Triassic atmospheric pCO_2 variation reflects a fundamental control of the carbon cycle by changes in continental weathering. *Geological Society of America Bulletin*, *127*(5–6), 661–671.

Schaller, M. F., Wright, J. D., Kent, D. V., & Olsen, P. E. (2012). Rapid emplacement of the Central Atlantic Magmatic Province as a net sink for CO_2. *Earth and Planetary Science Letters*, *323,* 27–39.

Schmieder, M., Buchner, E., Schwarz, W. H., Trieloff, M., & Lambert, P. (2010). A Rhaetian $^{40}Ar/^{39}Ar$ age for the Rochechouart impact structure (France) and implications for the latest Triassic sedimentary record. *Meteoritics & Planetary Science, 45,* 1225–1242.

Schmitz, B., & Asaro, F. (1996). Iridium geochemistry of volcanic ash layers from the early Eocene rifting of the northeastern North Atlantic and some other Phanerozoic events. *Geological Society of America Bulletin*, *108*(4), 489–504

Scholze, F., & Schneider, J. W. (2015). Improved methodology of "conchostracan" (Crustacea: Branchiopoda) classification for biostratigraphy. *Newsletters on Stratigraphy, 48,* 287–298.

Silvestri, S., & Olsen, P. E. (1988). Uniquely preserved trackway of the reptile ichnotaxon *Rhynchosauroides hyperbates Baird from the Late Triassic of Arcola, Pa., associated forms, and significance to Carnian-Norian tetrapod extinctions. Geological Society of America, Abstracts with Programs, 20*(1), 70.

Smith, R. C., Birkheiser, S. W., Jr., & Barnes, J. H. (1989). Strange clay baffles geologists. *Pennsylvania Geology*, *19,* 8–13.

Smoot, J. P. (2010). Chapter A: Triassic depositional facies in the Newark Basin. In , G. C. Herman & M. E. Serfes (Eds.), *Contributions to the geology and hydrogeology of the Newark basin* (pp. A1–A110). Trenton, N.J.: Geological Survey Bulletin 77.

Smoot, J. P., & Olsen, P. E. (1988). Massive mudstones in basin analysis and paleoclimatic interpretation of the Newark Supergroup. In W. Manspeizer (Ed.), *Triassic-Jurassic rifting and the opening of the Atlantic Ocean* (pp. 249–274). Amsterdam: Elsevier.

Smoot, J. P., & Olsen, P. E. (1994). Climatic cycles as sedimentary controls of rift basin lacustrine deposits in the early Mesozoic Newark basin based on continuous core. In A. J. Lomando & M. Harris, *Lacustrine depositional systems* (pp. 201–237). SEPM Core Workshop Notes, 19.

Spiker, E. C., Kotra, R. K., Hatcher, P. G., Gottfried, R. M., Horan, M. F. & Olsen, P. E. (1988). Source of kerogen in black shales from the Hartford and Newark basins, eastern United States. *United States Geological Survey Bulletin 1776,* 63–68.

Stahl, W. J. (1977). Carbon and nitrogen isotopes in hydrocarbon research and exploration. *Chemical Geology*, *20*(2), 121–149.

Steinen, R. P., Martin, L. G., Conti, A. A., Jorgensen, C. T., & Gierlowski-Kordesch, E. H. (2015). Stratigraphic observations on cored boreholes in the Mesozoic Hartford Basin, Hartford, Connecticut. *Geological Society of America Abstracts with Programs, 47*(3), 54.

Steinwehr, H. V. (1969). The pigment in red beds: A geologic thermometer. *Naturwissenschaften*, *56*(10), 513–514.

Sues, H-D., & Olsen, P. E. (2015). Stratigraphic and temporal context and faunal diversity of Permian-Jurassic continental tetrapod assemblages from the Fundy rift basin, eastern Canada. *Atlantic Geology*, *51,* 139–205.

Tagle, R., Schmitt, R. T., & Erzinger, J. (2009). Identification of the projectile component in the impact structures Rochechouart, France, and Sääksjärvi, Finland: Implications for the impactor population for the earth. *Geochimica et Cosmochimica Acta*, *73*(16), 4891–4906.

Tanner, L. H. (2010). The Triassic isotope record, the Triassic timescale. In S. G. Lucas (Ed.), *The Triassic timescale* (pp. 103–118). Geological Society, London, Special Publication 334.

Tanner, L. H., & Kyte, F. T. (2005). Anomalous iridium enrichment at the 1iiassic-Jurassic boundary, Blomidon formation, Fundy basin, Canada. *Earth and Planetary Science Letters, 240,* 634–641.

Tanner, L. H., & Kyte, F. T. (2016). New report of elevated Ir in Upper Triassic-Lower Jurassic strata of the Newark supergroup. *Geological Society of America Abstracts with Programs, 48*(2). doi: 10.1130/abs/2016NE–271941

Tanner, L. H., & Lucas, S. G. (2015). The Triassic-Jurassic strata of the Newark Basin, USA: A complete and accurate astronomically-tuned timescale? *Stratigraphy*, *12,* 47–65.

Tanner, L. H., Kyte, F. T., & Walker, A. E. (2008). Multiple Ir anomalies in uppermost Triassic to Jurassic age strata of the Blomidon formation, Fundy basin, eastern Canada. *Earth and Planetary Science Letters, 274,* 103–111.

Tanner, L. H., Kyte, F. T., Richoz, S., & Krystyn, L. (2016). Distribution of iridium and associated geochemistry across the Liassic-Jurassic boundary in sections at Kuhjoch and Kendlbach, Northern Calcareous Alps, Austria. *Palaeogeography, Palaeoclimatology, Palaecology 449,* 13–26. https://doi.org/10.1016/j.palaeo.2016.01.011

Tashiro, T., Ishida, A., Hori, M., Igisu, M., Koike, M., Méjean, P., Takahata, N., et al. (2017). Early trace of life from 3.95 Ga sedimentary rocks in Labrador, Canada. *Nature*, *549*(7673), 516–518.

Thulborn, T. (2003). Comment on "Ascent of dinosaurs linked to an iridium anomaly at the Triassic-Jurassic boundary." *Science*, *301*(11),169b.

Tollo, R. P., & Gottfried, D. (1992). Petrochemistry of Jurassic basalt from eight cores, Newark basin, New Jersey: Implications for the volcanic petrogenesis of the Newark supergroup. *Geological Society of America Special Paper 268*, 233–260.

Torrent, J., & Schwertmann, U. (1987). Influence of hematite on the color of red beds. *Journal of Sedimentary Research*, *57*(4), 682–686.

Tschudy, R. H., Pillmore, C. L., Orth, C. J., Gimore, J. S., & Knight, J. D. (1984). Disruption of the terrestrial plant ecosystems at the Cretaceous-Tertiary boundary, western interior, North America. *Science 225*, 1030–1032.

Tütken, T. (2011). The diet of Sauropod dinosaurs: Implications of carbon isotope analysis on teeth, bones, and plants. In N. Klein et al. (Eds.), *Biology of the Sauropod dinosaurs: Understanding the life of giants* (pp. 57–79). Bloomington and Indianapolis: Indiana University Press.

Vajda, V., & Bercovici, A. (2014). The global vegetation pattern across the Cretaceous-Paleogene mass extinction interval: A template for other extinction events. *Global and Planetary Change, 122,* 29–49.

Van Houten, F. B. (1964). Cyclic lacustrine sedimentation, upper Triassic Lockatong formation, central New Jersey and adjacent Pennsylvania. In D. F. Merriam (Ed.), *Symposium on cyclic sedimentation: Vol. 169* (pp. 497–531). Kansas Geological Survey Bulletin.

Van Veen, P. M. (1995). Time calibration of Triassic/Jurassic microfloral turnover, eastern North America: Comment. *Tectonophysics, 245,* 91–95.

Wade, J. A., Brown, D. E., Traverse, A., & Fensome, R. A. (1996). The Triassic-Jurassic Fundy Basin, eastern Canada: Regional setting, stratigraphy and hydrocarbon potential. *Atlantic Geology*, *32*, 189–231.

Walker, T. R., Larson, E. E. & Hoblitt, R. P. (1981). Nature and origin of hematite in the Moenkopi Formation (Triassic), Colorado Plateau: A contribution to the origin of magnetism in red beds. *Journal of Geophysical Research: Solid Earth*, *86*(B1), 317–333.

Warrington, G., & Ivimey-Cook, H. C. (1992). Triassic. In: J. C. W. Cope, J. K. Ingham, & P. F. Rawson (Eds.), *Atlas of palaeogeography and lithofacies* (pp. 97–106). Geological Society, London, Memoirs, 13.

Weems, R. E. (1992). The "terminal Triassic catastrophic extinction event" in perspective: A review of Carboniferous through Early Jurassic terrestrial vertebrate extinction patterns. *Palaeogeography, Palaeoclimatology, Palaeoecology, 94,* 1–29.

Weems, R. E., & Lucas, S. G. (2015). A revision of the Norian conchostracan zonation in North America and its implications for Late Triassic North American tectonic history. *New Mexico Museum of Natural History and Science Bulletin*, *67,* 303–317.

Whiteside, J. H., Olsen, P. E., Eglinton, T. I., Brookfield, M. E., & Sambrotto, R. N. (2010). Compound-specific carbon isotopes from Earth's largest flood basalt province directly link eruptions to the end-Triassic mass extinction. *Proceedings of the National Academy of Sciences, 107,* 6721–6725.

Whiteside, J. H., Olsen, P. E., Eglinton, T. I., Cornet, B., McDonald, N. G., & Huber, P. (2011). Pangean great lake paleoecology on the cusp of the end-Triassic extinction. *Palaeogeography, Palaeoclimatology, and Palaeoecology*, *301*(1–4), 1–17.

Whiteside, J. H., Olsen, P. E., Kent, D. V., Fowell, S. J. & Et-Touhami, M. (2007). Synchrony between the CAMP and the Triassic-Jurassic mass-extinction event? *Palaeogeography, Palaeoclimatology, and Palaeoecology*, *244*(1–4), 345–367.

Whiteside, J. H., Olsen, P. E., Kent, D. V., Fowell, S. J. & Et-Touhami, M. (2008). Synchrony between the Central Atlantic magmatic province and the Triassic-Jurassic mass-extinction event? Reply to comment of Marzoli et al. *Palaeogeography, Palaeoclimatology, Palaeoecology*, *262*(3–4), 194–198.

Withjack, M. O., Schlische, R. W., Malinconico, M. L., & Olsen, P. E. (2013). Rift-basin development: Lessons from the Triassic-Jurassic Newark Basin of eastern North America. *Geological Society, London, Special Publications, 369*(1), 301–321.

Wotzlaw, F. Jr., Guex, J., Bartolini, A., Gallet, Y., Krystyn, L., McRoberts, C. A., Taylor, D., et al. (2014). Towards accurate numerical calibration of the Late Triassic: High-precision U-Pb geochronology constraints on the duration of the Rhaetian. *Geology.* http://dx.doi.org/10.1130/G35612.1

Yager, J. A., West, A. J., Corsetti, F. A., Berelson, W. M., Rollins, N. E., Rosas, S., & Bottjer, D. J. (2017). Duration of and decoupling between carbon isotope excursions during the end-Triassic mass extinction and Central Atlantic Magmatic Province emplacement. *Earth and Planetary Science Letters*, *473,* 227–236.

Zaffani, M., Jadoul, F. & Rigo, M. (2018). A new Rhaetian δ13Corg record: Carbon cycle disturbances, volcanism, End-Triassic mass extinction (ETE). *Earth-Science Reviews*, *178*, 92–104.

APPENDIX 1: NOTES

1. The 1993 discoveries of a "fern spike" (Fowell, 1993; Fowell et al., 1994) and a thin coaly layer and underlying "strange white clay" (Smith et al., 1989) at the dramatic Triassic-Jurassic sporomorph turnover in the Jacksonwald Syncline of the Newark Basin, assumed at the time to be the system boundary, (Cornet 1977; Fowell et al., 1993, 1994), were so eerily similar to features found at the K-Pg boundary in the Raton Basin (text Fig. 12.1) (e.g., Tschudy et al., 1984), that it sparked a search for an Ir anomaly following the Alvarez et al. (1980) bolide impact paradigm. A modest Ir anomaly 2 to 4 times (0.100–0.300 ng/g) background was found at four localities precisely at the fern spike (Olsen et al., 2002a) horizon. These were temporally consistent with the tetrapod faunal turnover (i.e., both ichno- and skeletal fossils) in the Newark Basin of eastern North America (Olsen et al., 2002a, 2002b), strengthening the suggestion that another mass extinction was caused by an extraterrestrial impact, and suggesting that the ecological ascent of the dinosaurs, particularly large theropods, the footprints of which (*Eubrontes giganteus*) are limited to strata above the fern spike, was tied to the mass extinction by character release or immigration. This biotic transition was at the time identified with the Triassic-Jurassic system boundary in Europe by palynologists and placed at the extinction level but the establishment of the GSSP at the first appearance of the ammonite *Psiloceras spelae tirolicum* now places the system boundary well above the extinction level (Hillebrandt et al., 2013).
2. Griffin and Nesbitt (2019) argue that the osteological and footprint record does not reflect the maximum size of Triassic theropods, despite the fact that both independent data sets are mutually consistent. Instead they propose that morphological and histological data suggest the largest skeletal remains of Triassic theropods reflect immature individuals and Triassic theropods were significantly larger than both the skeletal and footprint records indicate. However, this argument makes unstated assumptions about sexual maturity and population dynamics and we regard the empirical data showing a 20% increase in the maximum size of footprints attributed to theropods to be a real phenomenon. *Eubrontes giganteus* and similar-sized footprints of 30–35 cm length are abundant (thousands of footprints) in just post-ETE strata and continuing through the next few million years of the Newark Supergroup record. There are none before the ETE in eastern North America reflecting a massive ecological shift at least in the tropics and subtropics, whether it is caused by evolution or immigration of larger-sized forms.
3. The abrupt increase in the size of theropod dinosaurs at the palynological transition has been questioned on the basis of very large, seemingly tridactyl footprints from much earlier in the Late Triassic (Carnian Age) that were asserted to be "identical" to *Eubrontes* [*giganteus*] known in eastern North America only above the palynological turnover, and therefore the rise of large theropods was not connected to the mass extinction (Thulborn, 2003). Such arguments against the mass extinction itself and the possible presence of a hiatus have since amplified (e.g., Kozur & Weems, 2005, 2007, 2010; Lucas & Tanner, 2007, 2008, 2018; Lucas et al., 2006). These occurrences of *Eubrontes* are dubious on morphological grounds, of dubious age, or in strata that actually postdate

the initiation of the ETE, even if being nominally latest Triassic age (e.g., in Sweden) (Olsen et al., 2011). In addition, the taxonomy of the ichnogenus *Eubrontes* is in need of revision, and we argue that it is the size of the footprints attributed to theropods that is of ecological and evolutionary interest, not if they are called *Eubrontes* sp. or *Kayentapus* sp., etc.

4. Below the Newark ETE there are two less dramatic intervals of change. One of these is in the lower Passaic Formation of the Newark Basin and occurs in sporomorph assemblages alone (i.e., there are no apparent changes in footprint assemblages) (Silvestri et al., 1988; Olsen et al., 2011). It is poorly resolved but is nominally between the New Oxford-Lockatong and overlying Lower Passaic-Heidlersburg palynofloras of Cornet (1977) and Cornet and Olsen (1985) between ~215 and 217 Ma on the Newark-Hartford APTS (Kent et al., 2017). This sporomorph transition was thought to correlate with the Carnian-Norian boundary but is now discounted on the basis of paleomagnetic and U-Pb correlations (Muttoni et al., 2004; Furin et al., 2006; Irmis et al., 2010; Olsen et al., 2011; Kent et al., 2017) (but see Lucas et al., 2012). The other biotic transition is seen in footprints and involves the last appearance of the nondinosaurian dinosauromorph footprint *Atreipus* between ~205 and ~207 Ma on the Newark-Hartford APTS (Kent et al., 2017), very close to the projected Rhaetian-Norian boundary (Maron et al., 2015; Wotzlaw et al., 2014).
5. *Sporomorphs:* Vesicate pollen taxa *Patinasporites*, *Enzonalosporites*, and *Vallasporites* disappear in nominally the late Norian or early Rhaetian strata in Europe, while in the Newark and Fundy basin sections, their last appearances are in strata just below the oldest CAMP flows, which has been identified as the ETE and hence at or very close in time to the Triassic-Jurassic boundary. Typical European Rhaetian sporomorph taxa are also missing (e.g., *Rhaetipollis*). Gradstein et al. (1994) and Van Veen (1995), echoed by Kuerschner et al. (2007) and Tanner and Lucas (2015), argued that these observations indicate that the Newark Basin interval was highly condensed with most of the Rhaetian omitted. The presence of *Patinasporites* above the upper basalt formation (Panfili et al., 2019) falsifies this argument, given that no CAMP flows are older than latest Rhaetian (Appendix Note 1). This is supported by the 201.566 ± 0.031 Ma zircon U-Pb dates from the Argana Basin Amalal Sill feeding the Alemzi Formation flows of intermediate basalt composition (Blackburn et al., 2013; Marzoli et al., 2019), which is significantly younger than any middle Rhaetian zircon U-Pb dates from marine strata (Wotslaw et al., 2014).
6. Hartford Basin assemblages close to the base of the Talcott Formation lack any taxa restricted to the Triassic, consistent with what is seen in the Newark Basin. Likewise, the sporomorph and footprint assemblages above the Talcott Formation are consistent with those above the Orange Mountain Basalt. The same is true for the footprint and sporomorph assemblages from the Deerfield Basin, although the equivalent of the Talcott basalt and immediately underlying strata are not known from outcrop.
7. The Fundy Basin has a similar palynological turnover below the North Mountain Basalt (Fowell & Traverse, 1994) to what is seen in the Newark and Hartford basins. In addition, the footprint and bone assemblages above the North Mountain Basalt are consistent with those in strata above the Orange Mountain and Talcott basalts. Cirilli et al. (2009) have also documented the presence of *Lunatisporites* spp. in the basal McCoy Brook Formation on top of the North Mountain Basalt, a typical latest Triassic form in Europe that is otherwise unknown from eastern North America.
8. Thus, in eastern North America the largest magnitude floral change occurs beneath the oldest basalt flows in each basin, and there is a distinct albeit thin interval with sporomorph assemblages similar to what is above the basalts between the interval of last appearances and the oldest basalts. This is not the case in the Moroccan basins (Marzoli et al., 2004; Panfili et al., 2019). In the Argana, Khémisset, and Central High Atlas basins, Triassic aspect sporomorph assemblages, characterized by abundant *Patinasporites* and *Enzonalosporites,* continue to the base of the oldest basalts, although the presence of E23r in the Argana Basin demonstrates that the youngest of those strata is still consistent with the *Patinasporites*-bearing strata in the Newark Basin.
9. *Clam shrimp:* The presence of the large *Shipingia olseni* (clam shrimp) is argued to indicate late Norian age, while the presence of smaller, nominal *Euestheria brodieana* in overlying strata (interbedded with the older CAMP lava flows) is interpreted to mean nearly all of the Rhaetian is missing based on correlation with European strata (Kozur & Weems, 2005, 2007, 2010; Weems & Lucas, 2015). There are major issues with the identification of these species and their counterparts in Europe due to a lack of quantitative morphological population analysis or precision (Scholze & Schneider, 2015) in the eastern North American forms and the strong interspecific and ecophenotypic variability in modern forms (Hethke et al., 2018, Hethke, 2014, Morton et al., 2017).
10. *Patinasporites* occurs above the upper basalt formation in the Central High Atlas Basin (Marzoli et al., 2004; Panfili et al., 2019). Three simple arguments could explain this observation: (1) the *Patinasporites* were produced by relict populations, extirpated earlier in eastern North America; (2) the *Patinasporites* grains were reworked from prebasalt strata; (3) the upper basalt formation in the Central High Atlas is older than any flows in eastern North America, which is favored by Panfili et al. (2019). Option 1, is ad hoc and makes that taxon less of an ideal index fossil for the ETE and the region. It would be analogous to the survival of the *Aquilapollenites* group of pollen in very few areas after the K-Pg boundary (e.g., Saito et al., 1986; Farabee, 1991; Vajda & Bercovici, 2014). Option 2 conflicts with the quality of sporomorph preservation. Option 3 clashes with the sequence of trace element geochemistry of CAMP flows in CAM basins that suggests the upper basalt formation is younger than the Orange Mountain and North Mountain basalts and that the carbonate-bearing units between the intermediate and upper basalt formations

resemble carbonates in the lower Feltville and McCoy Brook formations, overlying the Orange Mountain and North Mountain basalts, respectively (Whiteside et al., 2007). Although all are consistent with available U-Pb dates (Blackburn et al., 2013) and other biostratigraphic data, the preponderance of evidence favors Option 1. This hypothesized option could be falsified by zircon U-Pb dates showing that the upper basalt formation is older than the Orange Mountain or North Mountain basalt, or by showing that the paleomagnetic directional groups in the basalts in Morocco (Knight et al., 2004) were inconsistent with those in eastern North America.

11. Martinsville no. 1 core (40.611446° -74.574368°): Stratigraphically the youngest core of the Newark Basin Coring Project, it was spudded in the uppermost Feltville Formation, recovering 137.2 m, the complete 165 m of the Orange Mountain Basalt, and 882 m of upper Passaic Formation (core depths) with a total depth of 1223.8 m (Kent et al., 1995; Olsen et al., 1996a). It preserves a continuous sequence through the ETE interval, including the equivalent of the Jacksonwald Syncline section and the Woodland Park section with a highly resolved magnetostratigraphy (Fig. 34 in Olsen et al., 2016b). To date, this core has not been analyzed for PGEs.
12. The uppermost Passaic Formation in this core consists largely of red to purple cyclical laminated to massive mudstone and siltstone beds with thin (<20 cm) sandstone beds. Some siltstone and very fine sandstone beds contain oscillatory ripples and a few exhibit current ripple cross-lamination. At several levels, zones with casts of roots are present along with burrows, euhedral evaporite pseudomorphs, and gypsum nodules. Desiccation cracks are generally present and often extend through laminated intervals. The stratigraphy is similar to the Jacksonwald Syncline section, although grey strata are present. The thickest sandstone in the section (Fig. 34 in Olsen et al., 2016b) projects to the level of the "blue" sandstone in the Jacksonwald Syncline section.
13. This sequence exhibits abundant features characteristic of moderately deep to very shallow lakes, playas, and vegetated mudflats ("Cycle Type V" sequences, Smoot & Olsen, 1994; Smoot, 2010). Correlation pinned by the base of the Orange Mountain Basalt and magnetic polarity chron E23r show that these cycles are laterally equivalent to dark-shale-bearing cycles in the Jacksonwald Syncline (Fig. 34 in Olsen et al., 2016b). In general, cyclicity does become attenuated from the middle to upper Passaic Formation, but at the Martinsville no. 1 site and Jacksonwald, the context is still cyclical lacustrine, not fluvial as impugned by Tanner and Lucas (2015). While there is scant biological data from the cores themselves, including no sporomorphs; the spinocaudatan (clam shrimp) *Shipingia olseni* is present within the fine mudstones in E23r in the Martinsville core (Fig. 34 in Olsen et al., 2016b). The argument of a hiatus at this level based on this taxon is falsified by the data presented by Kent et al. (2018) and described in Appendix 5.
14. The original coordinates were reported in error as degrees, minutes, seconds when they should have been in degrees, decimal minutes. Prior to more precise GPS and because a lack of paper map coordinates for the construction sites at the time, three of the four site coordinates were also inaccurate (the exception being "Grist Mills"). The approximate correct coordinates in latitude and longitude decimal degrees are Grist Mills, 40.314151°, -75.853339°; Section I, 40.313412°, -75.843879°; Section 2, 40.313247°, -75.843174°; Section 3, 40.313249°, -75.838236°. Our new data were collected at Section 2.
15. Woodland Park (40.875964°, -74.188455°): A former traprock quarry in the Orange Mountain Basalt (Gallagher & Hanczaryk, 2006; Olsen et al., 2016b) and now a residential community in Woodland Park, N.J., has produced important stratigraphic, sedimentological, and paleobiological information between E23r and the Orange Mountain Basalt. The section has ~50 m of uppermost Passaic Formation and most of the 55 m thick lowest of three major flows of the 150 m thick Orange Mountain Basalt (Tollo & Gottfried, 1992). In this area, the uppermost Passaic Formation consists of two units with contrasting facies: a lower interval of fluvial facies that is most common and an upper unit of marginal lacustrine facies. The fluvial facies are composed of upward fining cycles of poorly sorted pale red conglomerate and pebbly sandstone with poorly defined trough cross bedding grading upward into massive red mudstones and sandstones (described by Parker et al., 1988) that are intensely bioturbated with obscure bedding. This facies is overlain by red and much less common grey mudstones and sandstones with more distinct bedding and excellent preservation of small-scale sedimentary structures, which are far more heterogeneous than underlying units. There are cross-laminated sandstones with channel morphologies, tilted thin beds that toe laterally into mudstones suggestive of small deltas or crevasse splays, tabular beds of climbing ripple cross-lamination, and thin bedded mudstone beds suggestive of suspension deposits in standing water. Many sandstone beds are bound by clay drapes, and several surfaces are covered by ripples, desiccation cracks, and trace fossils, notably reptile footprints. The uppermost surface of this interval is capped by the Orange Mountain Basalt and locally seems to have preserved some depositional relief, including small channels. Vertebrate footprint assemblages (Olsen et al., 2016b) and floral remains from the upper facies completely lack all Triassic-aspect forms, indicating that the interval postdates the ETE. Chron E23r was identified in the north quarry wall at about 16 m below the Orange Mountain Basalt in the coarser, fluvial, conglomeritic facies (Fig. 34 in Olsen et al., 2016b) that is similar to typical Passaic Formation in this area (Parker et al., 1988).
16. The floral assemblage from discontinuous pods of grey mudstone and sandstone near the base of the footprint-bearing marginal lacustrine facies include abundant remains of *Brachyphyllum* cf. *scottii*, less common *Clathropteris meniscoides*, a large variety of casts of stems and rhizoliths, and poorly preserved pollen mostly of the genus *Classopollis*. This is a typical post-ETE assemblage very similar to that in the overlying Feltville Formation as well as what is above the fern spike in the Jacksonwald Syncline.

17. The Woodland Park quarry site became famous in the 1980s to 2000s because of the abundant and well-preserved footprints (Olsen at al., 2004, 2016b; Gallagher & Hanczaryk, 2006). Overwhelmingly abundant are a full size range of brontozoid dinosaur tracks from small *Grallator* to *Eubrontes giganteus*, several with unique preservation styles, abundant *Batrachopus* cf. *B. deweyii* tracks, and the lizard-like track, *Rhynchosauroides* sp. Possibly thousands of tracks from this site have been examined by amateur collectors, with many finding their way into museum collections, notably the Princeton collection at Yale, the New Jersey State Museum (Trenton, N.J.), and the Morris Museum (Morristown, N.J.). Despite the very large numbers of tracks this site has produced, there have been no examples of any other footprint taxa, nor any typical Triassic forms, some of which have been found nearby in lower strata (e.g., Baird, 1986) in Essex County.
18. Although the section has not been analyzed for PGEs, salient features of this site are important to the ETE transition and the other CAM rift sections with Ir anomalies because of the robust correlation to the Jacksonwald Syncline section and the Martinsville no. 1: (1) the lack of Triassic aspect sporomorphs such as *Patinasporites*; (2) the lack of tetrapod footprints such as *Brachychirotherium*; and (3) the first appearance of large brontozoid footprints attributed to *Eubrontes giganteus* (Olsen et al., 2002, 2016b).
19. The coring transect of the Army Corps of Engineers (ACE) Passaic River Diversionary Tunnel Project recovered a series of short cores (<200 ms) through the uppermost Passaic Formation and lower Orange Mountain Basalt (Fedosh & Smoot, 1988; Tollo & Gottfried, 1992; Olsen et al., 1996b; Olsen et al., 2002) in this area. These cores show the same facies transition and chron E23r is identified at the appropriate levels as well along strike [PT-38 (40.8647, -74.2030), C-87 (40.8735°, -74.2007°), and C-84 (40.8658, -74.1946)] over a total distance of ~2.1 km southwest (Olsen et al., 2016b). These data corroborate the lateral traceability of chron E23r and correlation to the Martinsville no. 1 core and the Jacksonwald section.
20. Cornet (1977) retrieved numerous *Clathropteris* from this locality and recovered specimens of the spore *Granulatisporites infirmus* from sporangia of fertile pinnae (Cornet & Traverse, 1975). The mat itself and the underlying claystone make up a fern spike dominated by *Granulatisporites infirmus* (the dominant spore in the Jacksonwald Syncline fern spike), *Converrucosisporites cameronii* (which grades morphologically into the former), and *Corollina meyeriana* with subordinate amounts of *Dictyophyllidites paramuensteri*, *Dictyotriletes* sp., *Pilasporites allenii*, *Podocarpidites* sp., *Classopollis torosus*, *Corollina murphyi, Classopollis simplex*, *Circulina simplex*, *Cycadopites andrewsii*, and *Cycadopites* sp. (Cornet & Traverse, 1975).
21. The Holyoke exposure (Cornet & Traverse, 1975; Olsen et al., 2003b) consists of (from the bottom up) a few meters of red and brown sandstone and mudstone, followed by ~5 meters of grey and tan and yellow-weathering pebbly sandstone and siltstone. These coarser units are draped by a few cm of grey rooted light grey clay, covered by a mat of *Clathropteris* and *Equisetities* in growth position (albeit compressed). The mat is overlain by tan and yellow-weathering fine conglomerate, pebbly sandstone, and siltstone. It is clear from surrounding outcrops that this exposure lies below the Holyoke Basalt and is within the lower Shuttle Meadow Formation, as defined lithologically. The Talcott Formation that underlies the Shuttle Meadow Formation in most of the southern Hartford Basin is absent from this part of the northern Hartford Basin. Lithologically, the sequence resembles the Shuttle Meadow Formation although such lithologies begin in the uppermost New Haven Formation. While this unit is conventionally mapped as New Haven Formation, the chronostratigraphic meaning is unclear. Cornet (1977) positions this section 148 m below the Holyoke basalt, however, the irregular topography suggests to us the presence of a series of faults, making speculative any thickness estimate outside the existing exposure.
22. In core B-2, the lower 56.5 m (below 164.5 ft) of typical New Haven Formation is characteristic of the alternating "red stone" and Lamentation facies of Krynine (1950), typical of the Meriden area. The Redstone facies consists of a red micaceous feldspathic sandstone and interbedded bioturbated mudstones while the Lamentation facies is composed of often conglomeritic coarse grey or purplish white arkose. Both facies tend to be heavily bioturbated with roots and the burrow *Scoyenia*, and consequently there is little preservation of ripples and other fine sedimentary structures. Above 164.5 ft in core B-2 and 166.9 ft in core B-3, the New Haven Formation has an abrupt facies change to finely interbedded, red and tan fine sandstone that grades upward into grey fine sandstone and minor mudstone with abundant plant fragments, including conifer shoots (text Fig. 12.2). This facies is more similar to the overlying Shuttle Meadow Formation in the preservation of small-scale sedimentary structures, the reduction of bioturbation, and the preservation of organic matter. The contact with the overlying Talcott Formation at 156 ft in core B-2 is sharp, but there is some deformation of the uppermost New Haven Formation. From 156 ft to 70 ft, the Talcott Formation is pillowed and brecciated.
23. The depositional environment of the strata proximal to and below CAMP flows in most Moroccan basins (and the Fundy Basin) is nonmarine and largely lacustrine, despite assertions of marine environments in Morocco (e.g., Biron, 1982; Beauchamp & Petit, 1983; Fabuel-Perez, et al., 2009; Dal Corso et al., 2014). While marine carbonate deposits with definitive marine invertebrates such as echinoids occur in eastern Morocco (Oujda Mountains), interbedded with CAMP basalts (Whiteside et al., 2008), the only documented invertebrate fossils that have been found thus far in the outcrops to the west are either exclusively nonmarine forms, such as the hydrobiids (Whiteside et al., 2007) and spinocaudatans (Weems & Lucas, 2015) and darwinulid ostracodes, or poorly preserved bivalves that could belong to any number of nonmarine or marine taxa (e.g., Biron et al., 1983). What is often described as bioturbation (e.g., Fabuel-Perez et al., 2009) is generally sand-patch fabric. That does not mean that marine waters might

not be the ultimate source of the brines from which some evaporites evolved, only that there was no open marine connection and there was significant freshwater involvement (Holser et al., 1988).

24. The locality of Deenen et al. (2010) appears be reported with incorrect coordinates (N30°46.4′, W9°10.0′, as reported) because those coordinates plot within a large area of basalt and younger strata. Based on the photograph of the site provided by Deenen et al. (2010), their site appears to be at 30.771707°, -9.152153°, placing it less than 200 m south of the Whiteside et al. (2007) locality (text Fig. 12.3).
25. Both the Alemzi and "Aguerouine" (presumably Aguersouane) locations are problematic as given in the supplemental information of Marzoli et al. (2004). It is necessary to assume that Alemzi with coordinates given as 30° 43' 71"N, 9 14' 47"W, is actually 30° 43.710'N, 9° 14.470'W to fall on a suitable outcrop area, and if Aguerouine is Aguersouane, the given coordinates of 30° 44'N, 9° 15'W do not fall near the village of that name and not on the contact, repeated in Panfil et al. (2018). Both sites seem to be more than 6 km southwest of the Whiteside and Deenen sites. Because the palynological data were not plotted in a stratigraphic section, it is not possible to judge whether the discrepancy is due to a lower accumulation rate or some other cause.
26. In the Berrechid Basin, the contact between the lowest basalt in the basin and underlying red sequence is poorly exposed (33.626179°, -7.289546°) along a ravine leading northeast into the Oued Nfifkh. There, ~1 m of variegated red, grey, and dark grey mudstone is present just below the basalt, similar but thinner, to the sequence at Nif El Gour in the Khémisset Basin. Within 5 km to the east, down-dip is at least 20 m of halite in contact with the overlying basalt as seen in the PB43 core (Afenzar & Essamoud, 2017) close to the Société Sel de Mohammedia Mine (subsurface rock salt mine at 33.630031°, -7.330232°). As in the Argana sections, rapid changes in bed thickness occur laterally, even at small outcrops (text Fig. 12.5), consistent with the former presence of salt. Thick halite and potash salts are present down-dip in the same basin ~31 km northwest at the Pz1 core with more than 50 m of halite and sylvite (Et-Touhami, 1996) directly below the basalt.
27. This may be the same locality called Maaziz in Panfili et al. (2019), however, their coordinates do not plot in an outcrop area.
28. There is no agreed upon formal lithostratigraphic nomenclature for the Latest Permian to earliest Jurassic continental strata of the Central High Atlas region. Six pre-CAMP basalt sedimentary units are generally recognized (Biron, 1982), the uppermost of which is F6 or "upper siltstone" or "Siltite de Tafilant" of Mattis (1977). F6 is overlain by the CAMP basalts, which are named according to their position and chemistry: lower basalt formation, intermediate basalt formation, upper basalt formation, and recurrent basalt formation (e.g., Marzoli et al., 2018). These basalts are interbedded with, to a varying extent, sedimentary units, including thin carbonates (Whiteside et al. 2008). Other nomenclatures exist (e.g., Le Marrec, 1985).
29. The coordinates for the Tiourjdal section were reported with a typographic error by Dal Corso et al. (2014). The Tiourjdal section was reported as 31°07'74"N, 7°22'70"W, which should have been 31°07.74'N, 7°22.70'W equivalent to 31.129000°, -7.378333°.
30. The palynostratigraphies at Tiourjdal and Oued Lahr are difficult to compare with that at Sidi Rahal because the former are too sparsely sampled with *Enzonalasporites vigens* and/or *Patinasporites densus* at 1.7 m and 0.2 m below the contact with the CAMP strata, respectively. This pattern is consistent with that at the Sidi Rahal and Argana sites. Panfili et al. (2019) report *Patinasporites densus* at two sites, Oued Lahr (also reported by Marzoli et al., 2004) and Amassine (31.578889°, -7.501944° of Panfili et al., 2019) in the strata above the "upper basalt" and one site below the "intermediate basalt," which they interpret as an interval between the "lower basalt" and "intermediate basalts" (Panfili et al., 2019, Fig. 4) even though they point out no "lower basalt" is present at that section. These are the only sites from which *Patinasporites densus* has been reported above ANY CAMP basalt.
31. In order to correlate the Fowell et al. (1995) section with the others from Partridge Island, it was necessary to assume the depth scale was measured in decimal feet rather than meters as reported.

APPENDIX 2: DATA TABLES

Table 12.A1 Data for Exeter Section, Pennsylvania, USA

Locality	Comment	sample	Depth mid–point	color	grain size	TOC	d13C	d13C wood	Au (ppb)	Ir (ppb)	Pd (ppb)	Pt (ppb)	Rh (ppb)	Ru (ppb)	Au/Ir–CI	Pt/Ir–CI	Pd/Ir–CI	section GM Ir ppb	section GM Ir±	section 1 Ir ppb	section 1 Ir±	section 2 Ir ppb	section 2 Ir±	section 3 Ir ppb	section 3 Ir±
Exeter			2794	1	1																				
Exeter			2709	0	1																				
Exeter		6/23/00–15	2634	0	0.5	0.207	–17.350		1.52	0.04	1.50	0.63	0.04	<0.08	12.19	7.32	31.14								
Exeter		6/23/00–14	2609	1	1	0.104	–17.414																		
Exeter		6/23/00–13	2584	1	1	0.09212	–17.503																		
Exeter		6/23/00–12	2566.5	2	0.5	0.151	–17.659																		
Exeter			2544	1	2																				
Exeter			2521.5	2	2.5																				
Exeter		6/23/00–11	2504	2	0.5	0.05288	–18.241																		
Exeter		6/23/00–10	2484	2	0.75	0.05248	–18.543																		
Exeter			2424	0	1																				
Exeter			2369	1.5	2																				
Exeter			2309	0	1																				
Exeter		6/23/00–8	2249	2	0.75	0.08676	–19.720																		
Exeter		6/23/00–8b	2214	0	1	0.18336	–20.060																		
Exeter		6/23/00–7	2179	1	0.75	0.09268	–19.990		3.92	0.10	2.15	1.14	0.06	<0.08	12.57	5.30	17.85								
Exeter		6/23/00–6	2169	1.5	0.5	0.09348	–20.020		4.17	0.12	2.27	1.49	0.06	<0.08	11.14	5.77	15.71								
Exeter		6/23/00–5	2156.5	2	0.5	0.09392	–19.580																		
Exeter		6/23/00–4	2141.5	2	0.5	0.08608	–20.150		3.83	0.08	3.13	1.40	0.07	0.11	15.35	8.14	32.49								
Exeter		6/23/00–3	2126.5	2	0.5	0.0556	–20.230		4.70	0.10	3.17	1.85	0.08	<0.08	15.07	8.60	26.32								
Exeter		6/23/00–2	2109	2	0.5	0.05616	–20.190																		
Exeter		6/23/00–1	2067	1.5	2.5	0.207	–20.610		3.12	0.10	2.35	1.61	0.09	<0.08	10.01	7.49	19.51								
Exeter			2030	0	1																				
Exeter		19/10/01–1	2010	0	1.5	0.1852	–20.610		2.99	0.12	3.17	1.83	0.11	<0.08	7.99	7.09	21.94								
Exeter		19/10/01–2	1980	0	1.5	0.15156	–21.613																		
Exeter		19/10/01–3	1951	0	1	0.11068	–24.439		1.37	0.07	1.65	0.55	0.04	<0.08	6.28	3.65	19.57								
Exeter		19/10/01–4	1929.5	2	1	0.11476	–21.613		2.54	0.08	1.15	0.48	0.03	<0.08	10.18	2.79	11.94								
Exeter	picked wood	19.10.01 05 and 06	1912	2	2			–22.462																	
Exeter		19/10/01–5,6	1912	2	2	0.046	–22.403		8.65	0.29	3.91	2.96	0.14	0.10	9.57	4.75	11.20								
Exeter		19/10/01–7	1887	2	2.5	0.05496	–23.012		3.40	0.13	2.00	1.60	0.08	0.15	8.39	5.72	12.77								
Exeter		19/10/01–8	1857	2	3	0.04076	–23.968																		
Exeter		19/10/01–9	1827	2	3.5	0.07356	–25.897		1.03	0.08	0.99	0.72	0.05	0.09	4.13	4.19	10.28								
Exeter		19/10/01–10	1797	2	3	0.32652	–22.866																		
Exeter		19/10/01–11	1767	2	3	0.05044	–23.924		0.72	0.05	0.78	0.73	0.04	<0.08	4.62	6.79	12.95								
Exeter		19/10/01–12	1736	2	3	0.097	–24.465		1.48	0.07	0.88	0.64	0.03	<0.08	6.78	4.25	10.44								
Exeter			1727.5	2	3																			0.158	0.025
Exeter			1725	3	3															0.097	0.019				
Exeter			1724	2	3																	0.021	0.009		
Exeter			1721.5	2	3													0.06	0.015						
Exeter			1720	2	3													0.083	0.018						
Exeter			1717.5	2	3																			0.285	0.033
Exeter	picked wood	19 10 01–13	1717.5	3	0			–23.420																	
Exeter	coaly layer	19/10/01–13	1717.5	3	0	50.16	–26.294		1.44	0.05	0.94	0.75	0.05	<0.08	9.24	6.98	15.61								
Exeter			1715.5	2	0																	0.119	0.021		
Exeter			1715	0	0													0.177	0.026						

(*Continued*)

Table 12.A1 (Continued)

Locality	Comment	sample	Depth mid-point	color	grain size	TOC	d13C	d13C wood	Au (ppb)	Ir (ppb)	Pd (ppb)	Pt (ppb)	Rh (ppb)	Ru (ppb)	Au/Ir-CI	Pt/Ir-CI	Pd/Ir-CI	section GM Ir ppb	section GM Ir±	section 1 Ir ppb	section 1 Ir±	section 2 Ir ppb	section 2 Ir±	section 3 Ir ppb	section 3 Ir±
Exeter			1713	3	0																			0.087	0.018
Exeter			1712.5	2	0															0.025	0.01				
Exeter		19/10/01–14	1711.5	2	0	0.5048	–26.697		2.78	0.05	1.36	0.64	0.03	<0.08	17.83	5.95	22.59								
Exeter			1711	2	0													0.113	0.021						
Exeter			1709	2	0																			0.114	0.021
Exeter			1708.5	2	0																	0.103	0.02		
Exeter			1708	2	0																	0.096	0.019		
Exeter		19/10/01–15	1705	2	0.5	0.1884	–24.328		1.39	0.04	0.85	0.48	0.04	<0.08	11.14	5.58	17.65								
Exeter			1702	2	0.5															0.076	0.017				
Exeter			1699	2	1													0.116	0.021						
Exeter		19/10/01–16	1694.5	2	2	0.07236	–21.348		0.79	0.03	0.54	0.31	0.02	<0.08	8.44	4.81	14.95								
Exeter			1694.5	2	2																			0.048	0.001
Exeter			1692	2	2															0.071					
Exeter			1690	2	2																	0.061	0.015		
Exeter			1689	2	2													0.019	0.009						
Exeter			1687.5	2	2																			0.039	0.012
Exeter			1682	2	2															0.04	0.012				
Exeter			1681	2	2																	0.023	0.001		
Exeter			1680	2	2													0.083	0.018						
Exeter			1673.6	2	2																				
Exeter			1673.5	2	2																				
Exeter			1673	2	2																	0.073	0.017		
Exeter	picked wood	19.10.01 17	1672	2	2.5			–22.804										0.097	0.019						
Exeter		19/10/01–17	1672	2	2.5	0.1248	–22.457		0.73	0.03	0.56	0.36	0.03	<0.08	7.80	5.58	15.50								
Exeter			1669	2	2.5													0.028	0.01						
Exeter			1667	2	2.5																	0.035	0.012		
Exeter			1664.5	2	2.5															0.056	0.015				
Exeter			1663	2	2.5													0.03							
Exeter			1656.5	2	2.5													0.025							
Exeter		19/10/01–18	1642	2	2.5	0.05156	–23.399		0.54	0.03	0.54	0.34	0.03	0.12	5.77	5.27	14.95								
Exeter		19/10/01–19	1624.5	2	0.5	0.05268	–23.066		2.73	0.06	1.59	1.29	0.05	<0.08	14.59	10.00	22.00								
Exeter		19/10/01–20	1613	2	2	0.29196	–19.575		0.56	0.03	0.53	0.39	0.02	<0.08	5.99	6.05	14.67								
Exeter		19/10/01–21	1601.5	2	0.5	0.25724	–19.545		1.83	0.04	1.08	0.67	0.04	0.08	14.67	7.79	22.42								
Exeter		19/10/01–22	1587.5	0	2	0.05408	–21.694																		
Exeter		19/10/01–23	1571	2	3	0.19292	–22.208		1.01	0.02	0.71	0.39	0.02	<0.08	16.19	9.07	29.48								
Exeter		19/10/01–24	1558	1	2.75	0.03223	–22.570																		
Exeter		19/10/01–25	1540	0.5	2.5	0.05396	–22.073		0.67	0.03	0.79	0.32	0.02	<0.08	7.16	4.96	21.87								
Exeter		19/10/01–26	1522.5	0.5	2.5	0.05556	–22.906																		
Exeter		19/10/01–27	1500	0.5	1.5	0.04144	–22.595		0.68	0.03	0.44	0.25	0.02	<0.08	7.27	3.88	12.18								
Exeter		19/10/01–28	1465	0.5	1.5	0.04168	–22.522																		
Exeter		19/10/01–29	1425	0	1.5	0.05204	–22.471		0.94	0.03	0.93	0.40	0.03	<0.08	10.05	6.20	25.74								
Exeter		19/10/01–30	1385	0	1.5	0.04436	–21.327																		
Exeter		19/10/01–31	1335	0	2	0.06656	–20.627		0.74	0.04	0.96	0.36	0.03	<0.08	5.93	4.19	19.93								
Exeter			1257.5	0	2.5																				
Exeter		19/10/01–32	1205	0	2.5	0.16308	–20.397																		
Exeter			1105	0	3.5																				
Exeter		19/10/01–33	1005	0	3	0.16176	–19.541		0.39	0.02	0.46	0.20	0.02	<0.08	6.25	4.65	19.10								

Exeter			905	0	3											
Exeter		19/10/01–34	805	0	2	0.35348	–19.613									
Exeter			740	0	2											
Exeter		19/10/01–35	675	0	0.5	0.4516	–19.426		1.65	0.02	0.91	0.32	0.03	<0.08	26.46	7.44	37.78
Exeter			625	0	2											
Exeter		19/10/01–36	575	0	2	0.16312	–21.044									
Exeter			522.5	0	2											
Exeter		19/10/01–44, 37	450	1.5	2	0.07748	–21.731									
Exeter			377.5	1	2											
Exeter		19/10/01–46	325	0	1	0.05224	–21.881		0.66	0.03					7.06	0.00	0.00
Exeter			272.5	0	1											
Exeter		19/10/01–45	210	0	1	0.12132	–21.551		0.53	0.03					5.67	0.00	0.00
Exeter		19/10/01–44	185	1.5	0.5	0.14352	–21.701		0.33	0.03					3.53	0.00	0.00
Exeter		19/10/01–43	165	2	0.5	0.21532	–22.461		0.35	0.03					3.74	0.00	0.00
Exeter		19/10/01–42	140	2.5	0.5	0.1158	–22.631		0.54	0.04					4.33	0.00	0.00
Exeter	picked wood	19.10.01 41	115	2.5	0.5			–22.872								
Exeter		19/10/01–41	115	2.5	0.5	0.6876	–23.512		0.57	0.04					4.57	0.00	0.00
Exeter		19/10/01–41	95	2.5	0.5	0.736	–23.447		7.19	0.19	7.39	3.96	0.25	<0.08	12.14	9.69	32.30
Exeter		19/10/01–40	77.5	2	1	0.5868	–24.041		1.92	0.04	1.50	1.01	0.06	<0.08	15.39	11.74	31.14
Exeter		19/10/01–39	45	2	1.5	0.4072	–21.852		2.85	0.05	2.15	1.26	0.07	0.11	18.28	11.72	35.71
Exeter		19/10/01–38	10	0	1.5				3.27	0.05	2.90	2.11	0.11	0.09			

Notes: For color: 0 = red; 1.5 = purple; 2 = gray; 2.5 = dark gray; 3 = black; for grain size: 0 = clay, 1 = mudstone; 2 = siltstone; 3 = fine sandstone.

Table 12.A2 Data for Sidi Rahal Section, Morocco

Locality	sample	depth mid point	comment	color	grain size	depth	TOC	$\delta^{13}C$	Ir (ppb)	Au (ppb)	Pt (ppb)	Pd (ppb)	Pt/Ir	Pd/Ir
Sidi Rahal	27 09 03–13	5.00	(1)	basaltic	basaltic	10.00	0.06	–33.825	0.03	1.17	0.98	1.43	15.19	39. 58
Sidi Rahal	27 09 03–14	12.50	(2)	2	1	15.00	0.06	–31.039	0.28	2.83	6.42	3.59	10.66	10.65
Sidi Rahal	27 09 03–15	18.50	(3)	basaltic	basaltic	22.00	0.12	–29.146	0.16	3.58	2.02	2.09	5.87	10.85
Sidi Rahal	27 09 03–16	24. 50	(4)	basaltic	basaltic	27.00	0.07	–32.158	0.10	3.30	1.98	4.14	9.21	34. 38
Sidi Rahal	27 09 03–17	28. 00		2	0	29.00	0.20	–30.184	0.05	1.45	1.13	2.19	10.51	36. 37
Sidi Rahal	27 09 03–18	32. 50		3	0	36.00	0.75	–24.075	0.05	3.09	1.75	2.00	16.28	33. 21
Sidi Rahal	27 09 03–19B	38. 50		2	0	41.00	0.07	–32.416	0.31	0.83	0.38	0.58	0.57	1.55
Sidi Rahal	27 09 03–19	46. 00	(5)	–0.5	0	51.00	0.07	–31.974	0.02	1.42	0.37	0.37	8.60	15.36
Sidi Rahal	27 09 03–20	53.00	(6)	3	0	55.00	1.08	–22.388	0.05	2.69	0.76	1.40	7.07	23.25
Sidi Rahal	27 09 03–21	57.50		2	0	60.00	0.23	–26.664	0.02	0.52	0.24	0.25	5.58	10.38
Sidi Rahal	27 09 03–22	62. 00		3	0	64.00	0.88	–23.908	0.04	2.16	0.42	0.56	4.88	11.63
Sidi Rahal	27 09 03–23	71.50	(7)	1.5	0	79.00	0.10	–31.932	0.01	0.72	0.20	0.16	9.30	13.29
Sidi Rahal	27 09 03–24	80. 00		3	0	81.00	0.95	–22.413	0.07	2.56	0.49	0.70	3.26	8.30
Sidi Rahal	27 09 03–25	85. 00	(8)	0.15	0	89.00	0.14	–28.556	0.02	0.31	0.25	0.29	5.81	12.04
Sidi Rahal	27 09 03–26	90. 00		2.5	0	91.00	0.28	–24.712	0.02	0.90	0.30	0.50	6.98	20. 76
Sidi Rahal	27 09 03–27	97. 50		0	0	104.00	0.13	–25.500	0.02	0.76	0.33	0.53	7.67	22. 00
Sidi Rahal	27 09 03–28	109.50		2.5	0	115.00	0.25	–25.521	0.03	1.04	0.37	0.68	5.74	18.82
Sidi Rahal	27 09 03–29	120.00		0	0	125.00	0.18	–27.149	0.02	1.10	0.39	0.83	9.07	34. 46

(1) soft basalt
(2) green and black mudstone soft
(3) soft basaltic breccia
(4) green volcanoclastic
(5) white clay
(6) black mudstone interbedded with white
(7) gray–green and red mudstone
(8) light gray, white and red mudstone

Notes: For color: 0 = red; 1.5 = purple; 2 = gray; 2.5 = dark gray; 3 = black; for grain size: 0 = clay, 1 = mudstone; 2 = siltstone; 3 = fine sandstone.

Table 12.A3 Data for Partridge Island, Nova Scotia, Canada

Locality	sample no	depth mid points	color	grain size	TOC (%wt)	$\delta^{13}C$ value	Hg (ppb)
Partridge Island		0	3	0			
Partridge Island		1	3	0			
Partridge Island	06_08_03 1	3.505	2	1	2.5		137.5
Partridge Island	06_08_03 2	6.505	2	1	0.1	−31.640	80.5
Partridge Island	06_08_033	8.505	2	1	0.5	−34.513	86.5
Partridge Island	06_08_034	10.005	0	1	0.2		111.5
Partridge Island	06_08_035	11.505	2.5	0	0.4	−32.988	103
Partridge Island	06_08_03 6	13.005	0.5	0	0.2	−33.091	109
Partridge Island	06_08_037	15.505	2.25	0	1.2	−30.464	337
Partridge Island	06_08_03 8	18.255	0	1	0.4	−25.631	78
Partridge Island	06_08_039	20.505	0	1	0.2	−26.246	63
Partridge Island	06_08_03 10	23.005	1	1	0.9	−26.998	117
Partridge Island	06_08_03 11	25.255	2	0	0.8	−28.710	138
Partridge Island	06_08_03 12	27.505	0.5	1	0.3	−24.300	108
Partridge Island	06_08_03 13	30.505	0.5	1	0.2	−27.193	132
Partridge Island	06_08_03 14	33.505	0.5	1	1.1	−23.240	232.5
Partridge Island	06_08_03 15	36.005	3	1	3.4	−27.693	92.5
Partridge Island	06_08_03 16	38.005	2.75	0	2.8	−27.770	207.5
Partridge Island	06_08_03 17	40.005	2	2	0.9	−30.339	143
Partridge Island	06_08_03 18	42.005	1	1	0.1	−28.167	88.5
Partridge Island	05_08_03 16	45.005	0	1		−27.753	
Partridge Island	05_08_03 17	49.005	0	1		−27.779	
Partridge Island	05_08_03 18	53.005	0	1		−26.594	
Partridge Island	05_08_03 19	57.505	1.75	1	0.6	−23.893	5.6
Partridge Island	05_08_03 20	62.005	1.5	1	0.5	−23.676	52.5
Partridge Island	05_08_03 21	66.005	0	1	0.1	−23.982	34
Partridge Island	05_08_03 22	70.005	0	1	0.1	−23.949	28.5
Partridge Island	05_08_03 23	74.005	0	1		−23.509	
Partridge Island	05_08_03 24	78.505	0.5	1.5		−23.937	
Partridge Island	05_08_03 25	83.005	0	1.5		−26.396	
Partridge Island	05_08_03 26	87.005	1	1.5		−26.848	
Partridge Island	05_08_03 27	91.505	1	1.5		−26.998	
Partridge Island	05_08_03 28	96.505	0.75	1		−27.306	
Partridge Island	05_08_03 29	101.005	0.5	1			
Partridge Island	05_08_03 30	105.005	0	1		−24.949	
Partridge Island	05_08_03 31	109.005	0	1		−24.416	
Partridge Island	05_08_03 32	113.005	0	1		−24.728	
Partridge Island	05_08_03 33	117.005	0	1		−24.009	
Partridge Island	05_08_03 34	119.505	1.5	1		−23.557	
Partridge Island	05_08_03 35	121.005	2.25	1.5		−23.983	
Partridge Island	05_08_03 36	124.005	0	1		−26.287	
Partridge Island	05_08_03 37	130.005	0.2	1		−25.531	
Partridge Island	05_08_03 38	134.755	1.75	1		−24.548	
Partridge Island	05_08_03 39	142.255	0	1		−25.460	
Partridge Island	05_08_03 40	156.505	0	1		−24.086	
Partridge Island	05_08_03 41	169.005	0	1.5		−26.615	
Partridge Island	05_08_03 42	179.005	0.75	1		−23.677	
Partridge Island	05_08_03 43	191.505	0	1		−27.322	
Partridge Island		209.005	0	1			

Notes: For color: 0 = red; 1.5 = purple; 2 = gray; 2.5 = dark gray; 3 = black; for grain size: 0 = clay, 1 = mudstone; 2 = siltstone; 3 = fine sandstone.

Table 12.A4 Data for Silver Ridge Core B-2, Berlin, Connecticut, USA

B–2 depth ft	B–2 depth m	grainsize	color	TOCbulk	$\delta^{13}C$ bulk	TOCwood	$\delta^{13}C$ wood	Comments
156.30	–0.06		2.00		–27.556			basalt
156.50	0.00	3.00	2.25	1.07	–25.611			
156.80	0.09	3.00	2.50	2.48	–21.278			conifers
157.00	0.15	3.00	2.25	0.58	–24.733			conifers
157.40	0.27	3.00	2.25	0.53	–24.754			
157.70	0.37	3.00	2.50	1.20	–24.675			(1)
157.90	0.43	3.00	2.25	0.41	–25.618	55.630	–26.827	(2)
158.30	0.55	3.00	1.50	0.38	–18.920			
158.60	0.64	3.00	2.50	0.36	–21.213			(3)
159.40	0.88	3.00	1.50	0.65	–18.436			(4)
159.50	0.91	3.00	1.50	0.25	–33.079			
159.90	1.04	2.00	1.50	0.27	–21.196			
160.30	1.16	2.00	1.50	0.21	–25.732			
160.60	1.25	2.00	1.00		–24.539			
161.10	1.40	3.00	1.75	0.17	–28.021			
161.60	1.55	2.50	0.00		–22.647			
162.70	1.89	2.50	1.00	0.64	–27.720			
163.70	2.19	1.30	0.00		–21.239			
164.00	2.29	1.25	1.00	0.32	–25.073			conifers
164.30	2.38	1.30	1.00	0.89	–24.420			
164.80	2.53	1.30	0.00		–21.568			(5)

(1) kerogen, mostly woody debris and leaf cuticle, black – very mature: oxidized, woody debris, leaf cuticle, rare *Corollina meyeriana*
(2) kerogen, almost all woody debris, black very mature: oxidized, woody debris, *Corollina meyeriana, Pilasporites*
(3) kerogen, almost all woody debris, black very mature: oxidized, woody debris, rare cuticle, rare *Corollina meyeriana, Alisporites*
(4) kerogen, woody debris, leaf cuticle, spores black to dark brown, spores consist almost entirely of *Pilasporites* (horsetail): oxidized, woody debris, rare cuticle, mostly *Pilasporites,* one *Deltaspora,* one *Corollina*
(5) from Farminaton Mb.

Notes: For color: 0 = red; 1.5 = purple; 2 = gray; 2.5 = dark gray; 3 = black; for grain size: 0 = clay, 1 = mudstone; 2 = siltstone; 3 = fine sandstone.

Table 12.A5 Data for Cinque Quarry, East Haven, Connecticut, USA

Locality	Comment	Sample	Depth mid points	color	grain size	TOC	$\delta^{13}C_{org}$	TOC wood (%)	$\delta^{13}C$ wood
Cinque Quarry	(1)	08.15.00.09	0			2.90	–22.559	42.04	–25.163
Cinque Quarry	(2)	08.15.00.08	10	2	4	2.90	–22.559		
Cinque Quarry	(3)	08.15.00.10 mat layer	21.01	2.5	2	3.44	–24.263		
Cinque Quarry		08.15.00.07	27.02	2	2	0.60	–24.825		
Cinque Quarry		08.15.00.06	38.53	2	3	0.44	–25.190		
Cinque Quarry		08.15.00.05	46.54	2	2	1.08	–25.171		
Cinque Quarry		08.15.00.04	50.05	2	1	0.63	–25.171		
Cinque Quarry		08.15.00.03	56.06	2	2	0.81	–25.618		
Cinque Quarry		08.15.00.02	61.07	2	1	0.52	–22.775		
Cinque Quarry		08.15.00.01	67.08	0	2.5	0.41	–23.186		

(1) stem in pillows
(2) interpillow sediments
(3) *Brachyphyllum* mat layer, pollen (*Corollina meyeriana*) and cuticle

Notes: For color: 0 = red; 1.5 = purple; 2 = gray; 2.5 = dark gray; 3 = black; for grain size: 0 = clay, 1 = mudstone; 2 = siltstone; 3 = fine sandstone.